Numerical Calculation of Manoeuvring Coefficients for Modelling the Effect of Submarine Motion Near the Surface

Christopher David Polis

Bachelor of Engineering in Naval Architecture
Graduate Diploma in Business Management

Submitted in fulfilment of the requirements for the degree of

Doctorate in Philosophy

Australian Maritime College

An Institute of the University of Tasmania

December 2016

Signed: Date: 23/12/2016

ABSTRACT

Given the significant amount of time modern submarines conduct operations near the surface of the ocean, there is significant value in the capacity to predict the behaviour of a submarine operating in the near surface region. During most near surface operations, the primary forces involved are due to transient ocean waves and are statistical in nature. Yet there is also a contribution from the motion of the submarine near the surface, which has received less attention from researchers.

The aim of this thesis is to determine the nature of the changes that occur in the manoeuvring forces acting on a submarine due to its own motion when operating near the ocean surface. Currently, coefficient-based manoeuvring models are utilised to predict deeply submerged submarine motion. However, research has shown that these coefficients change when near the surface due to the proximity and form of that surface.

Utilising numerical computation with validation against experimental results, the sources of coefficient variation from their deeply submerged values in the near surface region are identified. The parameters that this variation depends upon are assessed, and the coefficients of motion that vary as a result are identified.

Two novel methodologies based upon the use of numerical planar motion are proposed by which the variation found in the near surface region can be measured across the operating envelope and the changes found for a standard submarine form are thus determined.

The results of these tests show that, of the coefficients assessed, those that have the most significant impact upon submarine motions in the near surface region are:

- Coefficient of normal force as a function of square of the axial velocity;
- Coefficient of normal force as a function of velocity in the z-axis;
- Coefficient of normal force as a function of acceleration in the z-axis; and
- Coefficient of pitch moment as a function of velocity in the z-axis.

Note: the z-axis is vertical in the submarine's frame of reference.

It was also found that the amplitude of a numerical planar motion can be reduced to a minor fraction of a submarine's diameter without loss of accuracy. More significantly, motions of such scale were found to render the coefficients approximately constant over the period of oscillation. This allows the utilisation of this method for the numerical estimate of linear acceleration and velocity coefficients in the near surface region, which are not obtainable via conventional methods.

The ability to estimate these coefficients — along with those obtainable through extending these methods to simulating pure pitch — will enable substantially improved modelling of submarine motions in the near surface region, enabling better design choices and operational control.

CONTENTS

ACKNOWLEDGEMENTS

There are a number of people who I cannot thank enough for their contributions to the work required to complete this project.

Thank you to Professor Dev Ranmuthugala: for your persistence with me over these years. I appreciate the insight that you bring to such a broad range of topics, and your capacity to illuminate significant issues that I may have otherwise passed up as minor. Without you, this never would have started, and never would have been completed.

Thank you to Dr Jonathan Duffy: for your ongoing encouragement, presence and discipline; you kept me going through some tough periods. Thank you for sharing your expertise, and much of your own experience. It was very much appreciated.

Thank you to Professor Martin Renilson: for the deep understanding you presented me with of the topic and tasks set before me. For taking the time to see me, whether near or far, through the midst of what hasn't been the easiest of times for you. It was an honour.

Thank you to Charl Fourie: for granting me an understanding of myself that I lacked, and the tools and structures required to mitigate the limitations within myself.

Thank you to Alex and Esther Ashworth-Briggs, Allan Belle, Zhi Leong, Max Haase, Howan Kim and many others at the AMC Research Hub. Thank you for journeying with me, and for the countless contributions and exhortations you made that enabled me to complete this thesis.

Thank you to Luciano Mason, who was always right there, and always right.

Thank you to my son, Benjamin, who shared the research experience with me on our many 'university days', and sat with me over many evenings towards the end, keeping me focussed on the task at hand.

And finally, thank you to my wife Natalie, who has stood by me through the hard times, and celebrated with me in the good times. The seemingly never ending process does have an end, and your love and commitment to me has allowed me to reach it. I am yours, alone, always.

To each and every one of you: May God bless you and keep you. May you be granted life in its fullness and joy in the years to come.

Yours humbly,

Christopher Polis

NOMENCLATURE AND CONVENTIONS

Directional Conventions

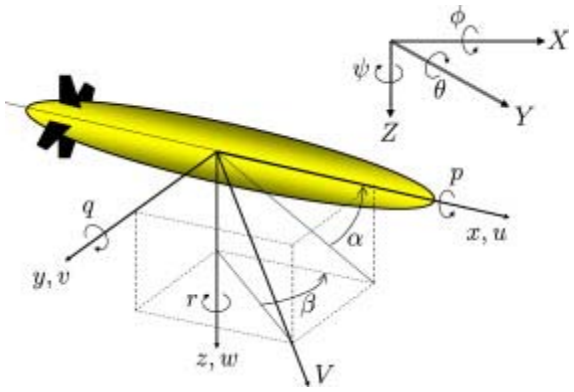

Linear and rotational axis system

X,Y,Z	Earth fixed axes
x,y,z	Body fixed axes
$\boldsymbol{u}$, $\dot{\boldsymbol{u}}$	Velocity, acceleration along the x axis
$\boldsymbol{v}, \dot{\boldsymbol{v}}$	Velocity, acceleration along the y axis
$\boldsymbol{w}, \dot{\boldsymbol{w}}$	Velocity, acceleration along the z axis
$\boldsymbol{p}$, $\dot{\boldsymbol{p}}$	Roll rate, acceleration
$\boldsymbol{q}$, $\dot{\boldsymbol{q}}$	Pitch rate, acceleration
$\boldsymbol{r}$, $\dot{\boldsymbol{r}}$	Yaw rate, acceleration
φ	Angle of Roll
θ	Angle of Pitch
ψ	Angle of Yaw

Nomenclature

B	Buoyancy Force
c	Uniform velocity of flow
$\boldsymbol{C}$	Centripetal-Coriolis Matrix
C	Model to Full Scale Thrust Coefficient
C_{R1}	Linear Resistance Coefficient
C_{R2}	Quadratic Resistance Coefficient
D	Diameter of submarine hull in metres
$\boldsymbol{D}$	Damping Matrix

f	Depth of doublet submergence
F_{xp}	Force due to Resistance and Propulsion characteristics
g	Acceleration due to gravity
$\boldsymbol{g(\eta)}$	Gravity vector
H	Depth from static free surface to the submarine hull centreline in metres
$H^{\star}$	Non-dimensionalised depth, H/D
I_y	Moment of Inertia about y-axis
k	Decay constant
L	Length of submarine hull in metres
m	Dummy integration variable
M	Doublet Strength
$\boldsymbol{M}$	Mass Matrix
M	Moment about y-axis
$M_q^{\star}$	Function of Pitch Moment across all values of $\boldsymbol{q}$
M_q	Coefficient of Pitch Moment as a function of $\boldsymbol{q}$
$M_{\dot{q}}$	Coefficient of Pitch Moment as a function of $\dot{\boldsymbol{q}}$
$M_q^{\star}$	Function of Pitch Moment across all values of $\boldsymbol{q}$
$M_u^{\star}$	Function of Pitch Moment across all values of $\boldsymbol{u}$
M_w	Coefficient of Pitch Moment as a function of $\boldsymbol{w}$
$M_{\dot{w}}$	Coefficient of Pitch Moment as a function of $\dot{\boldsymbol{w}}$
$M_{\lvert w\rvert}$	Coefficient of Pitch Moment as a function of $\lvert\boldsymbol{w}\rvert$
M_{ww}	Coefficient of Pitch Moment as a function of $\boldsymbol{w^2}$
$M_{w\lvert w\rvert}$	Coefficient of Pitch Moment as a function of $\boldsymbol{w}\lvert\boldsymbol{w}\rvert$
$M_{\star}$	Coefficient of Pitch Moment as a function of $\boldsymbol{u^2}$
$M_{\delta b}$	Coefficient of Pitch Moment as a function of δb
$M_{\delta s}$	Coefficient of Pitch Moment as a function of δs
$M_{\delta s\eta}$	Correction to $M_{\delta s}$ as a function of Command Ratio
N	Moment about the z-axis
N_r	Coefficient of Yawing Moment as a function of $\boldsymbol{r}$
$N_{\dot{r}}$	Coefficient of Yawing Moment as a function of $\dot{\boldsymbol{r}}$
N_v	Coefficient of Yawing Moment as a function of $\boldsymbol{v}$

$N_{\dot{v}}$	Coefficient of Yawing Moment as a function of $\dot{\boldsymbol{v}}$
P	Pressure
r	Radius
$S_{M,y}$	Strength of Momentum source in the y-axis direction
$S_{M,z}$	Strength of Momentum source in the z-axis direction
t	Time
Δt	Change in Time
U	Total velocity
U_0	Linear velocity of origin of body axes relative to fluid
U_y	Velocity component in y-axis direction
U_z	Velocity component in z-axis direction
u_i	Instantaneous Velocity Component
$\overline{u_\iota}$	Mean Flow Component
$u_i{}'$	Time Variant Flow Component
u_k	Instantaneous Velocity Component
u_c	Command Velocity
u_τ	Friction Velocity
W	Gravitational Weight
x_B	x-axis Distance from centre of rotation to centre of buoyancy
x_G	x-axis Distance from centre of rotation to centre of gravity
x_i	Flow component axis
x_k	Flow component axis
X	Axial Force
$X_\star$	Coefficient of Axial Force as a function of $\boldsymbol{u^2}$
$X_q^\star$	Function of Axial force across all values of $\boldsymbol{q}$
X_{qq}	Coefficient of Axial Force as a function of $\boldsymbol{q}^2$
$X_u^\star$	Function of Axial force across all values of $\boldsymbol{u}$
$X_{\dot{u}}$	Coefficient of Axial Force as a function of $\dot{\boldsymbol{u}}$
X_{vv}	Coefficient of Axial Force as a function of $\boldsymbol{v}^2$
$X_w^\star$	Function of Axial force across all values of $\boldsymbol{w}$
X_{wq}	Coefficient of Axial Force as a function of $\boldsymbol{wq}$

X_{ww}	Coefficient of Axial Force as a function of $\boldsymbol{w}^2$
X_{wwww}	Coefficient of Axial Force as a function of $\boldsymbol{w}^4$
$X_{\delta s \delta s}$	Coefficient of Axial Force as a function of δs^2
$X_{\delta b \delta b}$	Coefficient of Axial Force as a function of δb^2
Y	Lateral Force
Y_v	Coefficient of Lateral Force as a function of $\boldsymbol{v}$
$Y_{\dot{v}}$	Coefficient of Lateral Force as a function of $\dot{\boldsymbol{v}}$
$Y_{v\|v\|}$	Coefficient of Lateral Force as a function of $\boldsymbol{v}\|\boldsymbol{v}\|$
Δy	Distance from wall
y^+	Non-dimensionalised Distance from Wall
z_B	z-axis Distance from centre of rotation to centre of buoyancy
z_G	z-axis Distance from centre of rotation to centre of gravity
Z	Normal Force
$Z_q^\star$	Function of Normal force across all values of $\boldsymbol{q}$
Z_q	Coefficient of Axial Force as a function of $\boldsymbol{q}$
Z_{qq}	Coefficient of Axial Force as a function of $\boldsymbol{q}^2$
$Z_{\dot{q}}$	Coefficient of Axial Force as a function of $\dot{\boldsymbol{q}}$
$Z_u^\star$	Function of Normal force across all values of $\boldsymbol{u}$
$Z_\star$	Coefficient of Axial Force as a function of $\boldsymbol{u}^2$
$Z_w^\star$	Function of Normal force across all values of $\boldsymbol{w}$
Z_w	Coefficient of Axial Force as a function of $\boldsymbol{w}$
$Z_{\dot{w}}$	Coefficient of Axial Force as a function of $\dot{\boldsymbol{w}}$
$Z_{\|w\|}$	Coefficient of Axial Force as a function of $\|\boldsymbol{w}\|$
Z_{ww}	Coefficient of Axial Force as a function of $\boldsymbol{w}^2$
$Z_{w\|w\|}$	Coefficient of Axial Force as a function of $\boldsymbol{w}\|\boldsymbol{w}\|$
$Z_{\delta s}$	Normal force due to stern plane angle
$Z_{\delta b}$	Normal force due to bow plane angle
$Z_{\delta sn}$	Acceleration correction for Normal force due to stern plane
a_i, b_i, c_i	Coefficients for variation in drag due to command speed
δ	Boundary Layer Thickness
$\zeta(x, y)$	Surface height at position (x,y)

$\boldsymbol{\eta}$	Earth fixed position / orientation vector
η	Ratio of command velocity to velocity
κ_0	g/c^2
ν	Dynamic Viscosity
μ	Kinematic Viscosity
σ	Wave speed
$\boldsymbol{\tau}$	Control Vector
τ_x	x-axis force component of Control Vector
τ_y	y-axis force component of Control Vector
τ_z	z-axis force component of Control Vector
τ_ϕ	Roll moment component of Control Vector
τ_θ	Pitch moment component of Control Vector
τ_ψ	Yaw moment component of Control Vector
$\boldsymbol{\varphi}$	Stream Function

Non-Dimensionalisation

Coefficients

$$M' = \frac{M}{\frac{1}{2}\rho L^3 U^2}$$

$$M'_\star = \frac{M_\star}{\frac{1}{2}\rho L^3}$$

$$M'_q = \frac{M_q}{\frac{1}{2}\rho L^4}$$

$$M'_{\dot{q}} = \frac{M_{\dot{q}}}{\frac{1}{2}\rho L^5}$$

$$M'_w = \frac{M_w}{\frac{1}{2}\rho L^3}$$

$$M'_{\dot{w}} = \frac{M_{\dot{w}}}{\frac{1}{2}\rho L^4}$$

$$M'_{|w|} = \frac{M_{|w|}}{\frac{1}{2}\rho L^3}$$

$$M'_{ww} = \frac{M_{ww}}{\frac{1}{2}\rho L^3}$$

$$M'_{w|w|} = \frac{M_{w|w|}}{\frac{1}{2}\rho L^3}$$

$$M'_{|w|q} = \frac{M_{|w|q}}{\frac{1}{2}\rho L^3}$$

$$X' = \frac{X}{\frac{1}{2}\rho L^2 U^2}$$

$$X'_\star = \frac{X_\star}{\frac{1}{2}\rho L^2}$$

$$X'_{\dot{u}} = \frac{X_{\dot{u}}}{\frac{1}{2}\rho L^3}$$

$$X'_{qq} = \frac{X_{qq}}{\frac{1}{2}\rho L^4}$$

$$X'_{wq} = \frac{X_{wq}}{\frac{1}{2}\rho L^3}$$

$$X'_{ww} = \frac{X_{ww}}{\frac{1}{2}\rho L^2}$$

$$X'_{wwww} = \frac{X_{wwww}}{\frac{1}{2}\rho L^2}$$

$$X'_{\delta s \delta s} = \frac{X_{\delta s \delta s}}{\frac{1}{2}\rho L^2}$$

$$X'_{\delta b \delta b} = \frac{X_{\delta b \delta b}}{\frac{1}{2}\rho L^2}$$

$$Z' = \frac{Z}{\frac{1}{2}\rho L^2 U^2}$$

$$Z'_\star = \frac{Z_\star}{\frac{1}{2}\rho L^2}$$

$$Z'_w = \frac{Z_w}{\frac{1}{2}\rho L^2}$$

$$Z'_{|w|} = \frac{Z_{|w|}}{\frac{1}{2}\rho L^2}$$

$$Z'_{ww} = \frac{Z_{ww}}{\frac{1}{2}\rho L^2}$$

$$Z'_{w|w|} = \frac{Z_{w|w|}}{\frac{1}{2}\rho L^2}$$

$$Z'_{\dot{w}} = \frac{Z_{\dot{w}}}{\frac{1}{2}\rho L^3}$$

$$Z'_q = \frac{Z_q}{\frac{1}{2}\rho L^3}$$

$$Z'_{\dot{q}} = \frac{Z_{\dot{q}}}{\frac{1}{2}\rho L^4}$$

$$Z'_{w|q|} = \frac{Z_{w|q|}}{\frac{1}{2}\rho L^3}$$

$$N' = \frac{N}{\frac{1}{2}\rho L^3 U^2}$$

$$N'_r = \frac{N_r}{\frac{1}{2}\rho L^4}$$

$$N'_{\dot{r}} = \frac{N_{\dot{r}}}{\frac{1}{2}\rho L^5}$$

$$N'_v = \frac{N_v}{\frac{1}{2}\rho L^3}$$

$$N'_{\dot{v}} = \frac{N_{\dot{v}}}{\frac{1}{2}\rho L^4}$$

$$Y' = \frac{Y}{\frac{1}{2}\rho L^2 U^2}$$

$$Y'_\star = \frac{Y_\star}{\frac{1}{2}\rho L^2}$$

$$Y'_v = \frac{Y_v}{\frac{1}{2}\rho L^2}$$

$$Y'_{\dot{v}} = \frac{Y_{\dot{v}}}{\frac{1}{2}\rho L^3}$$

$$Y'_{v|v|} = \frac{Y_{v|v|}}{\frac{1}{2}\rho L^2}$$

$$Z'_{\delta s} = \frac{Z_{\delta s}}{\frac{1}{2}\rho L^2}$$

$$Z'_{\delta b} = \frac{Z_{\delta b}}{\frac{1}{2}\rho L^2}$$

$$Z'_{\delta s \eta} = \frac{Z_{\delta s \eta}}{\frac{1}{2}\rho L^2}$$

Velocities

$$\boldsymbol{u}' = \frac{\boldsymbol{u}}{U}; \boldsymbol{v}' = \frac{\boldsymbol{v}}{U}; \boldsymbol{w}' = \frac{\boldsymbol{w}}{U}; \boldsymbol{p}' = \frac{\boldsymbol{p}L}{U}; \boldsymbol{q}' = \frac{\boldsymbol{q}L}{U}; \boldsymbol{r}' = \frac{\boldsymbol{r}L}{U}$$

Accelerations

$$\dot{\boldsymbol{u}}' = \frac{\boldsymbol{u}L}{U^2}; \dot{\boldsymbol{v}}' = \frac{\boldsymbol{v}L}{U^2}; \dot{\boldsymbol{w}}' = \frac{\boldsymbol{w}L}{U^2}; \dot{\boldsymbol{p}}' = \frac{\boldsymbol{p}L^2}{U^2}; \dot{\boldsymbol{q}}' = \frac{\boldsymbol{q}L^2}{U^2}; \dot{\boldsymbol{r}}' = \frac{\boldsymbol{r}L^2}{U^2}$$

Distances

$$A^\star = \frac{A}{D};\ H^\star = \frac{H}{D}$$

$$A' = \frac{A}{L}$$

Angular Velocities

$$\omega' = \frac{\omega L}{U}$$

Speed-Length Ratios

$$Re = \frac{\rho L U}{\mu};\ Fr_L = \frac{U}{\sqrt{gL}}$$

ABBREVIATIONS

AMC	Australian Maritime College
AMCTT	Australian Maritime College Towing Tank
AUV	Autonomous Underwater Vehicle
BSL	Baseline
BSL-RSM	Baseline – Reynolds Stress Model
CFD	Computational Fluid Dynamics
DNS	Direct Navier Stokes
DTMB	David Taylor Model Basin
EARSM	Explicit Algebraic Reynolds Stress Model
EFD	Experimental Fluid Dynamics
FPM	Fractional Planar Motion
HPMM	Horizontal Planar Motion Mechanism
LCG	Longitudinal Centre of Gravity
PMM	Planar Motion Mechanism
RANS	Reynolds Averaged Navier-Stokes
RSM	Reynolds Stress Model
SLA	Sudden Linear Acceleration
SNAME	Society of Naval Architects and Marine Engineers
SST	Shear Stress Transport
UTAS	University of Tasmania
VOF	Volume of Fluids
VPMM	Vertical Planar Motion Mechanism

The following capitalised terms are used but are formal names, not abbreviations.

ANSYS
CFX
ICEM
MARNET
SUBOFF

LIST OF FIGURES AND TABLES

1. INTRODUCTION

1.1 Background

The relationship that submarines have with the surface of the water has evolved in a fascinating arc over the last 140 years. In the last thirty years of the 1800's, submarines progressed from being mere curios to promising but untried platforms. In World War 1, submarines — then vessels that primarily operated surfaced but with the capacity to submerge — showed significant naval value through their distinct capabilities. Early in World War 2, most retained a significant surfaced warfighting capability, including the possession of deck mounted guns. But by the end of the War, submarine designs had evolved to focus on underwater performance and capability. Figure 1-1 shows the evolution of Australian submarines over the last 100 years.

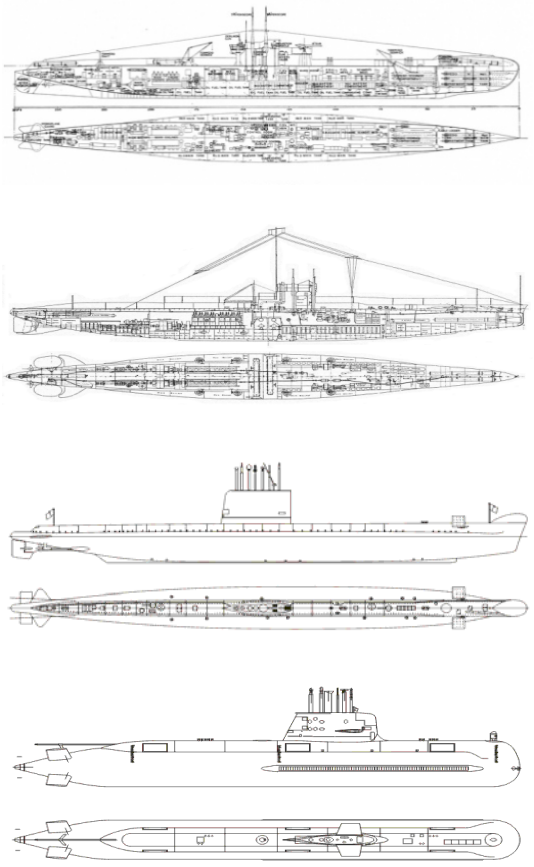

Figure 1-1 Changes in Australian Submarine Designs over Time
From Top: AE Class (1914); Odin Class (1927); Oberon Class (1967); Collins Class (1996);

However, the most substantial changes were yet to come, with the development over the next two decades of low drag underwater forms, and critically the development of nuclear propulsion. These advances moved the submarines preferred operating depth well below of the surface, eliminating most of the ties that made operating near the surface necessary.

Yet even today, near surface operations remain a significant consideration in the design and operation of submarines. A significant proportion of modern submarine operations require operation in the near surface region. Conventional diesel-powered submarines (SSK) such as those used in Australia spend a considerable portion of time near the surface in order to recharge batteries, and most submarines conduct operations that require access to the surface such as surveillance, communication and warfare (Joubert, 2006). There has been an arc of design and research focus that has progressed from first developing the capacity to move under the surface, then to optimise this capacity, and a renewed focus on the capacity to operate effectively, stealthily and safely in the water just beneath the surface where so many of the critical operations of a submarine take place.

Over this time, an immense amount of research has gone into developing ways to assess and predict the dynamic capabilities of a submarine in the design phase. The first mathematical models of the submarine in the near surface environment were

developed in the 1920's, developed further through the testing of physical models in the 1930's as nations prepared for a renewed outbreak of war (Weinblum et al, 1936). Primarily in these early periods, testing was focussed on the resistance of the models. In the post-war period efforts moved to the development of various means of assessing the manoeuvrability of a submarine using physical scale models in captive tests. By the 1960's, the nature of submarine manoeuvring was captured in six degree mathematical models of motion (Gertler & Hagen, 1967) utilising tests that isolated the response of a submarine to specific changes in its operational condition.

In the period since then, improvements in model testing have continued, with the development of models capable of self-propulsion and the systems required to accurately capture the actions and motions of the model in that state. Yet such testing remains expensive, requiring large and complex models, controlled facilities, and significant staffing. In the same period, there has also been a rapid rise in the development of Computational Fluid Dynamics (CFD), and the computational power required to effectively utilise it. This offers the potential of not only lower costs, but also of reduced timeframes and greater opportunity to explore different design options. Furthermore, CFD offers the capacity to model in detail the complex flows around the submarine and its appendages. This has offered insight into the basic fluid dynamic processes at work that were difficult to obtain experimentally. Despite these advances, it remains the case that both scale model and computational efforts must be able to be correlated to full scale results.

1.2 Problem Definition

Given the focus modern diesel-powered submarines have on operations in the near surface environment, there has been an understandable move towards research on the design of submarines specifically for this environment (Joubert, 2006). Their distinct differences from nuclear powered submarines — i.e. their need for air, finite range, reduced speed and lower cost — all skew the operational profile in practice. Blue water fleet support is of reduced significance — though not blue water fleet deterrence (Kopp, 2012) — and operation within the more complex environments of littoral waters and near the ocean surface is demanded. The capacity to reflect these changes in mission within the design process to achieve greater effectiveness in role performance is highly desirable.

In order to conduct a design optimisation focussing on operations in this space, the impact of operation near boundaries must be able to be estimated based upon the submarine's geometry. While these boundaries include the seabed and other large scale structures, and even discrete shifts in water density that occur as a submarine changes from one layer of water to another, the primary boundary of influence is the ocean surface. The additional effects that result from operating near the water surface can be grouped into environmental and self-generated classes. Under normal, low speed near-surface operating conditions, the transient environmental effects of passing ocean waves upon a submarine dominates the additional forces (Crossland

2013). Underlying this is a self-generated load derived from the motion of the submarine itself (Griffin, 2002), and at higher Froude Number this component increases in significance.

The estimation of the additional loads that occur in the near surface region is a complex matter. The creation and testing of self-propelled, scaled physical models are expensive and time consuming, but provides a level of accuracy that other methods have not yet delivered (Leong, Ranmuthugala, Penesis & Nguyen, 2012). Simpler physical models can be utilised in controlled testing to derive characteristics of motion for use in a mathematical model of submarine motion. The other methodology that is available and utilised today is the modelling of flows utilising CFD. Although CFD can be utilised to directly model the response in the near surface environment of full scale submarines in operation, this remains compute-resource intensive. Utilising CFD in a similar fashion to captive model testing to model a number of programmed conditions in order to determine the characteristics of motion opens up the possibility of relatively quickly and cheaply assessing a far wider range of design options, although costs and time can escalate.

In order to be able to model operations in the near surface environment, such that a wide variety of options may be considered without excessive demand on economic or computation resources, two basic components of research are required.

- CFD based predictions that produce outcomes within a validated error band.
- A mathematical model of submarine motion that accounts for the difference in behaviour between the well-studied deeply submerged environment and the near surface environment.

1.3 Research Question

The resolution of the entire problem outlined above is well beyond the scope of a single PhD study. However, in order to contribute to this, the thesis that follows seeks to resolve the following question:

What changes occur in the manoeuvring forces acting on a submarine due to its own motion when operating near the ocean surface compared to operating deeply submerged?

1.4 Research Objectives

In order to establish validated answers to the above question, a program of study and original research were undertaken. This program first set out to establish what is already known regarding the changes in manoeuvring coefficients near the ocean surface, and then to fill in the gaps in knowledge through research.

To do so requires the achievement of a number of specific objectives:

- Determine the significance of the coefficients within existing coefficient based mathematical models of submarine manoeuvring. Ascertain the sensitivity of these models to changes in the various coefficients therein.

- Determine which existing coefficients of motion vary significantly in the near surface environment and how the extent and nature of this variation can be modelled. Identify the parameters that this variation depends upon.
- Ascertain whether additional coefficients need to be included in the manoeuvring model to capture the motion response of a submarine in the near surface environment.
- Propose methodology by which the variation may be estimated through the simulation of planar motion tests in the near surface region, and how these results can be encoded into modified and/or additional coefficients.

1.5 Methodology

The following methodology has been utilised:

- A literature review was conducted into existing research on mathematical models of submarine motion, testing methodology, physical and model testing and numerical simulation conducted in the near surface region.
- The sensitivity of existing models to the various coefficients therein was examined in order to give insight into which of those coefficients were most significant in the modelling of submarine motion, and thus sensitive to change imposed by operation within the near surface region.
- A generic submarine form was be modelled undergoing standard testing manoeuvres, adapted as necessary to suit the near surface region. This was undertaken using CFD, validated against existing numerical and experimental test data, and utilised to assess the response associated with operating near the ocean surface.
- A preliminary investigation into the variation of the primary forces that occur in straight level motion as the submarine approaches a free surface was conducted. A more systematic mesh verification and validation was then undertaken for conditions both deep & near the surface. It considered both bare hull and sail appended configurations, with and without experimental apparatus attachments, for comparison against experimental data identified during the literature review.
- Research was then conducted into the effects of attitude variation of the submarine near the free surface, at a range of depths and Froude Numbers.
- Pure heave studies are customarily conducted with a significant amplitude of motion. Near the free surface, significant changes in depth invoke substantial changes in manoeuvring characteristics. To get around this problem, a study of planar motion a mere fraction of the diameter of the vessel (Fractional Planar Motion) was conducted to investigate its

capacity for determining hydrodynamic characteristics. This study was inferentially validated through validation against physical model testing in both the deeply submerged and near surface conditions.

- A study of small motions under instantaneous, constant acceleration (Sudden Linear Acceleration) was also conducted with the intent to derive acceleration coefficients in the near surface region. These results were compared with those obtained using Fractional Planar Motion.
- Finally, utilising these results, the significance of various coefficients to modelling operation near the free surface was assessed by evaluating the change that occurred in the coefficient near the free surface and the sensitivity of the model to change in that coefficient. The coefficients were then grouped into bands of significance on the basis of the expected effect of their near surface changes on the manoeuvring model.

1.5.1 Research Outcomes and Novel Contributions

The research outcomes of this work are summarised as follows:

- CFD based modelling of near surface test operations to determine relevant coefficients of motion in the vertical plane, including original work considering the effect of trim in the near surface region;
- Development of both Fractional Planar Motion and Sudden Linear Acceleration as means by which coefficients of acceleration can be determined in the near surface region.
- Assessment of a range of coefficients dependent upon motion in the z-axis for their significance in the modelling of the near surface motion of submarines.

1.6 Arrangement of this Thesis

Following this brief introduction, the remainder of this thesis is structured as follows:

- Chapter 2 contains a literature review, discussing the body of research underlying this thesis. The study of waves and the influence of bodies moving under them; the development of the coefficient based manoeuvring model; experimental and computational techniques are recounted, leading to the capability to develop this thesis.
- Chapter 3 discusses the theory and mathematical concepts underlying the modelling of submarine behaviour near the free surface. This includes the coefficient based manoeuvring model; its sensitivity to the changes in various coefficients; existing studies and calculations of the effect of the free surface on the model and its coefficients; choice of a deeply submerged, vertical plane manoeuvring model to develop the near surface model; and a method for assessment of coefficient consequence.

- Chapter 4 presents the verification and validation process underlying the CFD simulation conducted throughout this thesis. It then presents a study describing the relationship between depth, submergence, Froude Length Number, and the additional response observed in the vertical plane to steady state operation parallel to the free surface. This is then extended with a second study regarding the variation of these forces with changes in trim to the surface which assesses the significance of the coefficients based upon velocity in the x and z-axis for significance. However, these studies, given their steady state nature were unable to determine any change in the acceleration coefficients.
- Chapter 5 details the numerical modelling of pure sway in the deeply submerged regions and its validation against published data. This was a functional but a necessary step, providing a degree of assurity of process to obtaining the remaining coefficients in Chapter 6.
- Chapter 6 discusses the conceptual rationale and evaluation of both Fractional Planar Motion (FPM) and Sudden Linear Acceleration (SLA) efforts to develop a test methodology suitable for deriving acceleration based near surface manoeuvring coefficients. This is followed by the selection and use of FPM to provide a numerical estimate of the resultant coefficients at a series of depths.
- Chapter 7 summarises the conclusions resulting from this work and provides recommendations from the findings and for future work.
- A copy of a refereed conference paper presented by the author at PACIFIC 2013 is included as Appendix A. This presentation was based upon the data that would become the first half of Chapter 4 in this thesis. A second conference paper contributed to by the author was presented at WARSHIP 2014, and is included as Appendix B.

2. LITERATURE REVIEW

2.1 Historic Origins

The development of the theory of water waves (Craik, 2004 and 2005) has been touched by the work of some of the greatest scientific minds of the last 400 years: Newton (1687), Euler (1761), Laplace (1776), Poisson (1818), Cauchy (1827), Stokes (1847), Kelvin (1887), Michell (1893). Yet it was really only in the 20th century that work began in earnest on the understanding of the waves made by moving objects near the free surface, and only in the second half of that century that attention was truly brought to bear upon the manoeuvring of submarines, driven by the changing needs of modern navies.

The waves generated on the ocean surface by the passage of a submarine underneath are not simply a function of submergence and Froude Length Number, but also the form and current attitude of the submarine to that surface, along with the time history of those characteristics (Havelock 1950). At each point in time, energy is added to the surface wave system by the submarine in a manner dependant on the conditions of the submarine at that point. This energy is largely retained in the surface through the generation of waves, which travel away from the point of generation at a fixed speed. The integration of this continuous function of generation and travel of waves determines the effect of the nearby submarine on the water surface, and vice versa.

2.2 Coefficient Based Manoeuvring Models

The initial expression of the motion of a rigid body in a fluid — the first hydrodynamic models — were developed independently by Thompson & Tait (1867), Kirchhoff (1869) and Kelvin (1871). In these, the equations were developed as components of the impulse, obtained as the gradients of the energy relative to the components of motion. Lamb (1916 and 1932) refined the expression of these models and collated developments in the field into his *Hydrodynamics* text.

In 1946 Abkowitz prompted the development of a standard set of notation across the field, which was formalised through a series of committees into the notation that is still utilised today (SNAME, 1952). Abkowitz later wrote a summary text on stability and motion control, focussing on the derivation and evaluation of manoeuvring coefficients and models (Abkowitz, 1969).

Development was also occurring in the understanding, analysis and prediction of specific manoeuvring coefficients. Imlay (1961) brought together much of the preceding decade's developmental work on added mass, describing the added mass components of a coefficient-based system of equations for a submarine of standard form and the potential for their estimation by the reasonable assumption that the submarine takes the form of a finned prolate spheroid. Various methods for the description and estimation of the hydrodynamic damping terms were also being investigated: Thin-ship theory (Newman, 1964); Slender Body Theory (Newman &

Tuck, 1964); Flat Ship Theory (MacCamy, 1964); and Strip Theory (Vassilopoulos & Mandel, 1964).

A number of sets of standardised equations for modelling the motion of a submarine in deep water were developed. Early formulations like those produced by the Society of Naval Architects and Marine Engineers (SNAME, 1952) were built upon by the David Taylor Model Basin (DTMB), resulting in a standardised form published as *Standard Equations of Motion for Submarine Simulation* (Gertler & Hagen, 1967). This set of equations, with modifications to suit the data gathered and the arrangement of the particular submarine or submersible is still utilised today, however refinement of this general form continued (Feldman, 1979).

Working from this basis, the general equations are commonly either simplified or modified to suit a particular vessel (Healey & Lienhard, 1993; Prestrero, 2001). Other modifications are made based upon a preference for using alternate formulations for the non-linear components (Clarke, 2003) rather than the modulus quadratic form adopted to account for non-linearity in Gertler & Hagen (1967). There has also been a move to expressing the equations in vector notation (Fossen, 1994) which has allowed a more compact form of notation.

2.3 Near Surface Hydrodynamics

The theory of waves produced by submerged objects commenced in earnest with the work of Lamb (1913). Initially offering a reprise of the formulation employed by Cauchy (1827) nearly a century earlier, stating the stream function describing two-dimensional flow, Lamb then went on to develop a boundary condition for the free surface and derive a general solution. From this point, by supposing an oscillating source some distance below the surface, Lamb developed an expression for the response due to an infinite cylinder of small radius oscillating near the surface. He then further developed this to the surface response due to an infinite cylinder transverse to a constant flow and calculated the resulting wave resistance.

Havelock (1917a) reproduced the same problem by an alternate method considering the pressure on the cylinder surface, before extending the work further (Havelock, 1917b) to consider the resistance of a submerged sphere in the flow. Havelock (1919) subsequently repeated this result with a simpler if less direct method whereby the resistance was calculated by evaluating the moving pressure field required to form the same wave pattern. Lamb (1926) built upon this to provide an integral for determining the resistance of an arbitrarily shaped body moving below a free surface.

Havelock (1928) formulated the function of the free surface under potential flow conditions over a doublet. The approach mirrored a three-dimensional doublet about the plane of the free surface, in order to develop a flat streamline on that plane. It then applies a distortion to that plane that satisfies the boundary condition at the free surface. This approach allowed the construction of arbitrary forms through the combination and distribution of these ‘Havelock sources’.

Havelock continued his studies and development of this theory across the following decades, leading to works in the 1950's considering the flow resulting from a specified body following a specified path at a specified speed.

Havelock's body of work was later developed further by Tuck (1971 and 1987) and Lazauskas (2005) to deal with complex forms utilising numerical methods. Tuck, building on the thin-ship theory of Michell (1898), allowed any zx-plane symmetrical hull form to be represented by a source plane of strength determined by the hull demi-beam at each point.

A number of alternate approaches have also been developed, applying different numerical methods to the problem of modelling the manoeuvring of a submarine that are potentially applicable in the near surface. Some approaches, such as that employed in Jensen, Chislet & Romeling (1993) and Eloot & Vantorre (2003) replace the practice of utilising one or more fixed manoeuvring coefficients that serve to approximate a nonlinear curve with a tabulated and interpolated response across the range tested. Others such as Nahon (1996) utilise alternate formulations where established empirical formulae for the different responses are utilised instead of coefficients of form. Typically, these methods exchange a requirement for additional data and/or calculation for the ability to follow a response that departs from the coefficient-based estimate.

2.4 Experimental Methods

Alongside the theoretical development that was occurring throughout this period, the capacity to carry out physical model experiments to ascertain the response of the submarine also developed over this period. One of the earliest formal studies of the wave resistance of submarines was conducted by Weinblum, Amtsberg & Bock (1936) in Germany. This work compared the theoretical models of the day against a series of model tests of bodies of revolution, leading to a series of resistance curves showing wave resistance at various Froude Numbers.

After the Second World War, a substantial program of experimental and developmental works was carried out, developing methods for deriving the hydrodynamic characteristics of submarines, not only in terms of their drag (either submerged or near the surface), but also the manoeuvring characteristics.

The techniques and equipment developed included the Rotating Arm (Brownell, 1956) and Planar Motion Mechanism (Gertler, 1967). In addition to oblique tow tests conducted with the vessel in a normal towing tank, these tests sufficed to provide the primary coefficients for both velocity ($Y_v, Z_w, N_v, M_w, Y_r, Z_q, N_r, M_q$) and acceleration ($Y_{\dot{v}}, Z_{\dot{w}}, N_{\dot{v}}, M_{\dot{w}}, Y_{\dot{r}}, Z_{\dot{q}}, N_{\dot{r}}, M_{\dot{q}}$) terms (see the nomenclature for definitions of these coefficients).

In order to obtain the manoeuvring coefficients, a series of tests were conducted to identify the form and value of forces due to a specific variable. For instance, the graph in Figure 2-1, taken from Roddy (1990), shows the results of 24 different tests

with a submarine held at a fixed pitch angle to a water flow, from which the coefficients are then determined by means of a best fit.

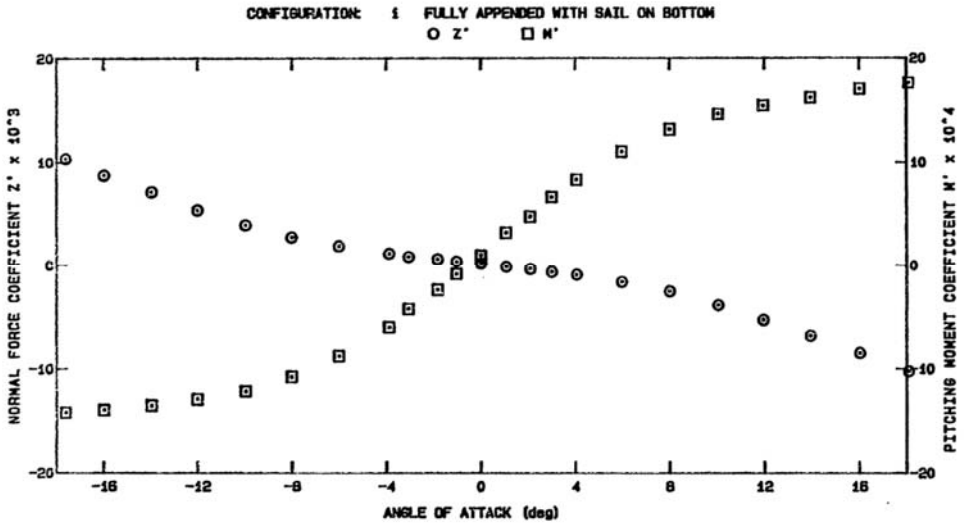

Figure 2-1 - Pitch and Normal Force Coefficients as a function of Pitch Angle (Roddy, 1990)

Utilisation of these techniques for the study of near surface effects remains relatively recent. The development (Anderson, Campanella & Walker, 1995) of sting mounted Horizontal Planar Motion Mechanisms (HPMM) such as that at the Australian Maritime College (AMC) has provided the means for direct measurement of manoeuvring forces when operating in the near surface region (Wilson-Haffenden, Renilson, Ranmuthugala & Dawson, 2010; Neulist, 2011). However, for any given submergence the height of wave generated by the passage of a submarine is dependent upon the speed at which that submarine travels and other factors mentioned earlier. This effect scales with the Froude length number of the submarine, making the transition from deep water (where Reynolds scaling dominates) to near surface (where Froude scaling increases in significance) a complex region to reliably test and explore.

2.5 Computational Fluid Dynamics

Computational Fluid Dynamics (CFD) predicts complex fluid flows by breaking them down into a multitude of simpler problems — typically the flow through a geometrically defined cell. These cells may be bounded by other cells, or have faces upon which a boundary condition is imposed.

Rider & Matteson (2013) report that the origins of CFD are found in the development program for the first nuclear weapons. In documents sealed until 1993 (as cited in Rider & Matteson, 2013) it was revealed that Richard Feynman directed the first calculations, which calculated the progression of shock waves using a 1-D finite difference method. Von Neumann & Richtmyer (1950), describes the methods developed. Research continued to develop the field, however the approaches were limited by lack of computational capacity. Chorin (1968) presented one of the first methods for the solution of the time dependant, incompressible Navier Stokes

equations. By the 1980's, commercial application in the aircraft industry saw a massive growth in the field, but the complex viscous flow around ships and submarines required substantially more computational power that was not yet available. Larsson & Kim (1992) describe a hybrid solver that was part turbulent flow solver, part potential flow solver, increasing the calculation speed by limiting the volume where the more complex CFD were performed. Computational power and solver efficiency has continued to increase to the point where useably accurate predictions of hydrodynamic responses can be derived utilising a range of different turbulence models on a desktop machine (Menter, 2011).

2.5.1 Modelling the Reynolds Averaged Navier Stokes Equation

One area of research has been the development of improved turbulence models. Although the Navier-Stokes equations are directly solvable — and for small scale and $Re<1000$, are now directly solved — the computing time required for the Direct Navier Stokes (DNS) approach scales as Re^3, making it unworkable for analysis of submarines which typically function at $Re \sim 10^8$.

Reynolds (1894) proposed that the motion of a turbulent flow could be devolved into a mean flow and a time-variant component (Equation 2.9), and that doing so would render the difference between turbulent flow and laminar flow to a single group of terms in each equation that together form the Reynolds Stress Tensor.

By adopting this approach in a numerical form, the amount of calculation required in order to resolve an engineering flow at high Re can be reduced by a factor in the order of 10^{10} (Menter, 2011). To do this requires some empirical solution to the Reynolds Stress Tensor. Over the last 50 years, there have been a number of different approaches to this, providing approximate results to the Navier Stokes equation that can with modern computational power be solved in a reasonable period of time.

2.5.2 Modelling the Reynolds Stress Tensor

Hellsten & Wallin (2009) describes the process by which the Reynolds Stress Tensor is broken down into component parts. These components are the production component P_{ij}, the viscous dissipation term ε_{ij}, the redistribution term Φ_{ij}, and the diffusion term $\mathcal{D}_{ij}$. The two basic engineering approaches to solving this are to provide either transport equations for each stress tensor component (Reynolds Stress Modelling) or to express the result of the Reynolds Stress Tensor as a function of the mean velocity gradient and two scale variables which together provide an estimate of the scale of the turbulence occurring. In these instances, the first scale variable, the velocity scale, is typically resolved from the turbulent kinetic energy. Jones & Launder (1972) utilised a formulation for ε as their second scale variable, leading to the $k-\varepsilon$ model. Wilcox (1988) alternatively utilised a model for ω, the turbulence frequency for the second transport model (the $k-\omega$ model). Menter (1994) utilises both of these formulations in different regions of the flow in his Shear Stress Transport(SST) modes, as $k-\omega$ is stronger near the wall and $k-\varepsilon$ is stronger in the open flow situation. Wallin & Johansson (2000) took a different approach, and

utilised explicit algebraic solutions (EARSM) to the implicit RSM equations to provide a production to dissipation ratio derived from a transport equation.

2.6 Experimental and Numerical Studies utilising the SUBOFF hullform

Huang, Liu & Groves (1989) set out a series of testing and computational studies that would be carried out by the David Taylor Research Centre (DTRC) based around the DTRC model 5470, which came to be known as SUBOFF. Details of the model utilised were published in Groves, Huang & Chang (1989), and results from the testing that followed in a number of DTRC papers that followed, with significant data from the experimental testing presented in Roddy (1990). Gorski, Coleman & Haussling (1990) presented the results of CFD studies of the flow around the submarine in two of the arrangements tested. Papers from DTRC continued and a summary paper (Liu & Huang, 1998) collated the set of work and noted the data that had been collected and stored. This published body of work and the model underlying it has become the basis for a significant number of studies since, including a number exploring the performance of the model in the near surface region. For instance, Griffin (2002) presented an extensive numerical study considering the performance of a number of different submarine bodies (including the SUBOFF hull) in the near surface region. He reported on heave and pitch effects, however at that stage there was no experimental data to compare to. Toxopeus (2008) and Toxopeus, Atsavapranee, Wolf et al (2012) conducted a comparative validation study in conjunction with other participating institutions, exploring the capacity of numerical modelling to match the overall forces, pressures and flow velocities reported from physical model tests in linear and rotational domains. Wilson-Haffenden et al (2010) reported on the development of a smaller length, sting mounted SUBOFF model and the changes in wave making resistance at different Froude length number. Neulist (2011) reported on the level-operation forces and moments in the vertical plane over a wide range of Froude length numbers. Leong (2014) reported on the results of numerically modelled linear and rotating arm experiments utilising the BSL-RSM turbulence model, finding it outperformed previous turbulence models. Kim, Leong, Ranmuthugala & Forrest (2015) reported on the results of physical and numerical HPMM motion utilising the SUBOFF model and found good correlation. Gourlay & Dawson (2015) reported on the use of a Havelock source panel method, finding substantial agreement with experimental results.

2.7 Significance of this Thesis

The development of generalised submarine coefficient based manoeuvring models has been ongoing since the 1950's, and the model for deeply submerged motion was substantially settled by the end of the 1960's, with work thereafter serving to refine that model rather than replace it.

Theoretical description of the additional drag imposed upon a submarine in operation near the free surface was first put forward around 1913, and by the late

1930's had been validated against physical model testing. Detailed study of the non-axial forces took place much later, and much of this has focussed upon the additional buoyancy due to passing ocean waves which is the dominant additional force in this space. Measurement of the self-generated vertical plane forces utilising physical models and estimation via numerical methods has increased over the last decade, to the point where this work, analysing which coefficients are necessary, which are helpful, and which may be neglected, is now possible. While measurement of bulk manoeuvring forces and moments has been conducted, there is little work incorporating those measurements into the manoeuvring model for submarines, nor examination of the effect of those additional forces on any but the primary coefficients.

This work seeks to model the forces and moments in the vertical plane resulting from flow velocity normal to the motion of a submarine while near the free surface, and from those results, determine which of the relevant coefficients of motion which are non-negligibly affected. By doing so, allowance can then be made in manoeuvring models of submarine-like bodies for near surface operations.

3. MODELLING SUBMARINE BEHAVIOUR NEAR THE FREE SURFACE

This chapter discusses the theory underlying the modelling of submarine behaviour near the free surface, focusing on the mathematics and thought behind modern coefficient-based modelling. Working from that basis a methodology is proposed for modelling operations near the free surface. This proposed model is assessed and analysed over the remaining chapters of this thesis.

3.1 The Coefficient Based Manoeuvring Model

There are a number of approaches to understanding and deriving the behaviour of a complex system such as a submarine. The coefficient-based model considered here proceeds by treating the system as a whole, with a large but limited number of independent variables that sufficiently describe the state of the submarine at any one moment. The assumption is made here that the changes in state of the submarine from this known moment to the next (as yet undetermined) moment are a function of the current state, and moreover, of the current state of the descriptive independent variables. This assumption explicitly excludes history effects from consideration.

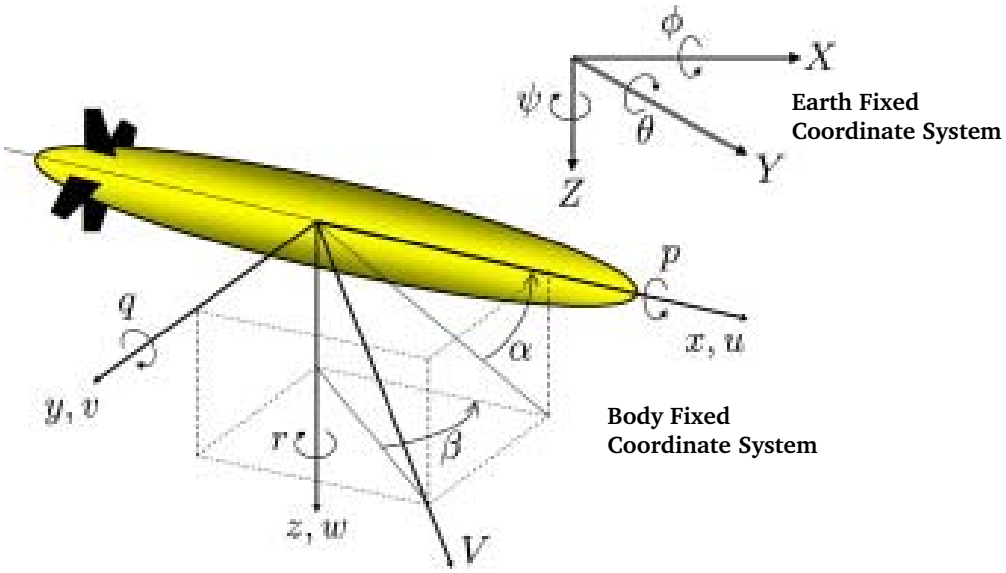

Figure 3-1 Linear and Rotational Axis System

To describe the state of a submarine requires knowledge of a significant number of variables. Firstly, its body fixed velocity vector $\boldsymbol{\nu} = [u\ v\ w\ p\ q\ r]^T$ — both linear and angular components — (see Figure 3-1). These values are to be taken about a known, body-fixed origin. For the SUBOFF model referenced throughout this document, the origin is located as per the original DTRC model; on the axial centreline, at the centre of rotation (Roddy, 1990). Secondly, its earth fixed position $\boldsymbol{\eta} = [x\ y\ z\ \phi\ \theta\ \psi]^T$, which allows the derivation of a vector $\boldsymbol{g}(\boldsymbol{\eta})$ for the (inherently earth fixed) gravitational components of weight and buoyancy. Thirdly, the control vector of forces and moments acting upon it (propulsion, dive & rudder planes) $\boldsymbol{\tau} = \left[\tau_x\ \tau_y\ \tau_z\ \tau_\phi\ \tau_\theta\ \tau_\psi\right]^T$. Fourthly, the physical characteristics of the vessel in terms of its

inertial matrix $\boldsymbol{M}$, including the effect of any acceleration upon the surrounding fluid. From this inertial matrix, a matrix $\boldsymbol{C}$ of the resulting coriolis and centripetal forces can be calculated directly. Finally, the damping response of the fluid must be accounted for, which is done via a damping matrix $\boldsymbol{D}$. In the vector form utilised by Fossen (1994), the resultant equations of motion can be written:

$$\boldsymbol{M\dot{\nu}} = \boldsymbol{\tau} - \boldsymbol{g(\eta)} - \boldsymbol{C(\nu)\nu} - \boldsymbol{D(\nu)\nu} \tag{3.1}$$

In this thesis, motion and forces are limited to the vertical plane. Given the form above and this limitation, much of the system of equations can be simplified. The body fixed velocity vector becomes $\boldsymbol{\nu} = [\boldsymbol{u}\ \boldsymbol{w}\ \boldsymbol{q}]^T$, the earth fixed position vector $\boldsymbol{\eta} = [x\ z\ \theta]^T$. The gravity vector, reduced to three dimensions and transformed into the body-fixed frame of reference (by a rotation θ) becomes:

$$\boldsymbol{g'(\eta)} = \begin{bmatrix} (W-B)sin\theta \\ -(W-B)cos\theta \\ (x_G W - x_B B)cos\theta + (z_G W - z_B B)sin\theta \end{bmatrix} \tag{3.2}$$

The inertial matrix $\boldsymbol{M}$, including both the rigid body and non-negligible added mass terms:

$$\boldsymbol{M} = \begin{bmatrix} m - X_{\dot{u}} & 0 & mZ_G \\ 0 & m - Z_{\dot{w}} & Z_{\dot{q}} - mX_G \\ mZ_G & M_{\dot{w}} - mX_G & I_y - M_{\dot{q}} \end{bmatrix} \tag{3.3}$$

Note: values for the added mass terms $X_{\dot{u}}, Z_{\dot{w}}, Z_{\dot{q}}, M_{\dot{w}}, M_{\dot{q}}$ can be determined by or derived through linear or cyclic acceleration tests.

The corresponding Coriolis matrix $\boldsymbol{C}$, derived directly from the mass matrix $\boldsymbol{M}$ as per the methodology in Fossen (1994):

$$\boldsymbol{C} = \begin{bmatrix} 0 & 0 & Z_{\dot{w}}\boldsymbol{w} + m\boldsymbol{w} + m\boldsymbol{q}x_G \\ 0 & 0 & -X_{\dot{u}}\boldsymbol{u} - m\boldsymbol{u} - m\boldsymbol{q}z_G \\ -Z_{\dot{w}}\boldsymbol{w} - m\boldsymbol{w} + m\boldsymbol{q}x_G & X_{\dot{u}}\boldsymbol{u} + m\boldsymbol{u} - m\boldsymbol{q}z_G & 0 \end{bmatrix} \tag{3.4}$$

The control vector $\boldsymbol{\tau} = [\tau_x\ \tau_z\ \tau_\theta]^T$ typically contains expressions of the forces actively exerted on the vessel, primarily those derived from propulsion and the action of the various dive planes and rudders. For example, the expression in Feldman's (1979) general equations of motion reduces under these conditions to:

$$\boldsymbol{\tau} = \frac{\rho}{2}L^2 \begin{bmatrix} X'_{\delta r\delta r}\boldsymbol{u^2}{\delta_r}^2 + X'_{\delta s\delta s}\boldsymbol{u}^2{\delta_s}^2 + X'_{\delta b\delta b}\boldsymbol{u}^2{\delta_b}^2 + a_i\boldsymbol{u}^2 + b_i C\boldsymbol{u}u_c + c_i C^2\boldsymbol{u}_c^2 \\ Z'_{\delta s}\boldsymbol{u}^2\delta_s + Z'_{\delta b}\boldsymbol{u}^2\delta_b + Z'_{\delta s\eta}\boldsymbol{u}^2\delta_s\left(\eta - \frac{1}{C}\right)C \\ L\left[M'_{\delta s}\boldsymbol{u}^2\delta_s + M'_{\delta b}\boldsymbol{u}^2\delta_b + M'_{\delta s\eta}\boldsymbol{u}^2\delta_s\left(\eta - \frac{1}{C}\right)C\right] \end{bmatrix} \tag{3.5}$$

Evident in these equations are terms expressing the position of the bow planes, stern planes and rudder planes (left in for illustration), as well as terms that capture the effect of the propulsion system given the command speed u_c (methods for calculation

of a_i , b_i , c_i , C, η are given in Feldman, 1979). These terms assume a specific control surface arrangement and would have to be altered to capture an alternate form: see Healey & Lienhard (1993) for an alternate expression featuring rudders fore and aft, as well as utilising propeller rate rather than command speed.

The hydrodynamic damping matrix consists of nine terms which approximately express the non-linear nature of the damping forces imposed upon a submarine in the course of its motion. In this approximation process — seeking a sufficiently accurate yet simple representation of the forces modelled — a degree of art is expressed, leading to a number of alternate models being found in the literature and in practical use.

Assuming briefly a linear response, the results for the damping matrix are obtained by setting the velocity vector to $\boldsymbol{\nu} = [u_0\ 0\ 0]^T$, and then perturbing the components of that vector by some small amount independently. Under these conditions, the following damping matrix is obtained:

$$\boldsymbol{D}(\boldsymbol{\nu})\boldsymbol{\nu} = \begin{bmatrix} \frac{\partial X}{\partial \boldsymbol{u}} & \frac{\partial X}{\partial \boldsymbol{w}} & \frac{\partial X}{\partial \boldsymbol{q}} \\ \frac{\partial Z}{\partial \boldsymbol{u}} & \frac{\partial Z}{\partial \boldsymbol{w}} & \frac{\partial Z}{\partial \boldsymbol{q}} \\ \frac{\partial M}{\partial \boldsymbol{u}} & \frac{\partial M}{\partial \boldsymbol{w}} & \frac{\partial M}{\partial \boldsymbol{q}} \end{bmatrix} \begin{bmatrix} \boldsymbol{u} \\ \boldsymbol{w} \\ \boldsymbol{q} \end{bmatrix} \tag{3.6}$$

This simple model works well in the condition where the velocity vector is approximately $[u_0\ 0\ 0]^T$. However, in practice, it is desirable to be able model the response over a larger range than is covered sufficiently accurately by the simplification made in assuming a linear response. In order to achieve this, rather than assess a single perturbation in each direction, each component is assessed across a range of values and a function fitted to those results. These response curves will be expressed as per Sen (2000) e.g. $X_u^\star$ is the variation in the axial force X with variation in axial velocity. Using this notation, $\boldsymbol{D}(\boldsymbol{\nu})\boldsymbol{\nu}$ is more fully expressed as:

$$\boldsymbol{D}(\boldsymbol{\nu})\boldsymbol{\nu} = \begin{bmatrix} X_u^\star & X_w^\star & X_q^\star \\ Z_u^\star & Z_w^\star & Z_q^\star \\ M_u^\star & M_w^\star & M_q^\star \end{bmatrix} \begin{bmatrix} \boldsymbol{u} \\ \boldsymbol{w} \\ \boldsymbol{q} \end{bmatrix} \tag{3.7}$$

As mentioned in Chapter 2, Roddy (1990) summarises the experimental outcomes of a number of tests conducted on the SUBOFF model. In Figure 11 (reproduced below as Figure 3-2), the response obtained in the non dimensionalised axial force component X' is plotted as a function of angle of attack θ (uncertainty quoted as 5% for static derivatives).

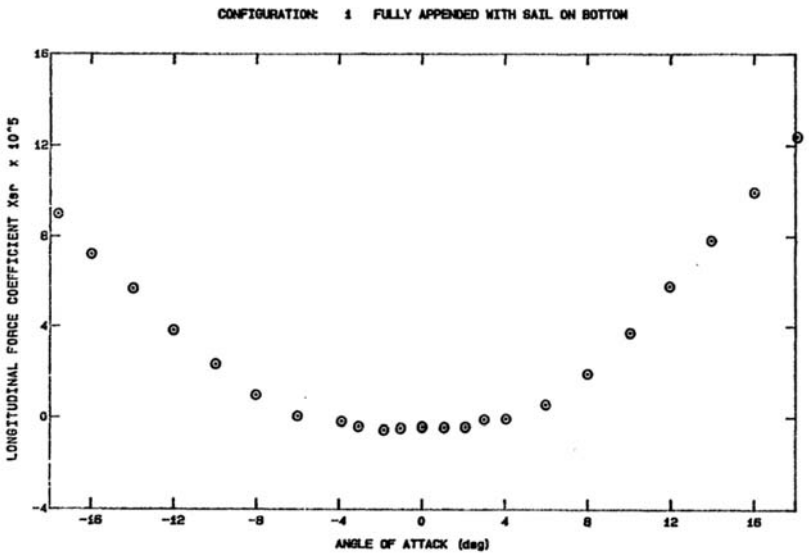

Figure 3-2 X' as a function of θ, Fig. 11 Roddy (1990)

This presents an approximately parabolic response for X as a function of w, (noting $w = U_0 \sin\theta$, which is close enough to linear in this range not to substantively change the curve). Thus, for instance in Feldman's (1979) equations for axial force, an expression is found approximating the response curve $X_w^\star$ (axial force X across a range of normal velocity w), as $X_{ww}\boldsymbol{w}^2$, capturing this basic form with a single coefficient.

Not all response curves can be captured well using a single coefficient. Figure 3-3 below, reproducing Figure 13 from Roddy (1990), shows the response of M' to changes in θ.

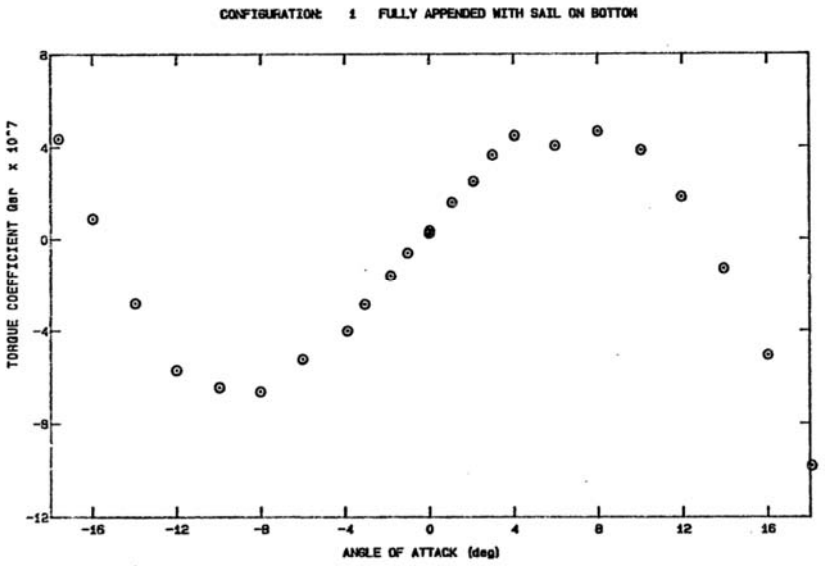

Figure 3-3 M' as a function of θ, Fig. 13 Roddy (1990)

While this appears approximately cubic in form, Feldman chose to capture $M_w^\star$, the response curve of pitch moment M across a range of velocity $\boldsymbol{w}$, using terms which reduce to $M_w\boldsymbol{uw} + M_{|w|}\boldsymbol{u}|\boldsymbol{w}| + M_{w|w|}\boldsymbol{w}|\boldsymbol{w}| + M_{ww}\boldsymbol{w}^2$ when considering the vertical

plane only. Doing this allowed the capture of the variation in pitch moment with direction of rotation that occurs due to the asymmetry of the body (primarily due to the presence of the sail). The selection of this more complex expression is an example of mapping what in some cases are complex and noisy experimental results into a relatively simple yet sufficiently representative mathematical form. Feldman's terms for the hydrodynamic response are:

$$\boldsymbol{D}(\boldsymbol{v})\boldsymbol{v} = \begin{bmatrix} X_{\star}\boldsymbol{u} & X_{ww}\boldsymbol{w} & X_{qq}\boldsymbol{q} \\ Z_{\star}\boldsymbol{u} & Z_{w}\boldsymbol{u} + Z_{|w|}\boldsymbol{u}\frac{|\boldsymbol{w}|}{\boldsymbol{w}} + Z_{ww}\boldsymbol{w} & Z_{qq}\boldsymbol{q} + Z_{wq}\boldsymbol{w} \\ M_{\star}\boldsymbol{u} & M_{w}\boldsymbol{u} + M_{|w|}\boldsymbol{u}\frac{|\boldsymbol{w}|}{\boldsymbol{w}} + M_{ww}\boldsymbol{w} + M_{w|w|}|\boldsymbol{w}| & M_{qq}\boldsymbol{q} + M_{q}\boldsymbol{u} \end{bmatrix} \begin{bmatrix} \boldsymbol{u} \\ \boldsymbol{w} \\ \boldsymbol{q} \end{bmatrix} \quad (3.8)$$

An alternate approach to evaluating these terms is as utilised in Jensen et al (1993) whereby a lookup table is created for each response curve. The lookup table has the advantage of more closely approximating the measured response, but at the cost of additional computation. Lookup tables can also be utilised in more than a single dimension to reduce approximation error where significant cross coupling between terms exists.

3.2 Sensitivity of Coefficients in typical manoeuvres

In order to judge whether the effects of a change in response due to the action of the free surface is:

a) sufficient to warrant the addition of a new term or modification of an existing term; and

b) sufficiently accurate in its modelling thereof;

some quantifiable measure must be determined.

Sen (2000) reports on the sensitivity of a general submarine model to the various coefficients utilised therein. His paper sets out a methodology for the assessment of sensitivity in terms of the relative change in the modelled submarine path resulting from variation in each coefficient from its reference value. The sensitivities noted are derived from vessel response during overshoot and turning circle manoeuvres — typical trial manoeuvres. While alternative manoeuvres, reference coefficients, and systems of equations would inherently derive different results, the results obtained provide a basis for assessment of which coefficients are the most sensitive and thus the highest priority to assess for variation. The system of equations modelled in Sen are based loosely on Feldman's equations and are thus largely similar to those utilised within this thesis.

The following vertical plane coefficients (Table 3-1) and their calculated maximum sensitivity are transcribed from Table 4 (Sen, 2000). These sensitivities will be utilised as described in Section 3.5.1 to derive a significance measure that will be applied to each of the coefficients derived from the simulations conducted in

Chapters 4 and 6 in order to judge under what conditions it is necessary that each coefficient should be treated as variable in the near surface regime.

Table 3-1 Sensitivities of various coefficients (Table 4, Sen 2000)

M_q	4.914	$M_{\delta s}$	3.154	$Z_{\delta s}$	2.305
Z_q	2.025	$Z_{\dot{w}}$	1.597	Z_w	1.290
$Z_\star$	1.203	$Z_{\|w\|}$	1.046	$Z_{\dot{q}}$	0.988
M_w	0.979	M_{ww}	0.959	$M_{\delta s\eta}$	0.959
X_{wq}	0.953	$M_{\|w\|}$	0.944	$M_{w\|w\|R}$	0.933
$M_\star$	0.889	$M_{\dot{q}}$	0.885	$X_{\dot{u}}$	0.319
X_{ww}	0.300				

Note: Details on the derivation of these values can be found in Sen (2000).

The vertical plane coefficients can be grouped roughly into four categories:

a) Pitch coefficients (M_q, $M_{\delta s}$);

b) Normal-force coefficients ($Z_{\delta s}$, Z_q, $Z_{\dot{w}}$, Z_w, $Z_\star$);

c) Shaping coefficients ($Z_{|w|}$, M_w, $Z_{\dot{q}}$, M_{ww}, $M_{\delta s\eta}$, $M_{|w|}$, $M_{w|w|R}$, $M_\star$, $M_{\dot{q}}$);

d) Axial-force coefficients (X_{wq}, $X_{\dot{u}}$, X_{ww})

Notably, no figure for the sensitivity of the equations to $X'_\star$ (X_{uu} in Sen, 2000) is provided. However, Perrault, Bose, O'Young & Williams (2003) suggests a maximum sensitivity of 0.387 in a similar series of tests, which will be utilised in this thesis. For comparison, they report a maximum sensitivity to Z'_w ($C_{L,hull}$ in Perrault et al, 2003) of 1.106, which is somewhat smaller than that reported in Sen (2000).

Some clear observations can be drawn. Variance of path due to coefficients of pitch is more significant than with heave, and linear coefficients (and control coefficients) are more sensitive than higher order terms. Still, other than the coefficients in X (which as noted, were not stressed in these tests as much as say a crash stop under jammed controls) the sensitivity of all coefficients tested were within a factor of 4 of each other.

3.3 Consideration of the Effects of Proximity to the Free Surface

Let us assume that near the free surface the existing damping matrix calculation for submarine motion is modified by the consideration of position as well as velocity:

$$\boldsymbol{M\dot{\nu}} = \boldsymbol{\tau} - \boldsymbol{g(\eta)} - \boldsymbol{C(\nu)\nu} - \boldsymbol{D(\eta,\nu)\nu} \qquad (3.9)$$

Where $\boldsymbol{D(\eta,\nu)\nu}$ is a function of both position $\boldsymbol{\eta}$ and velocity $\boldsymbol{\nu}$ that represents the hydrodynamic effects inclusive of the interactive effects of the free surface upon the submarine.

In order to develop terms that capture $\boldsymbol{D}$ as a function of $\boldsymbol{\eta}$ and $\boldsymbol{\nu}$, it is worth considering the extant literature on the observed effects of operating near the free

surface. There are two primary thrusts of the literature that will be referenced here: experimental results and theoretical development.

As noted in Chapter 2, the early experimental results of Weinblum et al (1936) reflected what had already been predicted by the theoretical considerations of Lamb and Havelock on the resistance of a submerged ellipsoid approximately 10 years earlier. Figures 3-4 and 3-5 (Weinblum et al, 1936) show residual resistance plotted against Froude Number for two different hull forms, at different submergences.

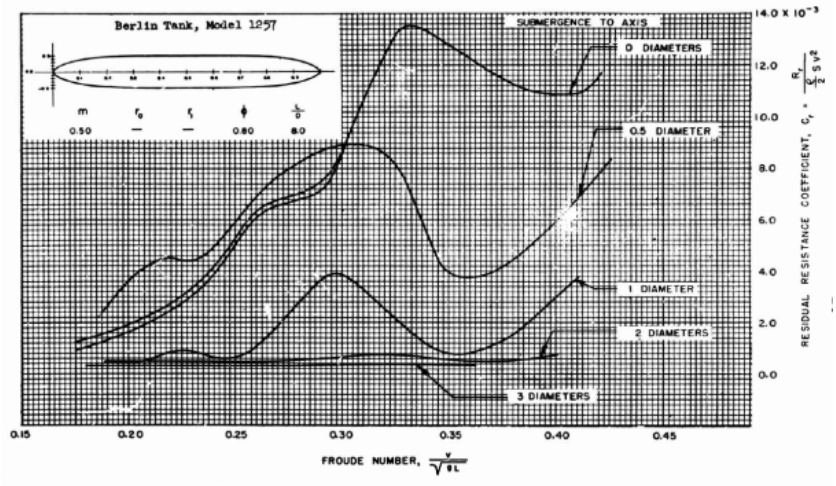

Figure 3-4 Resistance as a function of Froude Length Number, Model 1257, Weinblum et al (1936)

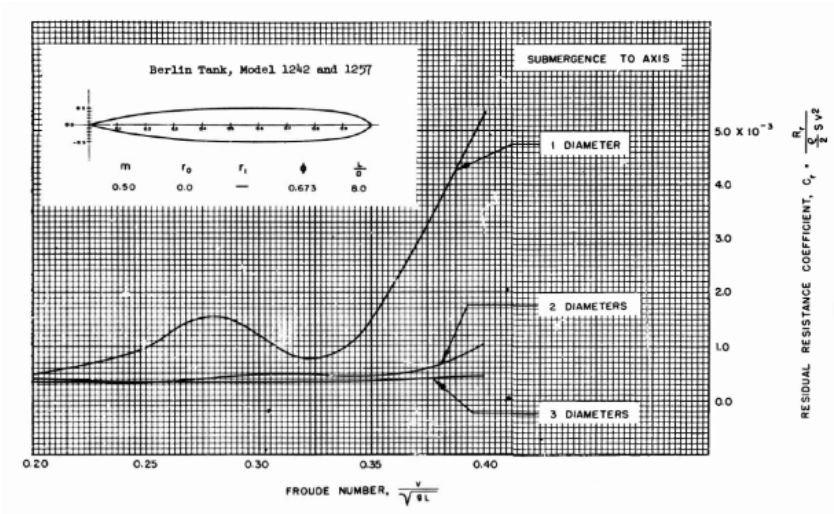

Figure 3-5 Resistance as a function of Froude Length Number, Model 1242, Weinblum et al (1936)

Weinblum investigated a wider range of forms (many of these more 'submarine-like') than the ellipsoids able to be considered using the potential flow theory of the day. Figures 3-4 and 3-5 show both the form-dependent changes in resistance with Froude number, as well as the dramatic effect that even small changes in submergence make as a submarine approaches and breaches the surface. It is evident from these that form plays a substantial part in wavemaking in submarines (as it does in surface vessels) and that the function of the additional resistance is not a simple polynomial.

Similarly, from the results of work conducted by Crook (1994) — see Figure 3-6, showing lift coefficients plotted against Froude Number — and Neulist (2011) — see Figure 3-7, showing pitch moment plotted against Froude Number and submergence — it is evident that the functions for heave and pitch are likewise neither simple nor simply periodic in nature.

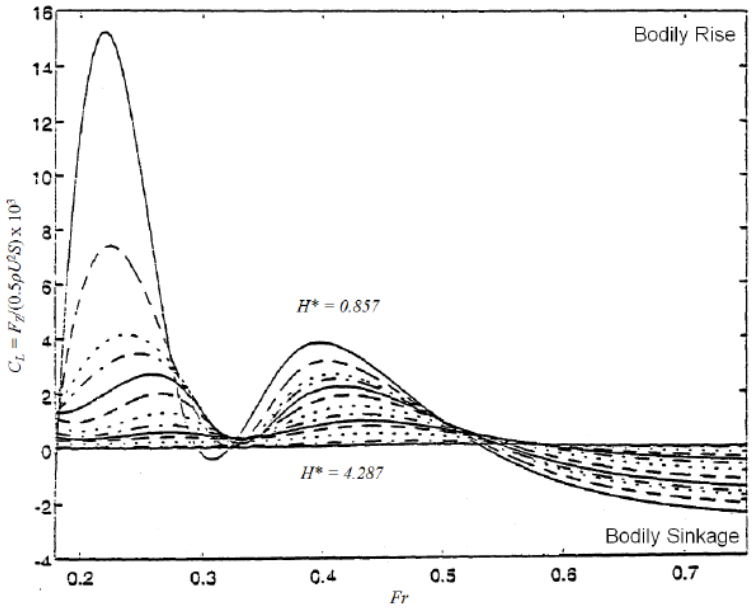

Figure 3-6 Lift Coefficient as a function of Froude Number and Submergence (Crook, 1994)

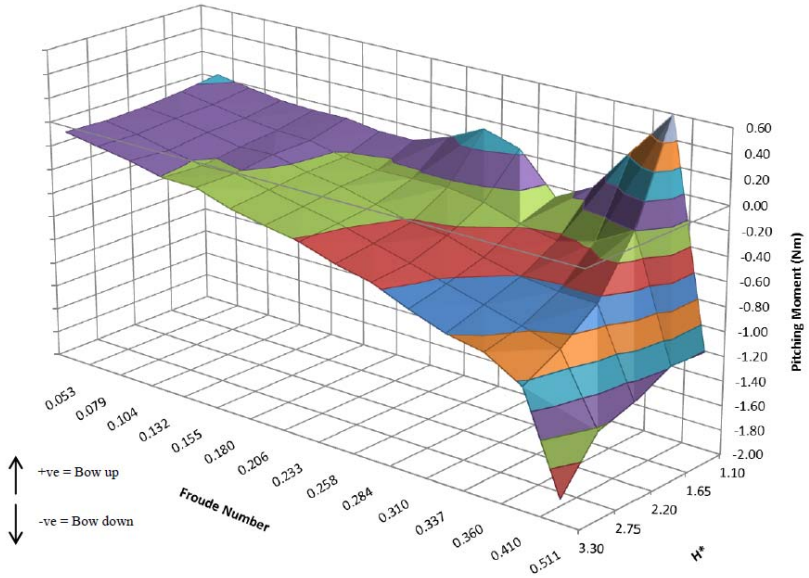

Figure 3-7 Pitch Coefficient as a function of Froude Number and Submergence (Neulist, 2011)

Inspection of the results in these papers led to some simple observations relevant to the problem at hand.

- The form of these curves is not obviously periodic;

- The surface effect fades quite quickly with submergence and is negligible at depth;
- Change in submergence result in slight changes in the speed at which peaks and troughs occur.

The near surface effect on the submarine is composed of two components: change in pressure, and change in skin friction. In all cases tested as a part of this thesis, change in skin friction is less than 4% of the total variation, in most cases less than 1%. In assessing suitable mathematical functions for the change in pressure it is worth considering the results of potential theory.

Havelock (1928) formulated the function of the free surface under potential flow conditions over a doublet of strength M submerged at a depth f in a uniform flow of velocity c.

$$\zeta(r,\theta) = \frac{2Mf}{c(r^2+f^2)^{3/2}} + \frac{2\kappa_0 M}{c}\int_{-\frac{1}{2}\pi}^{\frac{1}{2}\pi} sec^2\,\theta d\theta \int_0^{\infty} \frac{\kappa_0\, sec^2\,\theta\, cos\, mf + m\, sin\, mf}{m^2+\kappa_0^2\, sec^4\,\theta} e^{-mr|cos(\theta'-\theta)|} m dm + \frac{4\kappa_0^2 M}{c}\int_{-\frac{1}{2}\pi}^{\theta'-\frac{1}{2}\pi} sec^4\,\theta\, e^{-\kappa_0 f sec^2\theta}\, sin\,\kappa_0 r\, cos(\theta-\theta')\, sec^2\,\theta\, d\theta \qquad (3.10)$$

Where $\kappa_0 = g/c^2$ and m is a dummy variable for integration.

Lazauskas (2005) utilised a simplified version of the above derived by Tuck (1971) where:

$$\zeta(x,y) = \Re \int_{-\pi/2}^{\pi/2} A(\theta) e^{-ik(\theta)\omega(x,y,\theta)} d\theta \qquad (3.11)$$

with $A(\theta) = k_0 \sec^2\theta$, $\omega(x,y,\theta) = x\, cos\,\theta + y \sin\theta$ and $A(\theta)$ as the complex amplitude function derived by any of the various means noted in their paper. The function was found to develop rapid oscillations as $|\theta| \to {}^{\pi}/_{2}$, leading regular quadratures such as Simpson's to result in significant error. Both Tuck and Lazauskas utilised Filon's (1926) quadrature to evaluate the double integral above numerically.

Significantly for this work, Havelock's equation nor the later simplification do not lead to an expression for the flow over the submarine nor for the form of the free surface that is simple enough to utilise as a basis for expressing the effects of the free surface on a generalised submarine within a coefficient based manoeuvring model. Thus, either an approximate form will need to be developed for modelling these effects, or a 'look up' table or segmented equation will be required.

The first term in equation 3.10 above is simple and consideration will be given to treating this component of the waveform independently. Furthermore, equation 3.11 suggests that any effect due to the free surface will reduce exponentially with submergence. This corresponds with wave theory for deep water, where the velocity field also reduces exponentially with depth.

3.3.1 Notation Selected for Free Surface Manoeuvring Coefficients

Given the general structure of the equations of motion near the free surface noted in Equation 3-9, $\boldsymbol{D}(\boldsymbol{\eta},\boldsymbol{\nu})\boldsymbol{\nu}$ represents the matrix of the damping forces inclusive of the proximity, orientation and motion relative to the free surface. It is anticipated that the variation of pressure due to the generated waves during operations in the near surface will vary with submergence, velocity and attitude.

In describing the variation of an individual coefficient in the near surface region, Renilson (2015) utilises the notation $Z'_{\star}(H^{\star},Fr)\boldsymbol{u}^2$, denoting the previously constant manoeuvring coefficient $Z'_{\star}$ as now a function of the pertinent components of $\boldsymbol{\eta}$ when in the near surface region. This *coefficient function* can be computed either through the use of a multi-dimensional look up table, though some explicit function of $\boldsymbol{\eta}$, or some combination thereof.

Using this notation $\boldsymbol{D}(\boldsymbol{\eta},\boldsymbol{\nu})\boldsymbol{\nu}$ can be written:

$$\boldsymbol{D}(\boldsymbol{\eta},\boldsymbol{\nu})\boldsymbol{\nu} = \begin{bmatrix} X^{\star}_{u}(\boldsymbol{\eta}) & X^{\star}_{w}(\boldsymbol{\eta}) & X^{\star}_{q}(\boldsymbol{\eta}) \\ Z^{\star}_{u}(\boldsymbol{\eta}) & Z^{\star}_{w}(\boldsymbol{\eta}) & Z^{\star}_{q}(\boldsymbol{\eta}) \\ M^{\star}_{u}(\boldsymbol{\eta}) & M^{\star}_{w}(\boldsymbol{\eta}) & M^{\star}_{q}(\boldsymbol{\eta}) \end{bmatrix} \begin{bmatrix} \boldsymbol{u} \\ \boldsymbol{w} \\ \boldsymbol{q} \end{bmatrix} \tag{3.12}$$

3.4 Adoption of a General Form

Starting from the Feldman equations of motion (See Appendix C), the following equations have been adopted as standard equations of form for three degrees of freedom in the vertical plane. Each Feldman equation has been reduced to the three degrees of freedom within the vertical plane; i.e. $\boldsymbol{p} = \boldsymbol{r} = \boldsymbol{v} = 0$. In addition, the expressions for combined heave/pitch found in Gertler & Hagen (1967) are adopted rather than the integral forms utilised in the later Feldman model as these moved away from the coefficient-based nature of the model and have not been widely adopted. Control surface forces are neglected; i.e.$\delta_s = \delta_b = \delta_r = 0$. All terms are herein expressed in their non-dimensional forms for consistency with current conventions.

Given constant self-propulsion speed, (i.e. $u_c = \boldsymbol{u}, \eta = \boldsymbol{1}$) the propulsion function F_{xp} is reduced to:

$$F_{xp} = X'_{\star}\boldsymbol{u}'^2 \tag{3.13}$$

AXIAL FORCE EQUATION

$$(\boldsymbol{m}' - X'_{\dot{u}})\dot{\boldsymbol{u}}' + \boldsymbol{m}' Z'_G \dot{\boldsymbol{q}}' = \tag{3.14}$$

$$X'_{\star}\,\boldsymbol{u}'^2 + X'_{wq}\boldsymbol{w}'\boldsymbol{q}' - \boldsymbol{m}'\boldsymbol{w}'\boldsymbol{q}' - \boldsymbol{m}' x'_G \boldsymbol{q}'^2 + X'_{ww}\boldsymbol{w}'^2 + X'_{qq}\boldsymbol{q}'^2$$

$$+(W' - B')\ sin\theta$$

NORMAL FORCE EQUATION

$$(\boldsymbol{m}' - Z'_{\dot{w}})\dot{\boldsymbol{w}}' - \left(\boldsymbol{m} X_G + Z'_{\dot{q}}\right)\dot{\boldsymbol{q}}' = \tag{3.15}$$

$$Z'_{\star}\boldsymbol{u}'^2 + Z'_{w}\boldsymbol{u}'\boldsymbol{w}' + Z'_{|w|}\boldsymbol{u}'|\boldsymbol{w}'| + Z'_{ww}\boldsymbol{w}'^2 + Z'_{w|w|}\boldsymbol{w}'|\boldsymbol{w}'|$$

$$+Z'_q\boldsymbol{u}'\boldsymbol{q}' + Z'_{w|q|}\boldsymbol{w}'|\boldsymbol{q}'| + \boldsymbol{m}'\boldsymbol{q}'(\boldsymbol{u}' - \boldsymbol{q}' z'_G) + (W - B)cos\theta$$

PITCH MOMENT EQUATION

$$\boldsymbol{m}' z'_G \dot{\boldsymbol{u}}' - (\boldsymbol{m}' x'_G + M'_{\dot{w}})\dot{\boldsymbol{w}}' - (M'_{\dot{q}} + I'_y)\dot{\boldsymbol{q}}' = \tag{3.16}$$

$$M'_{\star}\boldsymbol{u}'^2 + M'_w\boldsymbol{u}'\boldsymbol{w}'\ M'_{|w|}\boldsymbol{u}'|\boldsymbol{w}'| + M'_{w|w|}\boldsymbol{w}'|\boldsymbol{w}'| + M'_{ww}\boldsymbol{w}'^2$$

$$+M'_q\boldsymbol{u}'\boldsymbol{q}' + M'_{|w|q}|\boldsymbol{w}'|\boldsymbol{q}' - \boldsymbol{m}'(\boldsymbol{u}' x'_G + \boldsymbol{w}' z'_G)\boldsymbol{q}'$$

$$+(x'_G W' - x'_B B')cos\theta - (z'_G W' - z'_B B')sin\theta$$

These equations will be used from here on as the general equations of vertical plane motion for a submarine in deep water.

3.5 Compiling a Complete Model of the Near Surface Static Response

The compilation of a first model of the near surface response of a submarine requires the derivation of response curves in three axes (axial, normal, pitch). From the sensitivity study by Sen (2000) it is known that any changes that affect the forces imposed by the control vector are significant. Changes to the added mass coefficients in the near surface must also be considered.

3.5.1 Matrix for Assessment of Coefficient Consequence

In order to be able to address the significance of any change in response due to the presence of the near surface, a metric of consequence is utilised. As noted in Section 3.2, the performance of the model is sensitive to each coefficient to distinctly different degrees. Furthermore, as could be anticipated, the relative variance of each coefficient under the influence of the near surface is markedly different from coefficient to coefficient. As such, for the assessment of each coefficient i, a Consequence (C_i) will be determined as the product of the sensitivity (S_i) of the model to that coefficient and the scale of change in that consequence noted as a result of the studies conducted in Chapters 4 and 6.

Consequence will thus be a guide to the value to be obtained from consideration of the near surface variability of each coefficient in a manoeuvring model. It should be

noted that consequence is equivalent to the sensitivity of the manoeuvring model to variation of the near surface component. As such, values for consequence can reasonably be compared with values obtained for sensitivity.

A consequence of 0.5 or greater will be referred to as of primary significance; it is similar in effect to the M and Z coefficients listed in Table 3-1. A consequence of between 0.1 and 0.5 is referred to as minor significance and is similar in scale of effect to the X coefficients listed in Table 3-1. Any significance less than 0.1 is referred to as minimal significance. A special category called "conditional significance" is also included where the near surface aspect of the coefficient is of minimal significance in the band of submarine operational Froude Length Number (i.e $< 0.250\ Fr_L$), but increases in significance at greater Froude Length Number.

Table 3-2 Coefficient Significance Bands

Coeffieicnt Significance (C_i) **Sensetivity × Relative Response**	
$C_i > 0.5$	Primary Significance
$0.1 > C_i > 0.5$	Minor Significance
$C_i < 0.1$	Minimal Significance
$C_i > 0.1$ only where $Fr_L > 0.250$	Conditional Significance

3.6 Summary

In this chapter, the mechanism by which coefficient based manoeuvring models provide a mathematical basis for characterising a submarine has been outlined. Information about the current state of the submarine is used to sufficiently accurately predict the future path of the submarine through the characterisation of the vessel in a series of coefficients that scale the modelled response of the submarine to the various components of the current state. The model can then be arranged in a rapidly solvable matrix form to obtain linear and rotational acceleration.

It was discussed how the choices of which coefficients to model are driven by the sensitivity of the model to each coefficient and the range of values over which those coefficients commonly vary. Standard models have been identified in which the coefficients that typically matter have been included; the practice of making variations to these to take account of the nature of a specific submarine has also been noted. The Feldman (1979) model has been reduced to a basis suitable for use in assessing the vertical plane components. Finally, a method has been set out by which an assessment is made in Chapters 4 and 6 regarding which coefficients need to be included and/or varied to allow the model to account for the changes that occur when a submarine is operating in near the free surface.

4. MODELLING AT CONSTANT SPEED AND TRIM NEAR THE FREE SURFACE

4.1 Objectives

The objective of this study is to identify and characterise the variance in response of a submarine in steady motion near the free surface of the water, in order to be able to express that variance within a manoeuvring model.

In order to achieve this, a representative submarine model (SUBOFF) is modelled at model scale using ANSYS CFX conducting steady state operations at various Froude Numbers, depths and attitudes to the free surface.

This model is verified to ensure it is accurately modelling the situation, and validated against data collected by DTRC (Roddy, 1990). The results are checked for self-consistency, converted into non-dimensional form and transformed to the body fixed reference frame in order to analyse the data and derive manoeuvring coefficients.

Utilising the results of the investigations presented in this chapter, the significance of the near surface to each of the:

- axial force coefficients $X_\star, X_w$ and X_{ww};
- the normal force coefficients $Z_\star, Z_w, Z_{|w|}, Z_{ww}$ and $Z_{w|w|}$;
- and the pitch moment coefficients $M_\star, M_w, M_{|w|}, M_{ww}$ and $M_{w|w|}$

is assessed in the context of the sensitivity of the overall manoeuvring model. These coefficients represent the vertical plane coefficients that can be readily determined under steady state motion.

4.2 Scope and Methodology

The term *near surface region* is herein used to describe the operational layer that exists between the depth where the submarine risks breaking the surface and the depth at which the effects of the surface become negligible. The point at which surface piercing occurs at rest in calm water varies with submarine design, primarily via the relative height of the sail — but typically a centreline submergence of about 1.1 diameters (D). However, with allowance for ocean waves, a useful bound of range is periscope/snorkelling depth, which is at a submergence of approximately $1.6D$ – $1.8D$ (Gertler, 1950). The effect of the surface drops exponentially with depth; at somewhere between $3.3D$ and $5.0D$ depending on form and speed, these forces become negligible.

Submarines in operation near the surface typically travel at relatively low speed — in the order of 4-6 knots. The wave train from a surfaced submarine, like any surface vessel, is detectable at a significant distance, and travelling at these low speeds aids in avoiding detection through wake detection. In addition, control of a submarine becomes increasingly difficult at higher speeds as there is less margin available for counteracting the pitching and heaving motions imparted by the ocean waves. Only in unusual circumstances would this be exceeded; an upper limit of 10-12 knots (Fr_L

0.250) for the design envelope is utilised to account for emergency actions (Dawson, 2014). Existing studies from Weinblum et al (1936) show that at a near surface operating depth, the effects of self-generated waves become minimal below a Froude Length Number of approximately 0.200. This leaves a reasonably tight window of study strictly relevant to a submarine's design envelope. However, in order to properly characterise the effects of the surface upon a submarine (or submarine-like body) and provide extensibility for future development, it is necessary to understand the nature of the reaction somewhat beyond that limit.

In terms of trim, at the upper end of the selected submergence envelope, changes in attitude reduce the minimum distance to the surface, such that at somewhere around 12-15° (depending on arrangement) the body will pierce the surface at bow or stern. In order to establish the effect of attitude on the pressure forces, given the form of the response in deep water, the region between ±6° is selected for investigation herein.

4.2.1 Approach

Two series of tests were conducted, utilising the SUBOFF geometry. The first, preliminary series concentrated on the way the near surface affects the submarine while in level trim. From this information, values for $X_\star, Z_\star$ and $M_\star$ as a function of Froude Length Number and submergence is determined. The second series extends this work to include the effect of vessel trim, allowing the assessment of the remaining coefficients as noted in Section 4.1. The extent of these two series of tests are summarised in Table 4-1 below.

Table 4-1 Test Case Envelope, Series 1 and 2

Series 1	
Froude Length Number	0.380 to 0.470 (9 speeds)
Submergence (Diameters)	1.8, 2.2, 2.5, 2.8
Series 2	
Froude Length Number	0.190 to 0.520 (17 speeds)
Submergence (Diameters)	1.6, 1.8, 2.0
Trim (degrees)	-6, -3, -2, -1, 0, 1, 2, 3, 6

Figure 4-1 depicts the spread of cases simulated in Series 2.

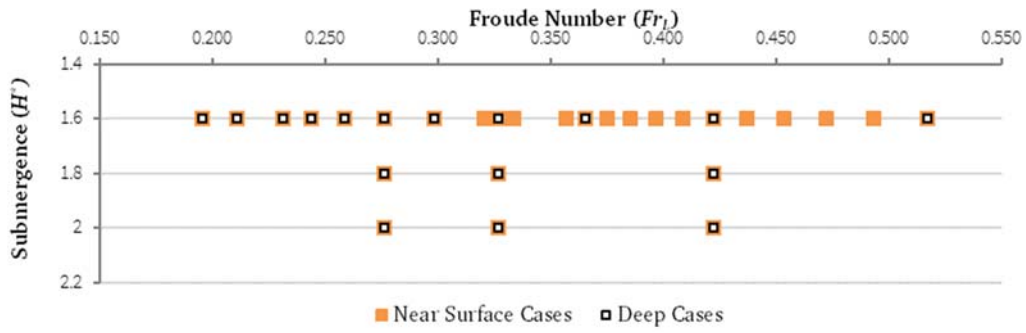

Figure 4-1 Series 2 Cases

In all of these tests the information being sought is primarily regarding the difference between the loads modelled in deep water and those modelled near the free surface. In each test, the arrangement is modelled twice; once with a free surface included at the nominated submergence (see Figure 4-2) and once without, albeit utilising the same mesh. This allows the deep case to be subtracted out in the analysis process, leaving the variation due to the free surface.

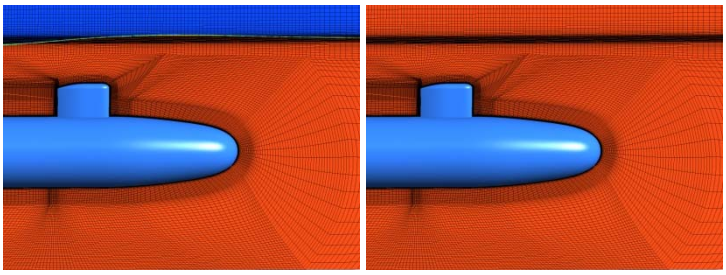

Figure 4-2 Identical mesh shown with water surface (left) and without (right) Water is shown here orange; air as dark blue.

The following subsections briefly set out the rationale for the arrangements utilised to undertake the modelling of the SUBOFF form across this range.

4.2.2 Surface modelling of SUBOFF Hull Geometry

The surface geometry for the bare hull utilised (see Figure 4-3) was produced inside ANSYS ICEM as a body of revolution, derived from a series of points generated from the SUBOFF equations found in Groves et al (1989). The sail utilised matches that found in Groves et al and was imported into ICEM as an IGES file from work carried out by Leong (2014). These forms were produced at model scale ($L_{OA} = 4.356m, D = 0.508m$) , matching those used at the DTMB. Neither the control surfaces nor the ring wing (require for comparison against other arrangements) were modelled. Two geometries were considered sufficient for validation purposes, and the sail was considered the appendage most likely to impose substantial variation in the surface response, given its scale and proximity to the surface. For consideration of the effect of operation in the near surface region on control surfaces, see Renilson, Polis, Ranmuthugala & Duffy (2014), included as Appendix B in this document.

Figure 4-3 SUBOFF Profile Calculated from Groves et al (1989)

This form was checked for accuracy and was found linearly accurate to within 0.02%. This was placed in a large rectilinear domain, shown in Figure 4-4 with a free surface for context. The domain extends for 2.5 body lengths (L) downstream, and 1.5L upstream, in order to reduce boundary effects (discussed in detail in Sections

4.2.7 and 4.2.8). The domain was modelled out to a distance of 2.0*L* from the centreplane, to avoid potential wave reflection from the side boundaries.

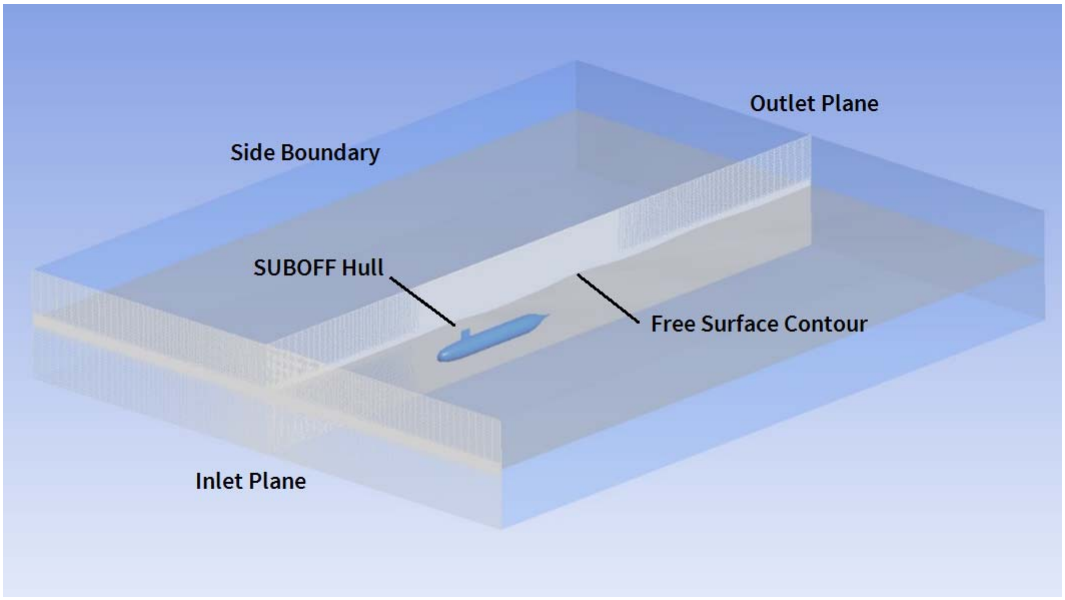

Figure 4-4 SUBOFF Model shown in Symmetric Domain

4.2.3 Mesh Arrangement

Hexahedral meshing is generated using a structured ICEM block model. Large rectilinear blocks are utilised to capture the free surface across the bulk of the mesh, however the blocking in way of the submarine itself is more complex in nature.

Primary characteristics of the block model near the hull (see Figure 4-5) include:

A. Initial O-grid block structure adjacent to the hull surface developed perpendicularly out to a shell in order to maintain near perpendicular meshing in the high aspect ratio region of the inflation layer.
B. A grid block structure wrapped around the O-grid layer in order to provide good capture of the vessel wake immediately downstream.
C. A double layered C-grid utilised to capture the form of the sail, with some manual editing to capture the sharp trailing edge of the sail.
D. Orthogonal blocking utilised throughout the near surface region in order to capture the free surface with as little mesh effect as possible.

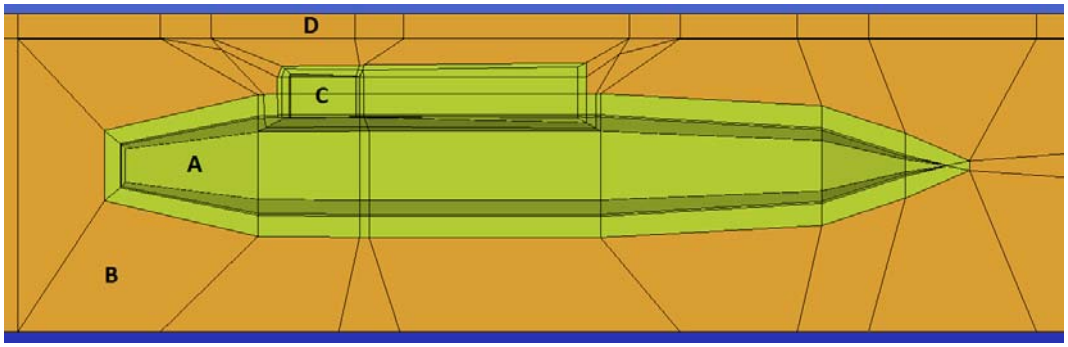

Figure 4-5 Near Hull Blocking Arrangement on Symmetry Plane

Figure 4-6 shows the resulting mesh. The meshing on the hull itself (A) is regular and consistent in order to minimise local pressure variations. A surface orthogonal mesh (B) is utilised to map the boundary layer. The more complex mesh region (C) serves to transition between the free surface and the rectilinear mesh (D) utilised to model the free surface and bulk fluids. This region is notable for its decreasing cell height approaching the water surface in order to smoothly transition to the relatively high aspect ratio cells required for accurate surface prediction, and constant cell pitch across the free surface over the submarine hull required to minimise any surface distortion from mesh effects.

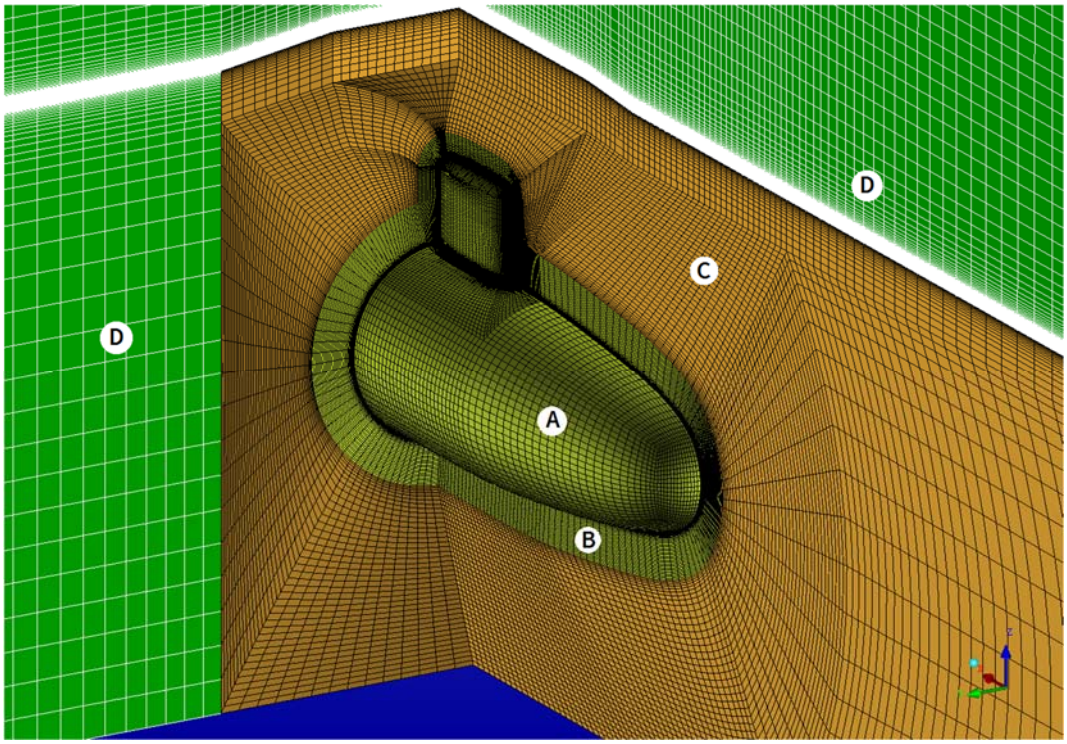

Figure 4-6 3D Sectional View of SUBOFF Meshing.

A) Outer Mesh B) Transitional Mesh C) Boundary Layer D) Hull Surface

4.2.4 Boundary Layer Modelling

In an open flow situation, such as the flow around a submarine, much of the small scale complexity takes place in the region immediately adjacent to the hull. At the very surface of the hull, the flow is 'attached' to the hull, moving along at the same velocity as the submarine. Over some small distance δ this velocity increases to the velocity of the local free stream velocity. Flow inside this boundary layer is viscous and may be laminar or turbulent in nature.

Near the hull surface, all flow can be considered, at a large enough time scale, to flow parallel to the surface. In a laminar flow situation, momentum is transferred normal to the hull by the action of shear due to the fluid viscosity. In a turbulent flow there is also momentum transfer through the bulk transfer effects of turbulent eddies in the flow. Turbulent boundary flow can be characterised by further subdivision into a viscous sub-layer in which the flow is almost laminar in which molecular viscosity

plays the dominant role in momentum transfer, and a logarithmic layer in which turbulence mixing dominates the transfer. Figure 4-7 below illustrates these subdivisions of the near-wall region.

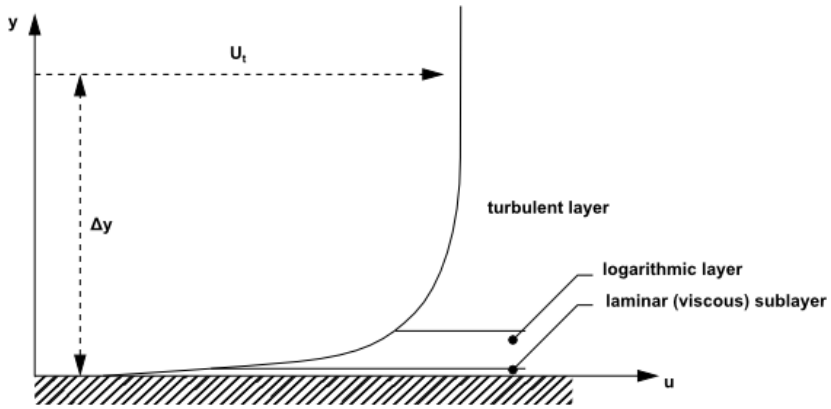

Figure 4-7 Subdivision of Turbulent Boundary Layer (ANSYS 2015)

For any full-scale submarine, laminar flow is limited to a small area at the nose of the submarine, typically extending between 2 and 10% of the distance along the submarine, depending on surface roughness and the form of the bow (Joubert, 2004). (Note: some sensors are situated in this region to improve their performance, and efforts are typically made to extend this region of laminar flow). At model scale this does not occur; laminar flow can extend over substantial portion of the model. In order to accurately model the flow over a submarine at model scale, turbulence is artificially instigated near the front of the model. Although capacity exists to model the transition from laminar to turbulent flow in CFD (Menter, Langtry, Likki et al, 2006), it does increase processing time due to increased meshing requirements (a halving of the expansion factor and finer surface meshing) and additional equations. It is simpler to initiate turbulence flow artificially. In CFD this can be achieved by specifying turbulent flow throughout the model. It should be noted that this is somewhat at variance with the practice for physical model experiments, where the turbulent flow is typically initiated 5-10% from the bow. As a consequence, some reduction in fidelity with results from physical models is expected.

Modelling boundary layer flow in CFD requires quite specific mesh arrangements to capture the flow accurately. Near the hull, change in velocity occurs at a very high rate normal to the hull surface, and in order to capture this flow accurately (and with it, the shear forces acting on the hull) very fine cells are required. While wall functions (analytical methods for resolving these two innermost layers) are available which can substantially reduce the numerical calculation required, in practice it is observed that the drag reported is sensitive to the span the wall function is required to bridge. This sensitivity leads to the practice of assessing the computed drag against the distance Δy between the first and second points off the wall. The non-dimensionalised form of Δy is referred to as y^+, and is scaled by the relationship

between the friction velocity u_τ, the density of the fluid ρ and the viscosity of the fluid μ), such that:

$$y^+ = \Delta y \frac{\rho u_\tau}{\mu} \qquad (4.1)$$

Typically, the characteristics of the boundary layer flow can be developed as a consistent function in y^+, as shown in Figure 4-8.

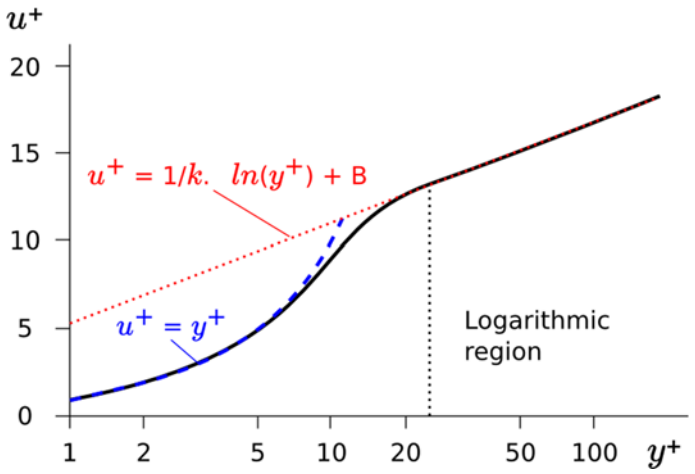

Figure 4-8 Law of the Wall (Geez, 2016)

CFX provides a wall function to bridge the final section between the wall and y^+=11, that reduces the sensitivity of results to the height of the first cells. As seen in Figure 4-9, a plot of y^+ cross-curves of skin friction against Reynolds number, the variance remains substantial for instances where y^+>11.

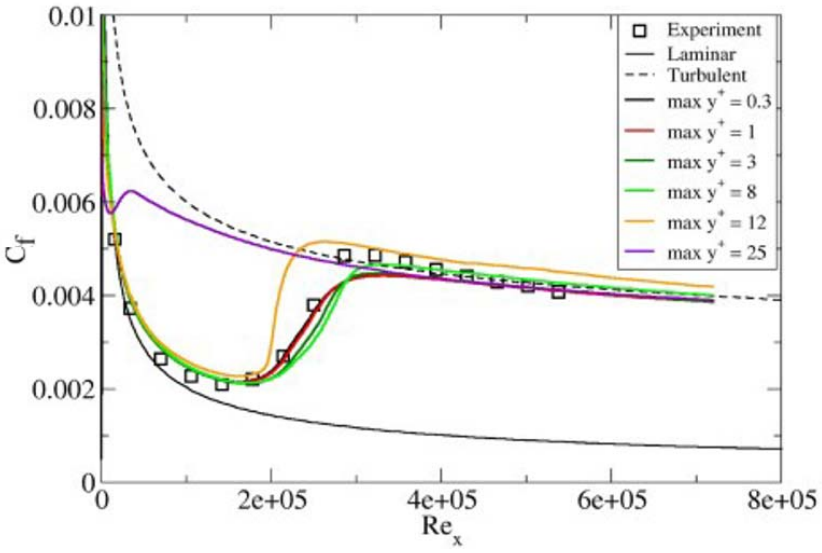

Figure 4-9 Variation of Skin Friction (C_f) on a flat plate with y^+ (ANSYS, 2015)

For the normal force and pitch coefficients, testing on a bare SUBOFF model, the independence of the coefficients falls away as the y^+ value exceeds 2. These results are in line with ANSYS recommendations for the Explicit Algebraic Reynolds Stress Model (EARSM) turbulence model (see Section 2.5), which suggests a y^+ value

below 1 to provide accurate lift forces and moments, but can provide drag results at low angles of incidence up to around a y^+ value of 8.

Constructing a mesh is a process that balances a preference for minimising the number of cells in order to be able to obtain results quickly and under limited resources with the need to discretise the volume involved in a manner which results in sufficiently accurate and stable calculation of the flow. Thus in constructing a mesh over a hull, constraints based upon the turbulence model and approach drive the characteristics of the mesh. Thus, given a y^+ of 1 (in order to resolve the flow to the surface) and selecting a height growth rate of 1.20, a minimum number of cell layers normal to the surface is obtained. Cell size along and around the hull surface is primarily constrained by the need to capture effects such as vortex shedding and wake along the hull and sail, as well as modelling the pressure variation over the hull itself. This leads directly to high aspect ratio cells (up to approximately 10 000:1) near the hull surface, and thus strong requirements for both orthogonality and arrangement parallel to the flow direction to minimise mesh effects. The result is a boundary region of cells that progress normal to the surface, transitioning from these high aspect ratio cells to cells with lower aspect ratios at the outer edge of the boundary layer as seen in Figure 4-10 below.

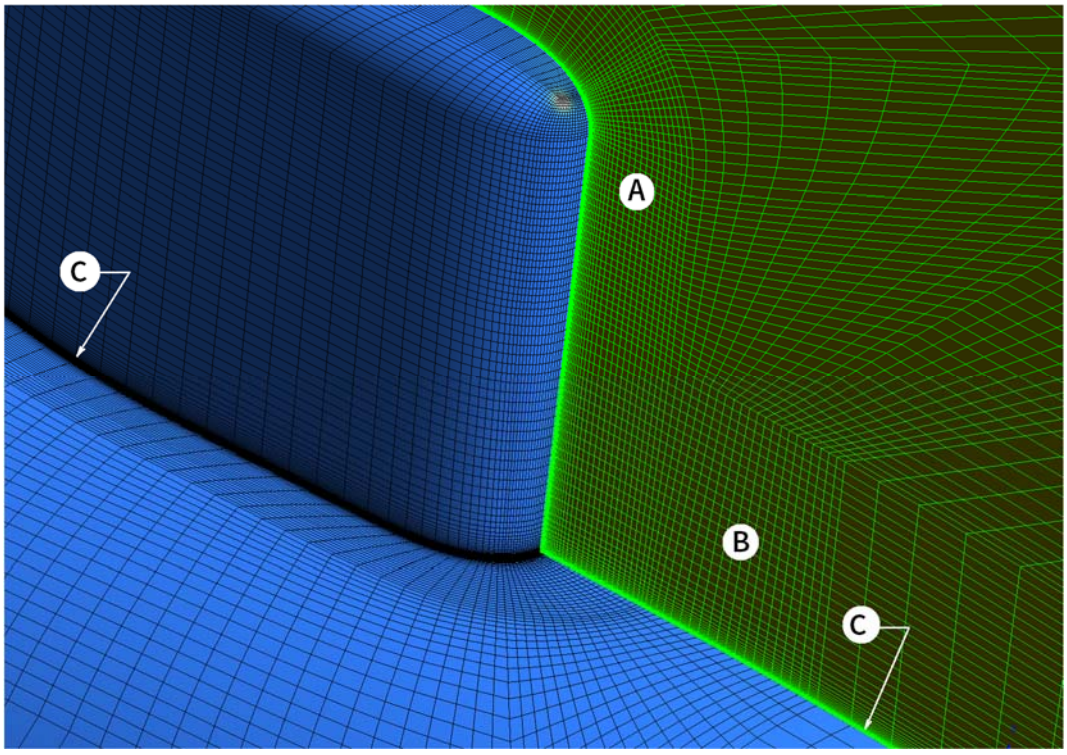

Figure 4-10 Boundary Layer Meshing

A – Orthogonal Meshing about Sail; B – Orthogonal meshing about Hull;
C – High Aspect Ratio Meshing in Boundary Region

4.2.5 Free Surface Modelling for the Volume of Fluids method

ANSYS CFX uses a Volume of Fluids (VOF) method to determine the location of the free surface during calculations. One of the difficulties in scenarios with a free

surface is that the location of the free surface is only generally known, and as such the mesh cannot easily be formed to follow the shape of the fluid. VOF resolves this difficulty by allowing different fluids to fill the domain (in this case air and water) and establishing a buoyancy constraint on the interface between the two fluids. The volume fraction is solved for by the use of an additional transport equation (ANSYS 2015).

Because of this methodology, the mesh utilised must include domain space for both the water and air. Furthermore, despite not needing to deform the mesh in the region where the interface between the two fluids will occur, particular attention does need to be paid to the form of the mesh in this region. Testing with CFX indicated that the waveform produced using the VOF method was highly susceptible to the density and consistency of the mesh in the region of the waveform.

In the course of attempting to resolve early issues with surface detail and convergence, a general arrangement of meshing in way of the free surface was arrived at, illustrated in Figure 4-11.

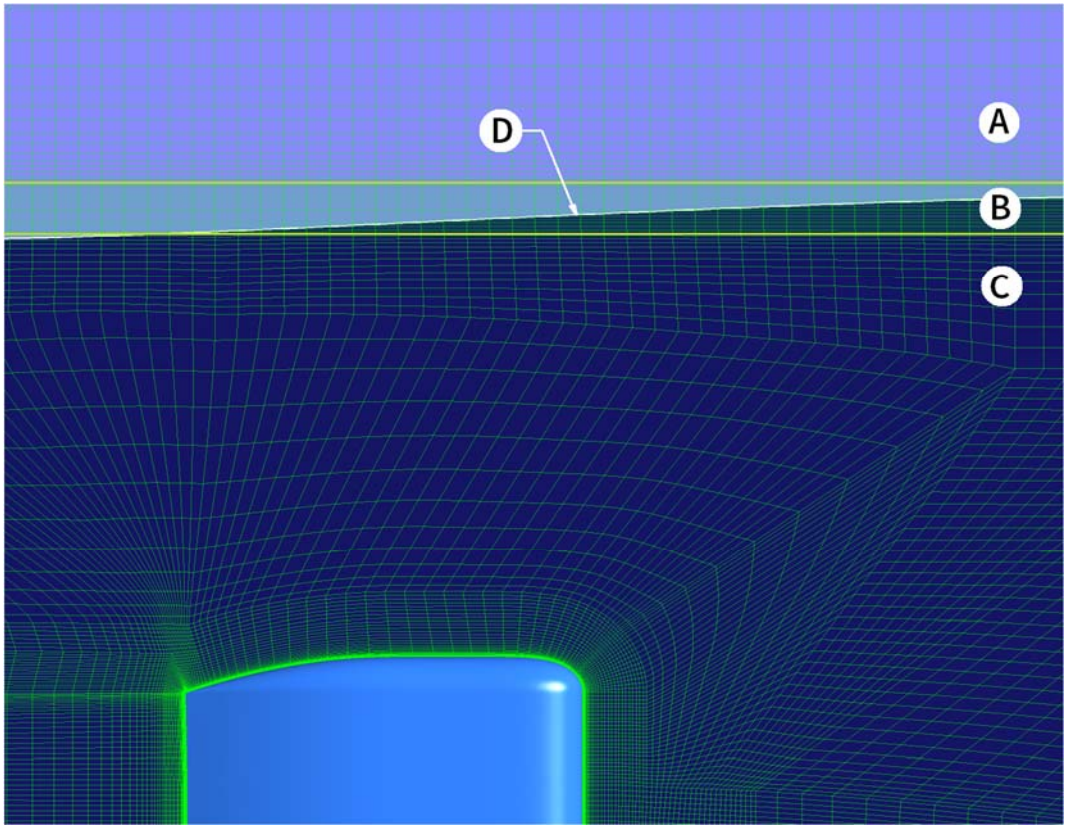

Figure 4-11 Free Surface Mesh Layering

A – Air mesh; B – Surface Interface mesh; C – Water Mesh; D – Typical Free Surface

The following guidelines were developed and utilised consistently throughout the process:

- Wherever possible, the mesh was kept regular and orthogonal throughout the volume swept by the wave form (see Region B, Figure 4-11). Hexahedral

mesh is preferred to triangular prisms (as it is difficult with this software to keep the prisms sufficiently uniform to avoid distorting the wave propagation); unstructured tetrahedral mesh is to be avoided in way of the surface (as these result in an uneven surface and/or exceptionally high mesh density).

- In both transverse and longitudinal directions, in the region where the surface form and resultant pressure field are significant to the study, at least 20 panels per wavelength were utilised. Small improvements were seen in the waveform at densities beyond this point however the sub-surface pressure field was well resolved.
- Changes were gradually made to the scale of cells in the transverse and longitudinal directions, as sudden changes could lead to visible reflections of wave energy and distortion of the wave field. If modelling the wave pattern is of significance, a constant pitch was maintained over the entire wave field. If the pressure on the submarine body under the surface is the primary concern, it was sufficient to maintain a constant pitch for at least half a diameter out from the plan-projection of the submarine.
- Arrange vertically at least 10 equally spaced cells either side of the waterline (see Region B above), before gradually inflating away from this dense layer to a smooth transition to the mesh either side. (Regions A, C). The vertical extent of Region B should approximate the anticipated wave height.
- Locate the centre of a cell (rather than the edge) at the inlet height of the waterline to reduce inlet sourced perturbations.

4.2.6 Turbulence Model

The selection of a turbulence model is significant in CFD as it impacts both the computation time and the ability of the computation to effectively model the flow. A turbulence model describes the methodology used to close the Navier-Stokes momentum transfer equations, by resolving the Reynolds stresses and the Reynolds Fluxes.

Reynolds (1894) introduced the notion of breaking down the components of an instantaneous velocity component u_i into two separate components, the mean flow $\bar{u}_i$ and the time variant component u_i'. This allowed the modelling of momentum transport perpendicular to the mean flow in both unsteady and turbulent flows by separating out the effects of stress (perpendicular variation in local mean velocity) and flux (local unsteady components of velocity), each of which could then be derived. Substituting Reynolds decomposition:

$$u_i = \bar{u}_i + u_i' \qquad (4.2)$$

into the momentum transport equation (where x_k represents each of the component axis, u_k represents the velocity along that component axis, p is pressure, ν is the viscosity, t is time, and ρ is density):

$$\frac{\partial u_i}{\partial t} + u_k \frac{\partial u_i}{\partial x_k} = -\frac{1}{\rho}\frac{\partial p}{\partial x_i} + \frac{\partial}{\partial x_k}\left(\nu \frac{\partial u_i}{\partial t}\right) \quad (4.3)$$

and averaging yields the Reynolds Averaged Momentum equation, referred to as the Reynolds Averaged Navier Stoke (RANS) equations:

$$\frac{\partial u_i}{\partial t} + u_k \frac{\partial u_i}{\partial x_k} = -\frac{1}{\rho}\frac{\partial P}{\partial x_i} + \frac{\partial}{\partial x_k}\left(\nu \frac{\partial \overline{u_i}}{\partial t}\right) - \frac{\partial}{\partial x_k}\left(\overline{u_i' u_k'}\right) \quad (4.4)$$

This equation is a function of the mean velocity, except for the final term, which is the averaged convection component of the time variant components. It is this term that turbulence models are required to close to utilise the RANS model of fluid flow.

There are two primary classes of models utilised for this (Hellsten & Wallin, 2009): Eddy viscosity models (such as k-ω, k-ε, SST) and Reynolds stress models (RSM). Typically, Reynolds stress models are more computationally intensive than eddy viscosity models, but model turbulent flow features that an eddy viscosity model cannot. Primarily this difference arises as a RSM models anisotropic stress and directly calculates the stress production. As a result, in flows with strong effects of streamline curvature, adverse pressure gradients, flow separation or system rotation, RSM models tend to provide more accurate flow predictions.

Explicit Algebraic Reynolds Stress Models (EARSM) derived from work of Pope (1975) and later Wallin & Johansson (2000), combines the capacity of a Reynolds Stress Model to incorporate the effects of pressure gradients and flow curvature into the solution, with the simplicity (and thereby speed) of a classic two-equation model for turbulence. EARSMs can formally be seen as non-linear eddy viscosity models.

Typically, the flow around a submarine with any substantive cross-flow results in the formation of sizable vortices, with adverse pressure gradients found over the aftbody and around local features such as the sail and control surfaces. Thus there is reason to suspect that utilising a Reynolds stress model may have advantages in accuracy. Indeed, Leong et al (2012) conducted a survey of comparisons between computational and experimental modelling of the SUBOFF hull in the literature, and found that although there was typically a 20% increase in computational time involved in the utilisation of a RSM, the error in off axis forces was reduced by up to half. Importantly, the results from the Baseline Reynolds Stress Model (BSL-RSM) model produced off axis forces within the experimental error.

Given the above, and considering the available computational resources, the EARSM model was evaluated against the more established and more time consuming BSL-RSM turbulence model. A series of simulations utilising the sail appended configuration was conducted replacing only the turbulence model to evaluate the

comparative performance of the two models against the experimental results obtained by Roddy (1990). Reynolds number during the simulation matched that utilised by Roddy.

Table 4-2 and Figure 4-12 below show the results obtained for axial force plotted against angle of attack using each turbulence model:

Table 4-2 Axial Force Values, EA-RSM vs BSL-RSM

Configuration	Angle of Yaw	X' BSL-RSM	X' EA-RSM	% Difference from EA-RSM
Sail Appended	12°	-0.00073	-0.00072	2.4%
Sail Appended	10°	-0.00087	-0.00085	2.4%
Sail Appended	8°	-0.00097	-0.00095	2.0%
Sail Appended	6°	-0.00103	-0.00101	1.7%
Sail Appended	4°	-0.00107	-0.00105	1.6%
Sail Appended	2°	-0.00109	-0.00107	1.6%
Sail Appended	0°	-0.00109	-0.00109	0.1%

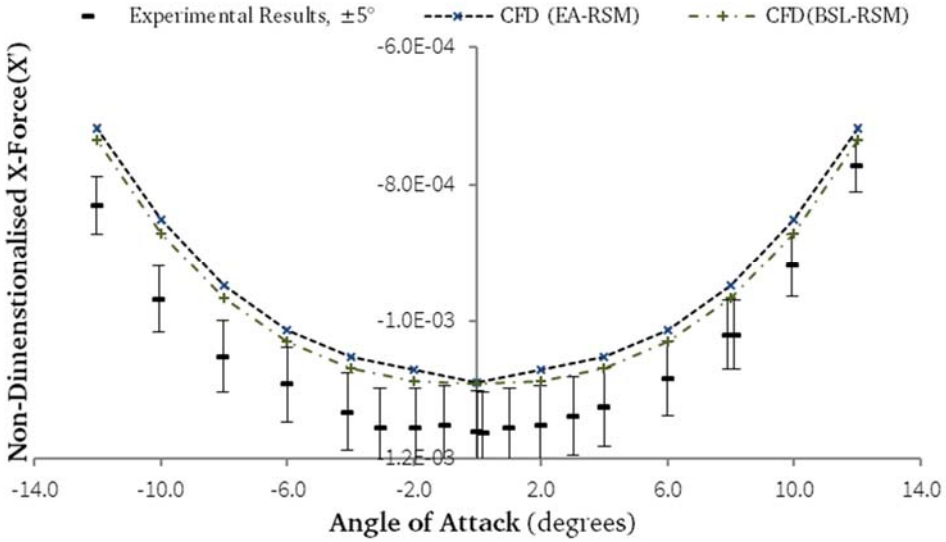

Figure 4-12 Axial Force at Different Angles of Yaw, SUBOFF with Sail

EA-RSM vs BSL-RSM (Roddy, 1990 Experimental data shown for reference)

From these results, a small difference in the axial force is evident in the results of the two different models, while there is a more substantial difference from both the modelled cases to that obtained by Roddy (1990).

Under these conditions, with consideration that these tests conducted in the horizontal plane, the relevant equation of motion is of the form:

$$X' = X'_{\star} cos^2\theta + X'_{vv} sin^2\theta \qquad (4.5)$$

Fitting a curve through the data obtained on this basis it is found:

Table 4-3 Axial Force Coefficient Comparison, Different Turbulence Models

Model	$X'_{\star}$	% Difference from Roddy	X'_{vv}	% Difference from Roddy
Roddy	-0.001169		0.006858	
BSL-RSM	-0.001107	-5.3%	0.007074	3.1%
EARSM	-0.001094	-6.4%	0.007276	6.1%

Table 4-3 clearly shown that both methods are under-predicting axial force due to axial velocity, and over-predicting axial force due to lateral velocity. These differences will be dealt with in Section 4.4 below.

Table 4-4 and Figure 4-13 below show the values obtained for force in the y-axis, plotted against angle of attack:

Table 4-4 Y-force Values, EA-RSM vs BSL-RSM

Configuration	Angle of Yaw	Y' BSL-RSM	Y' EA-RSM	% Difference from EA-RSM
Sail Appended	12°	-0.00731	-0.00711	2.8%
Sail Appended	10°	-0.00571	-0.00558	2.3%
Sail Appended	8°	-0.00429	-0.00422	1.7%
Sail Appended	6°	-0.00305	-0.00302	1.1%
Sail Appended	4°	-0.00195	-0.00194	0.7%
Sail Appended	2°	-0.00095	-0.00094	0.5%
Sail Appended	0°	0.00000	-0.00003	0.0%

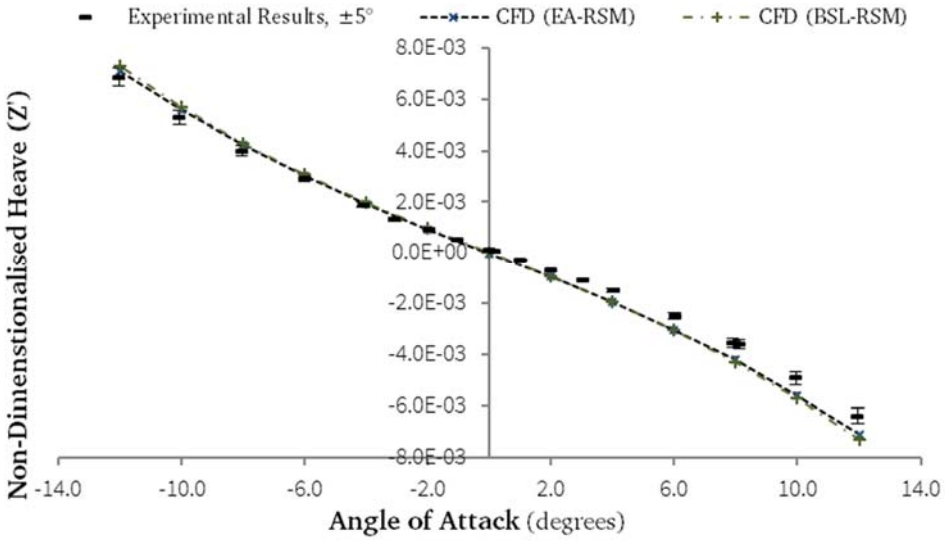

Figure 4-13 Y-Force at Different Angles of Attack, SUBOFF with Sail

EA-RSM vs BSL-RSM (Roddy, 1990 Experimental data shown for reference)

The relevant equation under these conditions is:

$$Y' = Y'_v \, cos\theta sin\theta + Y'_{v|v|} sin\theta |sin\theta| \qquad (4.6)$$

Fitting curves of this form by the least squares method, the following values are obtained for the coefficients:

Table 4-5 Lateral Force Coefficient Comparison, Different Turbulence Models

Model	Y_v'	% Diff	$Y_{v\|v\|}'$	% Diff
Roddy	-0.018948		-0.062676	
BSL-RSM	-0.022581	19.2%	-0.060912	-2.8%
EARSM	-0.022418	18.3%	-0.056712	-9.5%

The values for the linear coefficient Y_v are over-predicted in each case in comparison to Roddy — by nearly 20% — and the quadratic coefficient $Y_{v|v|}$ is underpredicted. Again, see Section 4.4 below regarding validation against Roddy (1990).

It is clear from these results that especially at smaller angles of attack, there are only minor differences in the results obtained utilising these two turbulence models on the appended SUBOFF model. Thus, there is no reason to incur the time penalty associated with the BSL-RSM model, and as such the EA-RSM turbulence model was utilised in the simulations.

4.2.7 Boundary Conditions

Given a steady forward velocity, it is possible to model submarine motion utilising a body fixed frame of reference. Utilising this simplifies the boundary conditions and setup as follows:

- The inlet is modelled as a dual fluid flow at the prescribed rate, with water below the free surface line, and air above. Critically, in order to minimise a wave making effect that can originate at the inlet, the mesh is arranged such that the free surface at the inlet lines up exactly in the centre of the mesh layer.
- The hull is modelled as a smooth wall, and a zx-symmetry plane and condition are utilised.
- All other boundaries are modelled as entrainment openings with hydrostatic pressure applied in scale with depth from the level water surface.

4.2.8 Damping Arrangements

One issue encountered in preliminary studies into modelling free surface flows in CFX was a degree of difficulty in converging to a stable solution when dealing with Froude Length Numbers below approximately 0.300. Investigation into the situation found that there were several complicating factors. These are illustrated in Figure 4-14, which uses a zebra style mapping to highlight the (small) waves in the wave train above a submarine. Note that:

- Waves were being induced at the leading edge of the mesh.
- Initial conditions created a small pulse that travelled at a slightly higher rate than the wave train, and thus progressed along the mesh, imposing a

small but noticeable variation in wave profile, heave force and pitch moment.

- Wave energy was found to reflect from all bounding edges, sudden changes in mesh density, and damping regions.

The result was that low amplitude waves not associated with the wave train were travelling up and down the modelled region, with minimal to negative loss of energy over time, leading to long solution times or failure to solve.

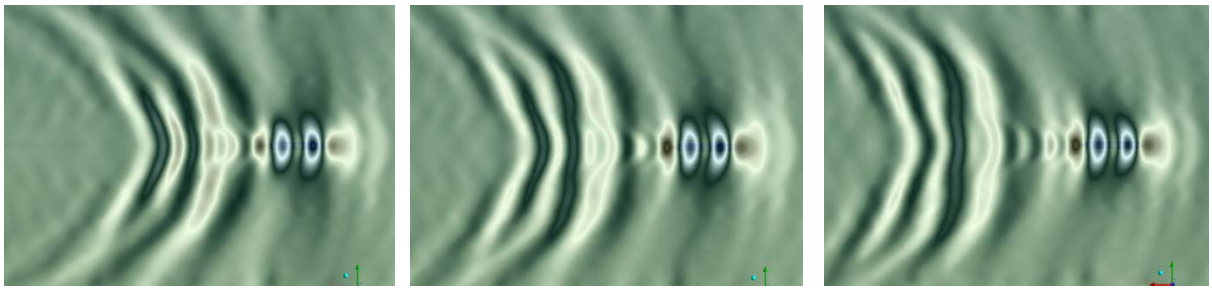

(a) **(b)** **(c)**

Figure 4-14 Unstable Small Amplitude Surface Waves Traversing Wave Train.

(a)300 iteration (b) 360 iterations (c)420 iterations

The issue with the waves originating at the forward bound of the water surface was found to be able to be minimised by the introduction of high aspect ratio cells at the forward bound, and eliminated when the free surface level at the inlet coincided with the centre of a cell rather than the original arrangement where it typically coincided with the edge.

Off axis damping was introduced exponentially once away from the region where wave effects have measurable effect on the forces acting on the submarine. CFX provides for off axis damping via a directional loss model (ANSYS, 2015). This is imposed via the addition of a directional momentum source throughout the volume of the damped region, in opposition to any velocity off the defined streamline (in this case, any velocity off the x-axis). The strength of these momentum sources ($S_{M,y}, S_{M,z}$) in the y and z-axis directions respectively are calculated as per:

$$S_{M,y} = -C_{R1}U_y - C_{R2}|U|U_y \qquad (4.7)$$

$$S_{M,z} = -C_{R1}U_z - C_{R2}|U|U_z \qquad (4.8)$$

where $C_{R1}$and $C_{R2}$are the linear and quadratic resistance coefficients, $|U|$ is the speed of the flow, and U_y and U_z are the flow velocities in the y and z axis directions respectively. It should be noted that in these models, $|U|$ is approximately constant throughout the damped regions (i.e. away from the hull) and thus the two coefficients are effectively equivalent.

Between these two changes the effect was mitigated sufficiently for convergence down to Froude Length Numbers below 0.2. It should be noted that slower Froude Numbers continued to take substantially longer to resolve with a Fr_L 0.195

simulation taking in the order of 1500 iterations compared to a Fr_L 0.512 taking in the order of 300 iterations, as wave speed remains lower and thus takes longer to establish itself over the field.

4.3 Mesh Verification

A series of five meshes with progressively finer resolution was produced to ascertain the point at which the solution obtained was independent of the mesh. These tests were conducted at a flow angle of 12° in order to test the mesh in its extreme case. Results in each axis are reported below in Table 4-6. For each mesh the density throughout was scaled in each direction by a Linear Factor – total mesh cell count varies approximately cubically with this factor.

Table 4-6 Axial force (X'), Lateral force (Y') and Yaw moment (N') Coefficients vs Mesh Density

Linear Factor	X'	Y'	N'
2.00	-0.0010088	0.0028622	0.0024784
1.60	-0.0010097	0.0028717	0.0024758
1.25	-0.0010122	0.0028808	0.0024746
1.00	-0.0010192	0.0028920	0.0024732
0.80	-0.0010257	0.0028939	0.0024772
Error (50D / 25D)	1.0%	1.0%	-0.2%

For the axial force (see Figure 4-15), a Richardson Extrapolation indicated a power of approximately 4.2, and an extrapolated value of mesh independent axial force coefficient of -1.0008×10^{-3} was derived.

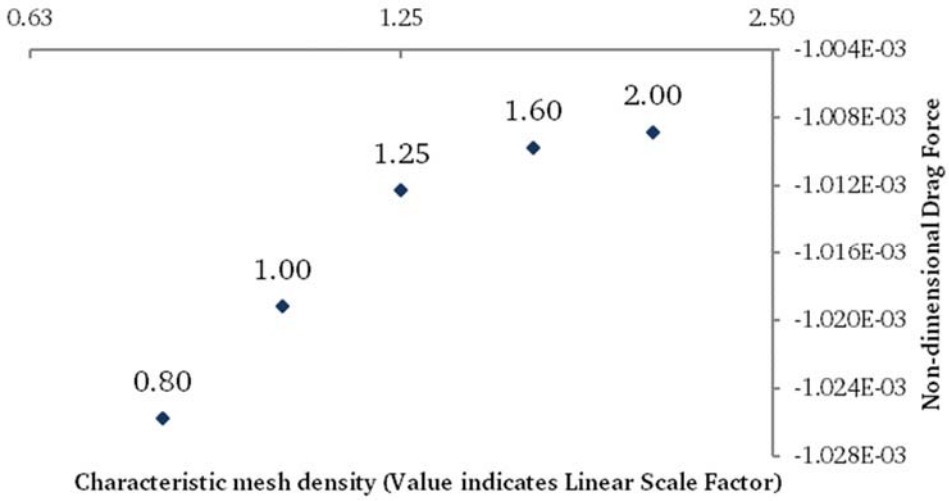

Figure 4-15 Axial Force as a function of Mesh Density

Based upon these results, simulation proceeded utilising a characteristic mesh with a linear mesh density increased by 25%. This implies an error of just over 1% due to mesh dependence in each case.

4.3.1 Free Surface Mesh

A series of tests was conducted to measure the effect of grid density on the formation of waves in CFX. In these tests, a tetrahedral mesh was used to meld a prismatic layer adjacent the submarine hull with a fixed pitch prismatic grid in which the free surface was captured.

SUBOFF was modelled operating at a submergence of 1.6D, and at a Froude Length Number of 0.447. These values were chosen in order to produce a reasonably large wave for examination. Figure 4-16 shows the resultant wave profile for the mesh cell sizes (as a proportion of submarine length).

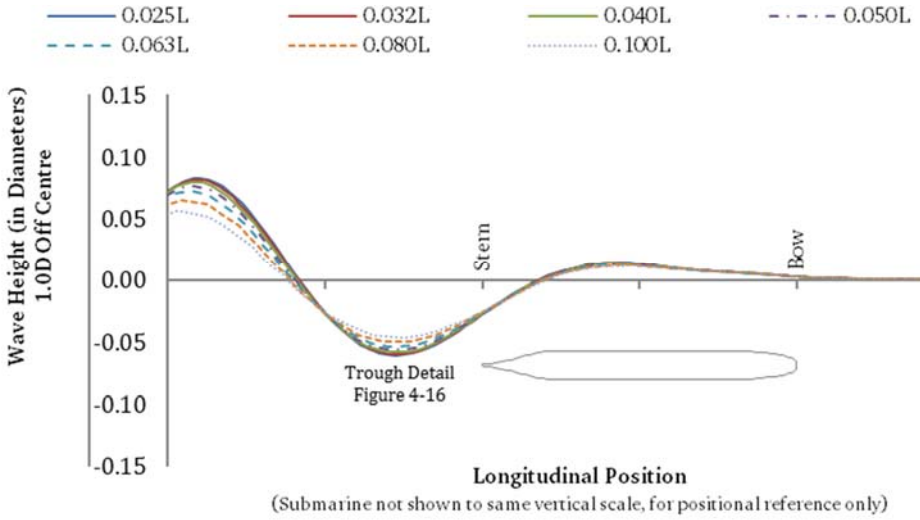

Figure 4-16 Effect of Mesh Density on Wave Height.

Wave Cuts 1.0D Starboard of Submarine Centreline.
All cases run at Fr_L 0.447 and H^* 1.6

At lower grid density, the wave length increased and wave height reduced. If the first wave trough is examined in detail, as shown in Figure 4-17, it is seen that the gradual increase in wave height with mesh density is still ongoing even at the finest mesh setting. A Richardson's extrapolation suggests that at infinite mesh density the wave would reach a depth of around 11.4mm. The trough minimum however has stabilised by a mesh density of 0.050L.

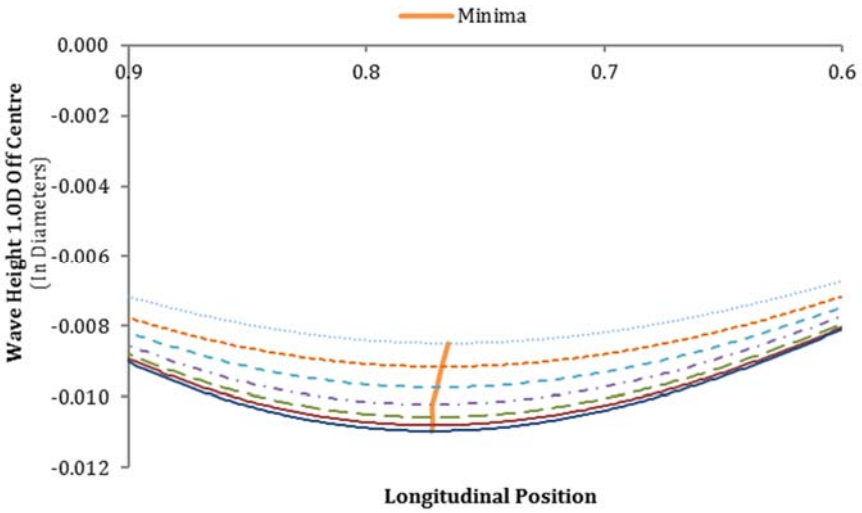

Figure 4-17 Detail of First Wave Trough at Different Mesh Densities,

Wave Cuts 1.0D off Model Centreline.
All cases run at Fr_L 0.447 and Submergence 1.6D

For the purposes of these simulations, a mesh density of 0.050L was adopted. This provides correct placement of the minima, and further variation in pressure forces on the hull beneath are not discernible with greater density.

4.4 Validation

Validation serves the purpose of ensuring that modelled results have a consistent relationship with real world data. It involves testing the results of the model against known values for the same or similar tests conducted in practice. Ideally, these are compared against full scale trials results, however these are typically unavailable and as such, comparison against physical model experiments is utilised as an alternative approach. The relationship between experimental results and full-scale results is well established, although some uncertainty remains. However, the experimental results themselves are known to the accuracy of the equipment used; assessing the model against those experiments allows validation without considering the full-scale outcome.

To validate the model against known physical data, consideration must first be given to the availability, accuracy and validity of the comparison data. Furthermore, the conditions under which that data was obtained need to be taken into consideration, including the manner in which the physical model was supported.

4.4.1 Raw Data correction

For each case modelled, raw values for X, Z and M are obtained using the ANSYS component CFX-Post. These values correspond to the modelled forces along the global x and z axes, and the moments about the global y axis. Note that to validate results against those produced by Roddy, the global y axis is located 2.013m aft of the model bow. This was the axis of support during the experiment (See Figure 4-18), but is otherwise arbitrary except in repeating those results.

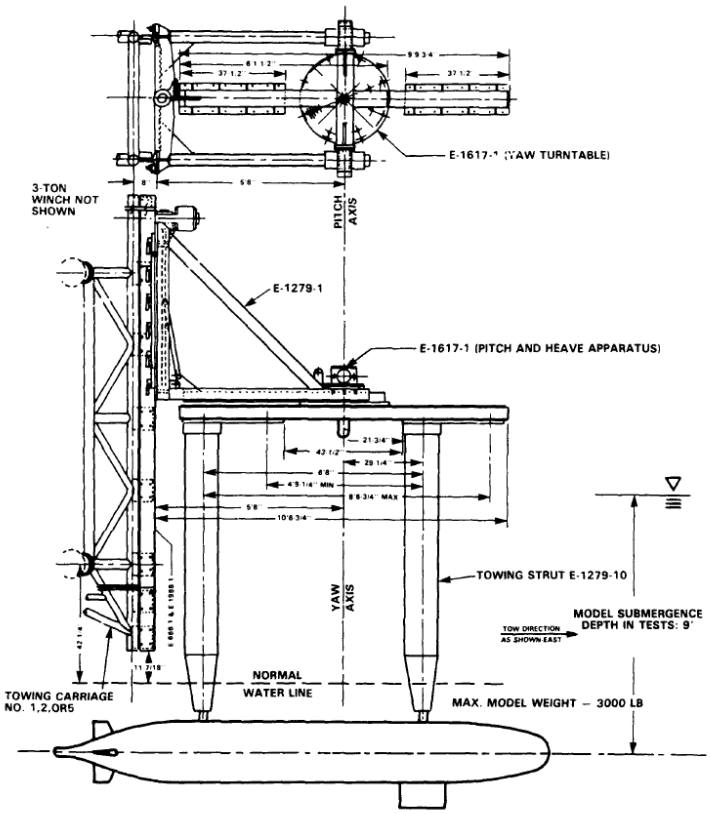

Figure 4-18 DTRC Equipment Arrangement (Huang et al, 1989)

In CFX, when operating with buoyancy modelled (as must be done in order to calculate the free surface), there is no model weight present, merely an absence of fluid. The weight (W) can be considered zero in these calculations and the hydrostatic buoyancy (B) and moment must be determined using surface integrals taken over the hull:

$$B = \oiint p_0 \left(\hat{n} \cdot \hat{k}\right)\hat{k}\, dA \tag{4.9}$$

$$B_x = \oiint p_0 \left(\hat{n} \cdot \hat{\imath}\right)\hat{\imath}\, dA \tag{4.10}$$

$$x_B B cos\theta + z_B B sin\theta = \oiint p_0 \; x\left(\hat{n} \cdot \hat{k}\right)\hat{k}\, dA + \oiint P_{hs} \; z(\hat{n} \cdot \hat{\imath})\hat{\imath}\, dA \tag{4.11}$$

where $p_0 = \rho g z$ is the calculated hydrostatic pressure from the undisturbed free surface, x_B and z_B are the distances to the centre of buoyancy along the x and z axes respectively. These calculations provide the hydrostatic buoyancy B, hydrostatic error in x B_x and hydrostatic moment $x_B B cos\theta + z_B B sin\theta$. The corrections for the x component both in buoyancy and leverage should be small as these are solely due to numerical error, given that hydrostatic pressure is dependant purely on depth. However, these corrections are necessary as otherwise calculation of the coefficients is affected by the addition of a constant error, leading to a hyperbolic curve once non-dimensionalised.

In summary, for each case, values for the force along the X and Z-axes, the moment about the Y-axis, the hydrostatic buoyancy and the buoyancy torque are collected and stored.

4.4.2 Validation against AMC Tank Test Data

Comparative CFD and experimental work at AMC (Neulist, 2011; Leong, 2013) has been used to validate the CFD results presented in Section 4.5, operating at level trim near the surface. The AMC has a 1.556m long physical model of SUBOFF which has been used to examine hydrodynamic characteristics, including near surface effects, in captive model testing within AMC's towing tank. The model is secured to a vertical strut and a stern entry sting that supports an internal force balance as shown in Figure 4-19.

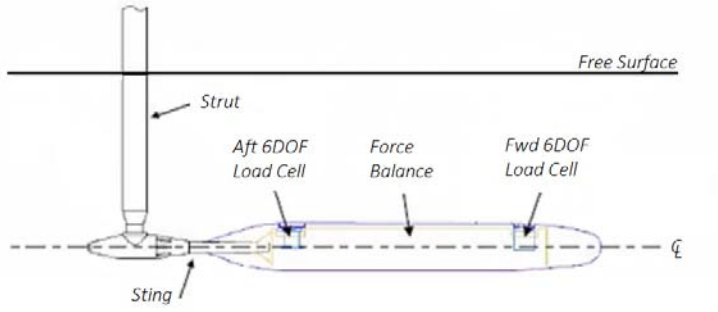

Figure 4-19 Sting Supported SUBOFF as used in the AMC Towing Tank

The effects of the mounting strut and sting upon the resistance recorded at different depths and Froude Numbers was modelled numerically, thus enabling the CFD models herein to be validated against this comparative data. Figure 4-20 shows that the coefficient of drag (C_D) of the CFD model developed for this study is in good agreement with that of a previously validated model (Leong, 2013) across a range of Froude Numbers.

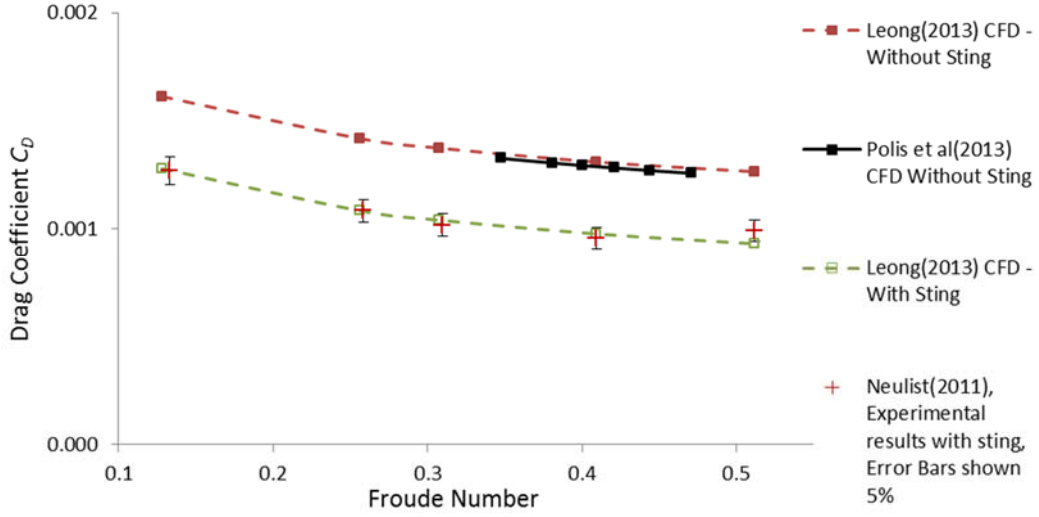

Figure 4-20 Comparison of CFD and Experimental Data for SUBOFF Model

4.4.3 Validation against DTRC SUBOFF data

As detailed in Section 2.6, the SUBOFF model was originally developed and tested by the David Taylor Research Center (DTRC). Roddy (1990) provides an overview of the characteristics of the model (detailed fully in Groves et al, 1989) and the test setup used (detailed more fully in Huang et al, 1989), as well as detailed results for the linear testing conducted.

Although the effects of the testing equipment were considered negligible at the time (Roddy, 1990), there was notable variation in some values obtained across the positive and negative portions of the runs. To confirm that the assertion of minimal impact of testing apparatus was correct, SUBOFF was modelled using ICEM in both bare hull and with sail conditions, with and without the testing apparatus to quantify the difference that resulted in each case.

The detailed drawings (see Figure 4-21) provided in Huang et al (1989) were used to generate a 3D solid model (see Figure 4-22) of the struts and their supports in Solid Edge. These were imported into CFX and mated with the SUBOFF geometry generated previously.

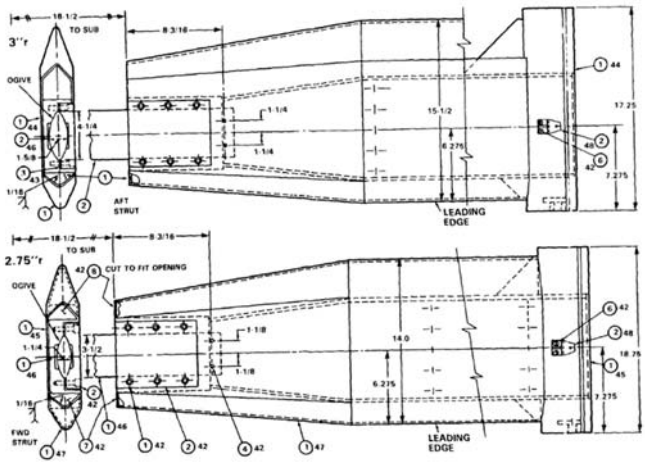

Figure 4-21 Details of DTRC Support Posts (Huang et al, 1989)

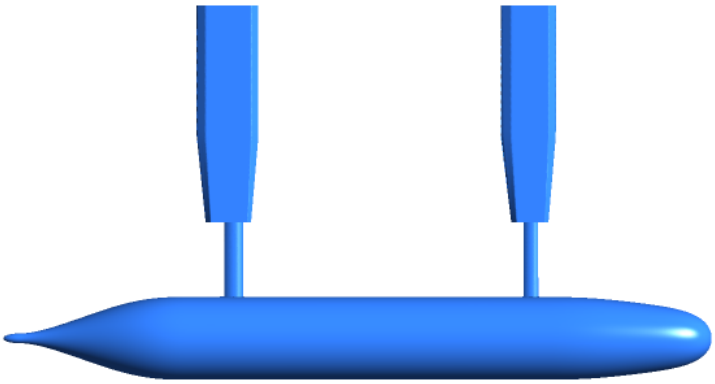

Figure 4-22 - Modelled DTRC Supports

The existing block structure was modified to encase each post in a O-grid, with a second O-grid encasing both posts and a central transition block. This arrangement allowed for clean expansion immediately around the post surfaces (see Figure 4-23) and transition back to the orthogonal mesh on the remainder of the submarine.

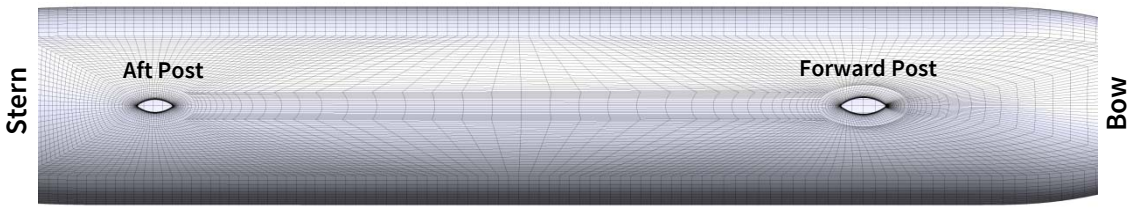

Figure 4-23 Mesh Arrangement on SUBOFF Surface around Posts

Similar variation was made to the blocking model with the sail, with the posts located on the opposite side of the model to the sail.

All four variants were tested across a range of flow directions. Those with posts were tested over -12° to +12° in pitch, while those without from 0° to +12°, given its symmetry. The model was held constant throughout and the direction flow over the model was changed. In each case the inlet velocity was held constant at 6.5 knots (3.34389 ms^{-1}) as per DTRC. These results were non-dimensionalised as per the methodology of Gertler & Hagen (1967) and plotted over that range in both axial and normal force.

Results for axial force plotted against angle of attack in the Bare Hull configuration are shown in Figure 4-24.

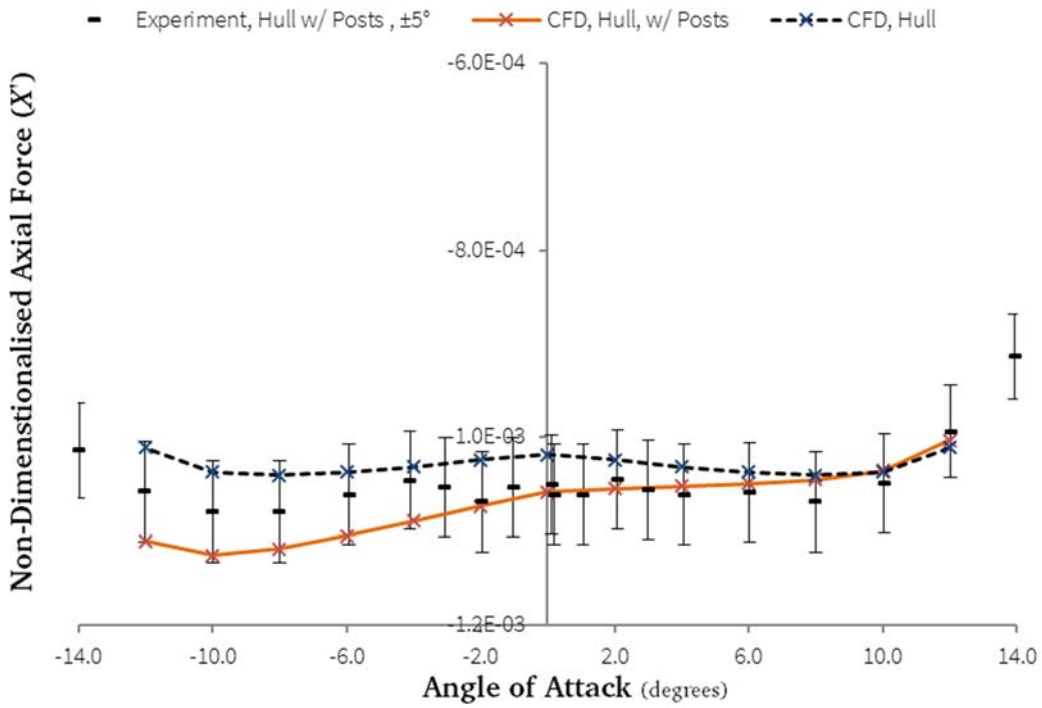

Figure 4-24 Variation in Drag with Angle of Attack, With and Without Supports

SUBOFF in Bare Hull Configuration, Experimental data Roddy(1990)

Coefficients are fitted by least squares method to the CFD and experimental results obtained, using equation 4.12:

$$X' = X'_{\star} cos^2\theta + X'_{w} cos\theta sin\theta + X'_{ww} sin^2\theta + X'_{wwww} sin^4\theta \qquad (4.12)$$

Note: This equation is **not** derived from the general model but rather developed specifically to deal with the task of validation. In addition to the standard $X'_{\star}$ and X'_{ww} terms, additional terms X'_{w} (being the coefficient of axial force in terms of $\boldsymbol{uw}$) is included to account for the linear bias due to the supports, and X'_{wwww} (being the coefficient of axial force in terms of $\boldsymbol{w^4}$) is included to allow for the reduction in axial force found near 0°.

Note also that the values from Roddy are derived directly from the tabulated data, rather than the published summary. In both cases, although data was available out to 18 degrees, only the data between -12° and 12° was utilised in order to maintain some commonality between the CFD and experimental results.

The results of the curve fitting are summarised in Table 4-7:

Table 4-7 Coefficients of Axial Force, SUBOFF Bare Hull

	$X'_{\star}$	X'_{w}	X'_{ww}	X'_{wwww}
Experiment w/ posts	-0.001052	0.000087	-0.003057	0.058756
Bare Hull	-0.001021	0.000000	-0.003140	0.053930
% Variance from Experiment	-2.9%	-100.0%	2.7%	-8.2%
Bare Hull w/ posts	-0.001061	0.000264	-0.003243	0.052097
% Variance from Experiment	0.8%	203.9%	6.1%	-11.3%

Results for axial force plotted against angle of attack in the Sail appended configuration are shown in Figure 4-25, and summarised in Table 4-8:

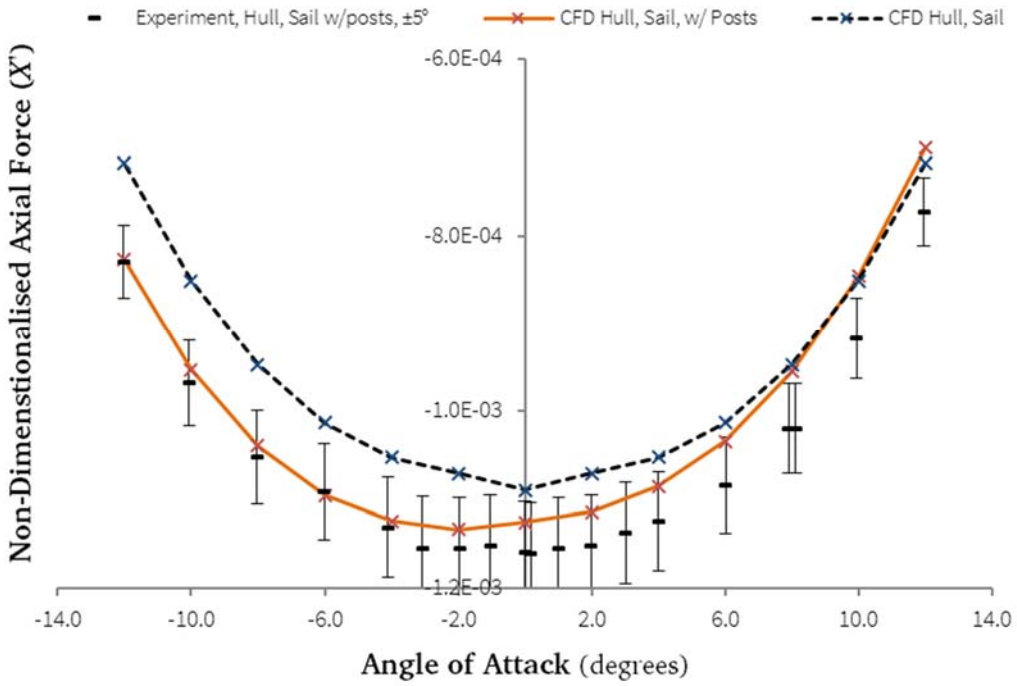

Figure 4-25 Variation in Drag with Angle of Attack, With and Without Supports

Table 4-8 Coefficients of Axial Force, SUBOFF with Sail

	$X'_{\star}$	X'_{w}	X'_{ww}	X'_{wwww}
Experiment w/ posts	-0.001158	0.000129	0.003600	0.081717
Hull , Sail	-0.001082	0.000000	0.004727	0.061089
% Variance from Experiment	-6.5%	-100.0%	31.3%	-25.2%
Hull , Sail, w/ posts	-0.001131	0.000307	0.004410	0.069282
% Variance from Experiment	-2.3%	138.1%	22.5%	-15.2%

In both cases, the inclusion of the posts in the modelling improves the prediction of the value of $X'_{\star}$, while significantly over-predicting the value of X'_{w}. In the sail appended condition, there is a slight improvement in the prediction of X'_{ww} and X'_{wwww}. Given that X'_{w} for a symmetric hull is zero by symmetry, and thus any non-zero value in the CFD results is a function of the support arrangement, the over-prediction of this impact, while notable, does not materially impact the prediction of the hydrodynamic coefficients utilised in the equations of motion.

Roddy (1990) estimates the uncertainty of the prediction of the static derivatives at 4-5%, and the value for $X'_{\star}$ is within this margin once the effect of the support is corrected for. The values for X'_{ww} and X'_{wwww} are under-predicted by less than 10% in the sail appended case, and consideration of results obtained in Toxopeus (2008) suggests that this under-prediction is consistent with other CFD modelling using similar turbulence models and could be allowed for.

4.5 Straight line motion at varying depth and speed, Bare Hull.

This section presents the results of the preliminary series of modelling conducted at level trim across the Froude Length Number range from 0.380 to 0.470. This material was first presented in Polis, Renilson, Ranmuthugala & Duffy (2013), which is included as an Appendix to this thesis. Operation of a 1.556m SUBOFF model in the bare hull configuration near the surface at nine different Froude Length Numbers was modelled at a submergence of 1.8D, and four Froude Length Numbers were modelled at each of three progressively greater depths (2.2D, 2.5D, 2.8D). The resultant axial force, normal force and pitch moment were non-dimensionalised and cross-plotted as a function of both Froude Length Number and submergence. These charts are replicated and discussed below.

4.5.1 Change in Axial Force

The difference in axial force between the deeply submerged case and the near surface case was presented as $\Delta X'_{\star}(Fr, H^{\star})$ — the change in the coefficient of axial force with u^2 from the deeply submerged condition as a function of Froude Length Number and submergence. In Figure 4-26, this is plotted against Froude Length Number for each of the submergences modelled.

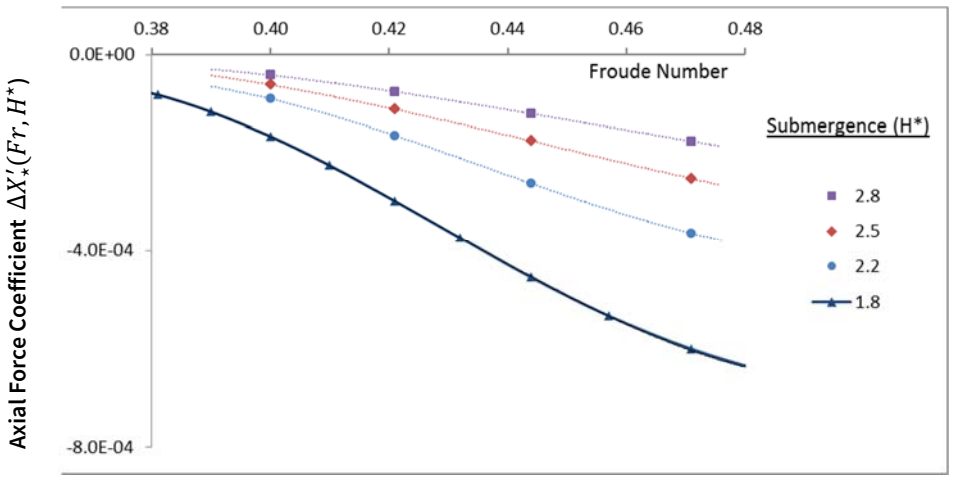

Figure 4-26 Axial Force Coefficient $\Delta X'_\star(Fr, H^\star)$ as a function of Fr_L at H* 1.8, 2.2, 2.5, 2.8

SUBOFF in Bare Hull Configuration, at Level Trim

Notable in this plot is that the axial force coefficient is smoothly modelled over the speed range, and that the reduction in the difference from the deeply submerged case is a consistent function of submergence. This is reinforced in Figure 4-27, where the logarithm of the same data is plotted against submergence for each of the Froude length numbers modelled.

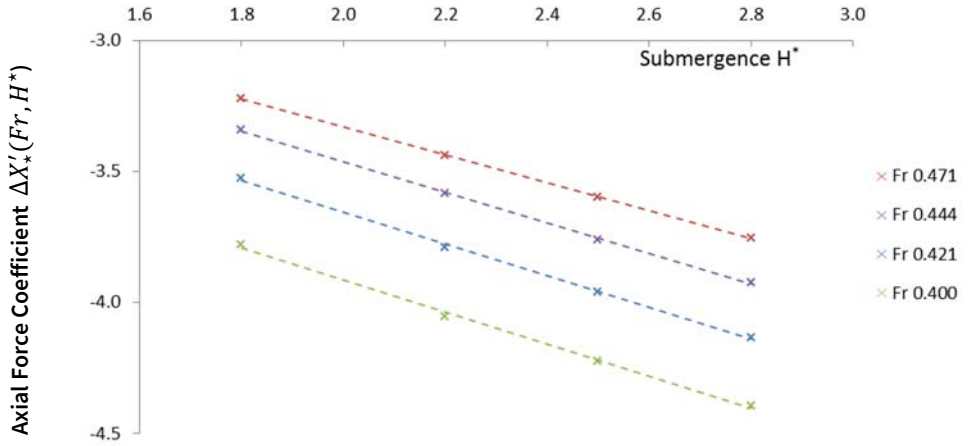

Figure 4-27 Axial Force Coefficient $\Delta X'_\star(Fr, H^\star)$ as a function of $H^\star$ at Fr_L 0.400, 0.421, 0.444, 0.471

SUBOFF in Bare Hull Configuration, at Level Trim

At each speed an exponential decay in the axial force coefficient with submergence is found, with a near constant decay rate of approximately$10^{-0.4H^*}$ regardless of speed in the range simulated.

4.5.2 Change in Normal Force

The difference in normal force between the deeply submerged case and the near surface case was presented as $\Delta Z'_\star(Fr, H^\star)$ — the change in the coefficient of normal force with u^2 from the deeply submerged condition as a function of Froude length number and submergence. In Figure 4-28, this is plotted against Froude length number for each of the submergences modelled.

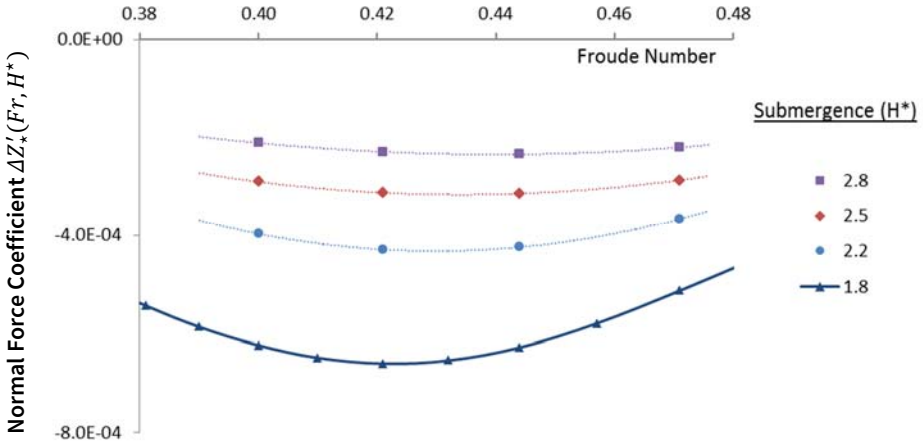

Figure 4-28 Normal Force Coefficient $\Delta Z'_\star(Fr, H^\star)$ as a function of Fr_L at H* 1.8, 2.2, 2.5, 2.8

SUBOFF in Bare Hull Configuration, at Level Trim

The normal force coefficient is smoothly modelled over the speed range, and the reduction in the difference from the deeply submerged case is a consistent function of submergence. Figure 4-29 bears this out, where the logarithm of the same data is plotted against submergence for each of the Froude length numbers modelled.

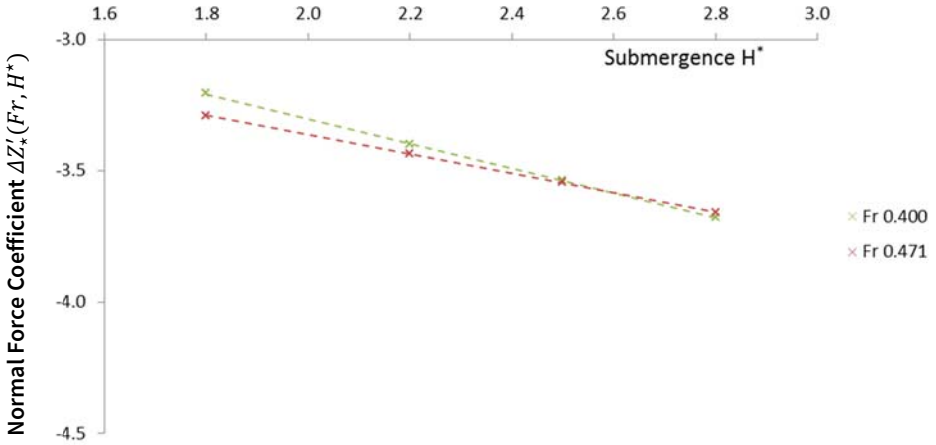

Figure 4-29 Normal Force Coefficient $\Delta Z'_\star(Fr_L, H^\star)$ as a function of $H^\star$ at Fr_L 0.400, 0.471

SUBOFF in Bare Hull Configuration, at Level Trim. Note that for clarity only two cases are shown. Cases at 0.421 and 0.444 overlay these results.

At each speed an exponential decay in the normal force coefficient with submergence is found, however in this instance the rate of decay appears somewhat dependent upon speed. Upon re-inspection of Figure 4-28, it can be seen that this corresponds to a change in the Froude Number at which the minima in normal force occurs. This could potentially be modelled as an increase in 'effective length' with increasing submergence, however the effect appears small and for manoeuvring purposes can be modelled as a constant.

4.5.3 Change in Pitch Moment

The difference in pitch moment between the deeply submerged case and the near surface case was presented as $\Delta M'_\star(Fr, H^\star)$ — the change in the coefficient of pitch moment with u^2 from the deeply submerged condition as a function of Froude length number and submergence. In

Figure 4-30, this is plotted against Froude length number for each of the submergences modelled.

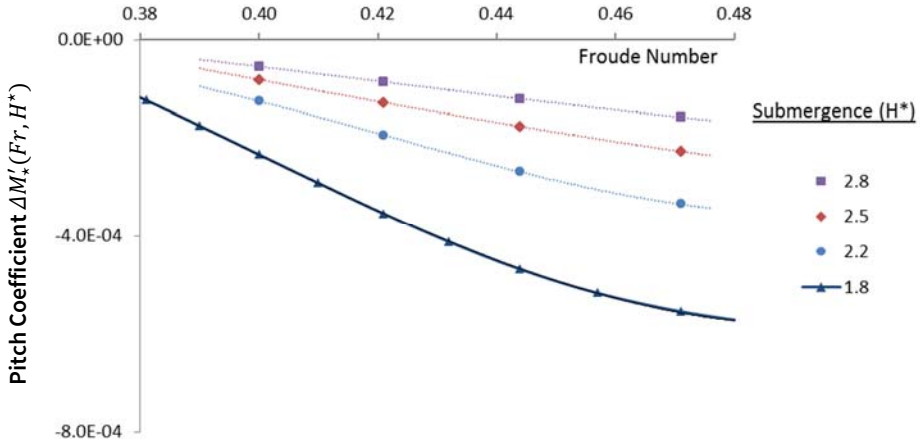

Figure 4-30 Pitch Moment Coefficient $\Delta M'_\star(Fr, H^\star)$ as a function of Fr_L at $H^\star$ 1.8, 2.2, 2.5, 2.8

As with the force coefficients, the pitch moment coefficient is smoothly modelled over the speed range, and the reduction in the difference from the deeply submerged case is a consistent function of submergence. Figure 4-31 bears this out, where the logarithm of the same data is plotted against submergence for each of the Froude length numbers modelled:

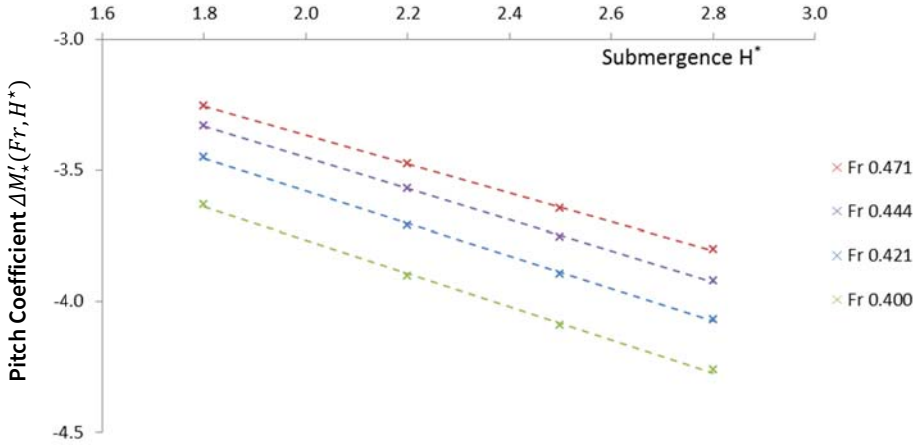

Figure 4-31 Pitch Moment Coefficient $\Delta M'_\star(Fr, H^\star)$ as a function of $H^\star$ at Fr_L 0.400, 0.421, 0.444, 0.471

As per the axial force coefficient, at each speed an exponential decay in the pitch moment coefficient with submergence is found, with a near constant decay rate of an order of magnitude per 2.0D submergence regardless of speed.

4.5.4 Discussion

In this preliminary study, the following general points were established:

- The change in all three coefficients is smooth in both submergence and Froude Length Number.
- The change with submergence is exponential in nature, with near fixed coefficients of decay found in both the pitch moment and the axial force.

There is some apparent variation in the decay rate in the case of the normal force, corresponding to some variance in the speed at which the coefficient minima occur at the different submergences modelled. However, given the rapid decay in values being noted, it is likely that this variation could be ignored in most utilisation cases.

- Providing further validation of the free surface modelling, previous physical model experiments have shown a corresponding minimum in axial force at around Fr_L 0.38 due to destructive superposition of the bow and stern wave systems. Figure 4-32 below, showing axial drag plotted against Froude Number for a range of submergences, is reproduced from Neulist (2011). Similar outcomes can be found in Figure 3-4 and Figure 3-5, sourced from Weinblum et al (1936).
- The smooth nature of the curves in Figure 4-26, Figure 4-28 and Figure 4-30 suggests that piecewise constructions of each curve at some minimum submergence (say 1.6*D*) could sufficiently accurately replicate these curves for manoeuvring use. Furthermore, the difference from the deeply submerged case at any greater submergence can then be adequately approximated by use of linear exponential decay.

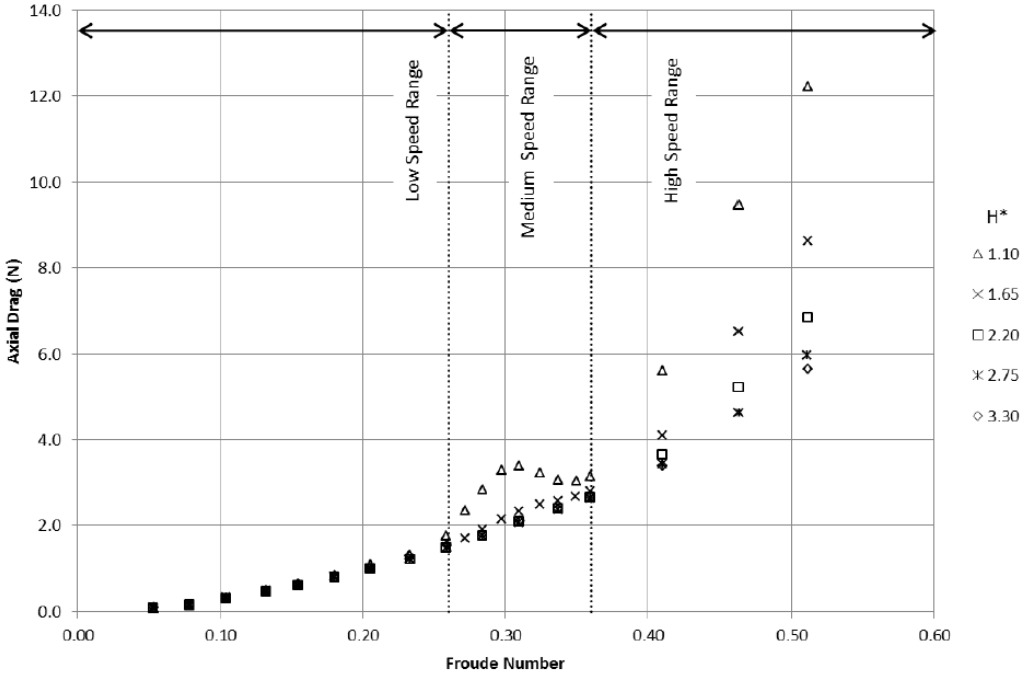

Figure 4-32 Experimental Variation in Axial Force (Neulist, 2011)

4.6 Axial Force due to Level Motion at an Angle of Trim, at Various Froude Numbers.

Upon completion of the preliminary series, a more extensive series of testing was conducted across a wider range of Froude Numbers, also introducing the effects of trim. The results from this series is presented across Sections 4.6, 4.7 and 4.8, examining axial force, pitch moment and normal force respectively. In each instance, an example of the derivation of the coefficient values is presented for a higher speed

(i.e. with greater forces and moments), before proceeding to present and analyse the results of the extended series of cases, with a focus on the changes in the relevant coefficients in the Froude length number range of interest from 0.200 to 0.250 (as detailed in Section 4.2). The significance of the variation in each coefficient is then assessed against the sensitivity of the overall manoeuvring model to changes in that coefficient.

As noted in Chapter 3, the coefficients are then grouped into four bands, based upon the significance of that coefficient to the performance of the overall model. These bands are restated here as Table 4-9 for ease of reference.

Table 4-9 Coefficient Significance Bands

Coeffieicnt Significance (C_i) **Sensetivity × Relative Response**	
$C_i > 0.5$	Primary Significance
$0.1 > C_i > 0.5$	Minor Significance
$C_i < 0.1$	Minimal Significance
$C_i > 0.1$ only where $Fr_L > 0.250$	Conditional Significance

4.6.1 Equation of motion for axial force under steady conditions at an angle of trim

Given an imposed force X' that leads to the conditions where a model maintains a steady speed, angle of trim and submergence:

$$u = U_0 cos\theta; \dot{u} = 0 \tag{4.17}$$

$$w = U_0 sin\theta; \dot{w} = 0 \tag{4.18}$$

$$q = 0; \dot{q} = 0 \tag{4.19}$$

The axial force equation (see Equation 3.14) reduces to:

$$X' = X'_\star \, cos^2\,\theta + X'_{ww} \, sin^2\,\theta \tag{4.19}$$

Allowing for the influence of the free surface (where $\boldsymbol{\eta}$ is the position vector as detailed in Chapter 3):

$$X'(\boldsymbol{\eta}) = X'_\star(\boldsymbol{\eta}) \, cos^2\,\theta + X'_{ww}(\boldsymbol{\eta}) \, sin^2\,\theta \tag{4.20}$$

4.6.2 Coefficient Evaluation

To verify the adequacy of this representation of the near surface manoeuvring response, a detailed series of simulations utilising the sail appended SUBOFF configuration at different angles of trim was conducted at a submergence of $1.6D$ and a speed of Fr_L 0.422. Values obtained from the simulations for X' are tabulated below.

Table 4-10 Results for X' for various angles of trim
Deeply Submerged (DS) and submerged 1.6D below Free Surface

Config	H*	Fr_L	Trim degrees	X' EA-RSM
Sail Appended	DS	0.422	-6	-5.539E-04
Sail Appended	DS	0.422	-3	-5.496E-04
Sail Appended	DS	0.422	-3	-5.476E-04
Sail Appended	DS	0.422	0	-5.470E-04
Sail Appended	DS	0.422	0	-5.442E-04
Sail Appended	DS	0.422	3	-5.446E-04
Sail Appended	DS	0.422	3	-5.416E-04
Sail Appended	DS	0.422	6	-5.328E-04
Sail Appended	1.6	0.422	-6	-7.985E-04
Sail Appended	1.6	0.422	-3	-7.269E-04
Sail Appended	1.6	0.422	-2	-7.158E-04
Sail Appended	1.6	0.422	-1	-7.004E-04
Sail Appended	1.6	0.422	0	-6.958E-04
Sail Appended	1.6	0.422	1	-6.895E-04
Sail Appended	1.6	0.422	2	-6.829E-04
Sail Appended	1.6	0.422	6	-7.066E-04

As can be seen in the table, multiple angles of trim were simulated for each submergence and Froude number. Taking multiple values (and sometime repeat values) allows the calculation of the coefficients required with some robustness to individually spurious values (several of which were discarded in the analysis).

The results tabulated above are plotted below on Figure 4-33 as a function of angle of trim. The fitted curves shown are calculated using a least squares fit to Equation 4.19:

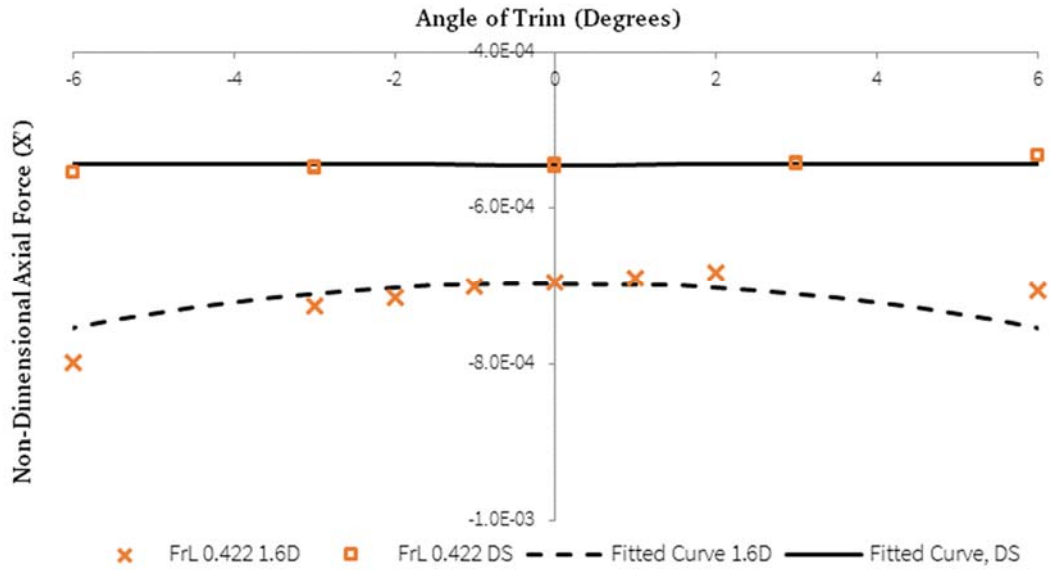

Figure 4-33 Variation in Axial force as a function of trim, SUBOFF with sail appended at Fr_L 0.422

Deeply Submerged (DS) and Near Surface (1.6D) cases
Curves Fitted as per Equation 4.20

One aspect is notable immediately: although the deeply submerged results are close to symmetrical about the axis, the near surface results tilt distinctly to one side. To capture this aspect, a term $X'_w(\boldsymbol{\eta})\boldsymbol{u'w'}$ is added to equation 4.20, which becomes:

$$X'(\boldsymbol{\eta}) = X'_\star(\boldsymbol{\eta})\, cos^2\,\theta + X'_w(\boldsymbol{\eta}) cos\theta sin\theta + X'_{ww}(\boldsymbol{\eta})\, sin^2\,\theta \qquad (4.21)$$

With this change, the fit of the equation improves markedly (see Figure 4-34):

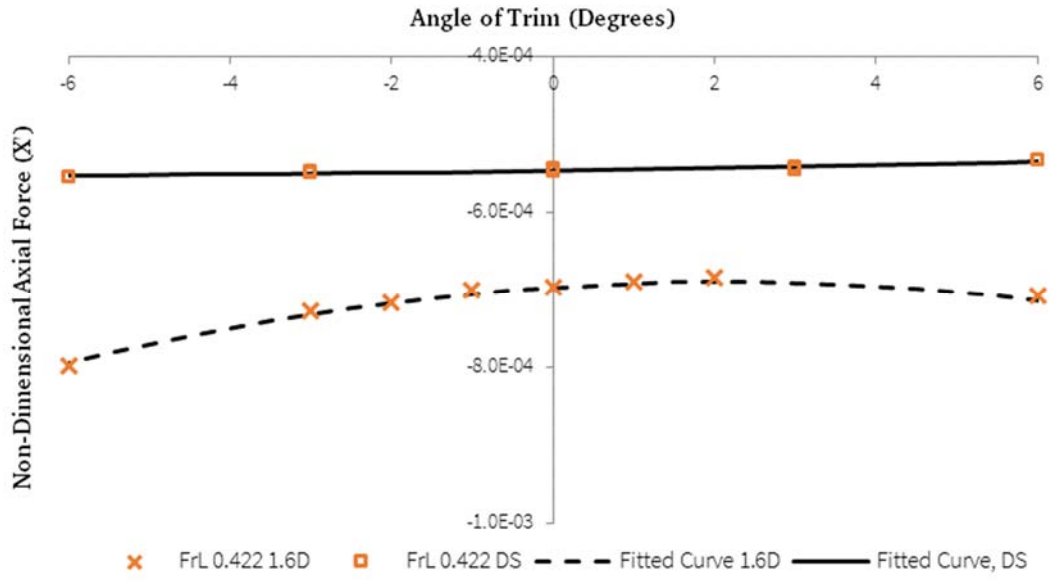

Figure 4-34 SUBOFF w/ Sail, Non-dimensionalised Axial force as a function of Trim at Fr_L 0.422

Fitted as per $X'_\star\, cos^2\,\theta + X'_w cos\theta sin\theta + X'_{ww}\, sin^2\,\theta$

Summarising the change found in the coefficients:

Table 4-11 Changes in Axial Force Coefficients Near the Free Surface

Coefficient	DS	1.6*D*	Difference	Change from DS case
$X'_\star$	-5.446E-04	-6.914E-04	-1.468E-04	27%
X'_{ww}	-4.320E-04	-1.615E-02	-1.572E-02	3640%
X'_w	8.885E-05	-6.795E-04	-7.684E-04	-865%

The distinctly different nature of the deeply submerged forces and those imposed in the near surface are evident. The deeply submerged component is derived primarily from friction drag, and the near surface dominated by pressure imposed by gravity waves over the submarine. The deeply submerged values are primarily driven by effects related to Reynolds Number, and those of the near surface effects to Froude Length Number. Conducting both deep and near surface tests with the same mesh and simply a different depth of water over allows the separation of the effect of the free surface from any viscous or mesh effects, which is shown in the following results.

4.6.3 Extended Series

Similar sets of simulations to the above were conducted from Fr_L 0.195 through to the above case at Fr_L 0.422. At the higher Froude Numbers, additional simulations were undertaken at increased submergence, in order to gain an understanding of the characteristic of the decay of each coefficient with depth. The coefficients obtained from these tests are presented below across the range of Froude Numbers tested.

4.6.4 $X'_\star$ –Coefficient of Axial force as a Function of u^2

For the case examining axial force as a function of $\boldsymbol{u}^2$, the values for X' at level trim are also plotted. Although there are minor discrepancies in the values for $X'_\star$ obtained as a result of the curve fitting to the trimmed values, these should be and are small as $X'_\star$ is the only component that has value when $\boldsymbol{w}$ is zero**.** Figure 4-35 shows $X'_\star$ plotted as a function of Froude number for both deeply submerged and near surface cases**.**

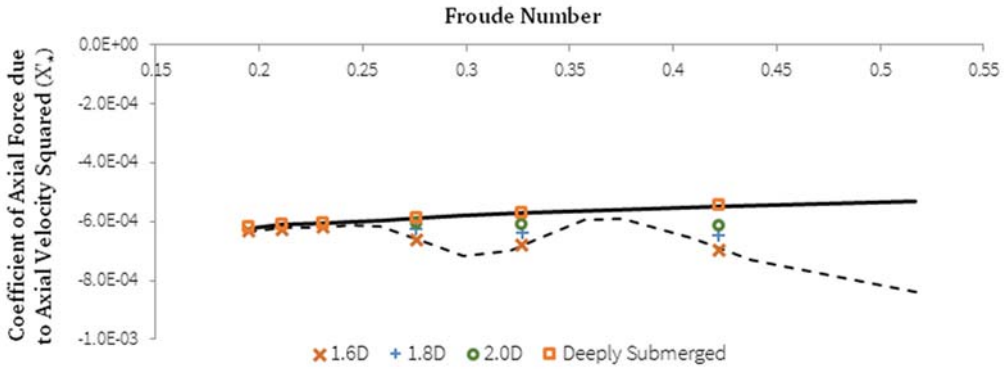

Figure 4-35 SUBOFF w/ Sail at Level Trim, $X'_\star$ as a function of Fr_L and $H^\star$

Detailed progression of 1.6*D* submergence series indicated. Trendline shown through DS cases.

Considering the results presented above in Figure 4-35, a significant increase in the near surface effect is found as the velocity passes a Froude Length Number of approximately 0.250. Below this value, there is a small but consistent increase in axial force of less than 4%, however the increase due to the presence of the surface increases substantially as Froude Numbers climb above this point. A peak variance of just over 40% is found in the region of Fr_L 0.300 before the effect drops away again to a minimum at a round Fr_L 0.365.

As per Section 3.5, Coefficient Significance can be evaluated by multiplying the sensitivity of the model to change in the coefficient by the greatest magnitude of such change observed. Given a nominal sensitivity of 0.387 (as per Table 3.1), and a maximum change of 4% in value at Froude Length Numbers between 0.200 and 0.250 (at which a submarine is potentially liable to travel near the surface), the significance of $X'_\star$ can be evaluated at a value of approximately 0.02. For modelling submarine like bodies or other special cases where the Froude Length Number is expected to exceed 0.250, this coefficient gains in significance (>0.16 Fr_L 0.300) at

due to the marked increases shown in Figure 4-35. $X'_\star$ is thus judged, according to Table 3-2, to have conditional significance.

4.6.5 X'_w —Coefficient of Axial force as a Function of uw

The effect of a near surface on X'_w is quite marked. As can be seen in Figure 4-36 where X'_w is plotted against Froude number, this change does not show the same reduction to minimal amounts as the axial velocity drops below Fr_L 0.250.

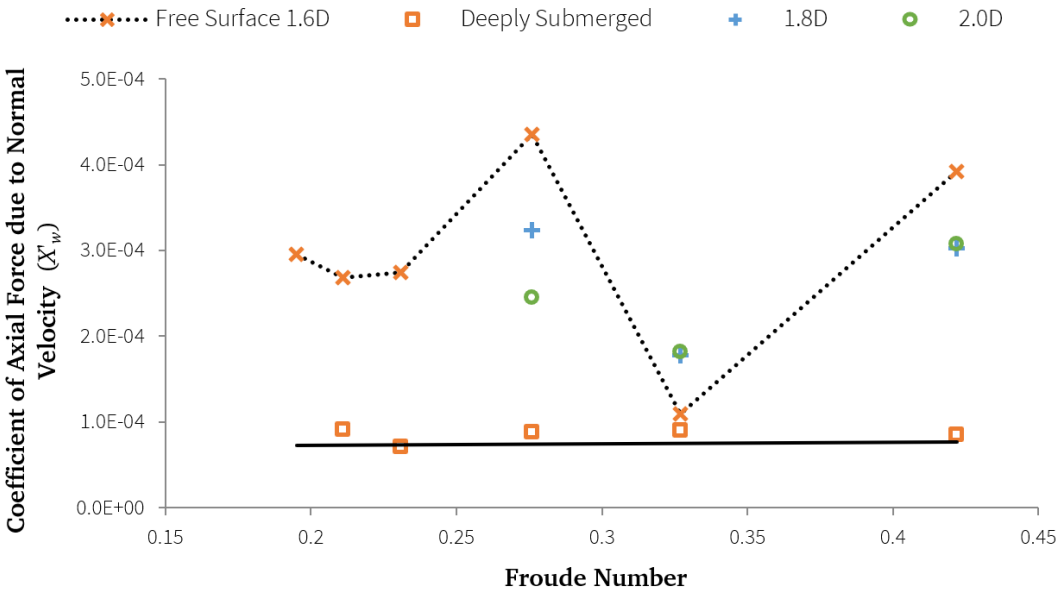

Figure 4-36 SUBOFF w/ Sail, X'_w as a function of Fr_L and $H^\star$

General progression of 1.6D submergence series indicated. Trendline shown through DS cases.

Across the range of interest between Fr_L 0.200 and Fr_L0.250, the surface effect dominates. The value calculated here for X'_w in the deeply submerged condition is ignored in the standard equations for modelling; it makes little difference to the axial forces in the deeply submerged condition whether the vessel is trimmed bow up or down. Near the surface this effect is around half an order of magnitude greater; the increase in axial force is noticeably more substantial when the vessel trims bow down than bow up as seen in the difference between the value at -6° and +6° in Figure 4-34. This is to be expected as the wave from the bow imposes itself over noticeably more of the submarine's length, and the bow wave increases in height more for a given trim up than it decreases for a trim down.

As X'_w is a coefficient introduced to capture near surface effects, there is not an established sensitivity for this coefficient. However, comparison can be made to other coefficients which are functions of uw such as Z'_w. While Z'_w has a reported sensitivity of 1.290 (Sen, 2000), this is off a substantially larger basis, typically between 10^{-2} and 10^{-3}, compared to the above values for X'_w between 10^{-3} and 10^{-4}. Furthermore, the equations of motion were typically less sensitive to X-axis coefficients in the battery of tests used in Sen (2000). These differences suggest that the sensitivity of the equations of motion to X'_w may well be below 0.05.

This view is reinforced when the proportion of axial force derived from each coefficient is assessed. Even at 6 degree down trim, the force due to X'_w is approximately 5% of that due to $X'_\star$ (see Table 4-12), and logically this reduces to 0% at level trim. Again, this suggests that sensitivity to X'_w is well below 0.05.

Unless a full sensitivity analysis suggests otherwise, X'_w may be considered of minimal significance.

4.6.6 X'_{ww} —Coefficient of Axial force as a Function of w^2

Figure 4-37 shows a steadily increasing surface effect upon X'_{ww} across the range of Froude Numbers. However, as in the case with X'_w , at these angles of trim and in this range of Fr_L, the absolute scale of the force produced remains small.

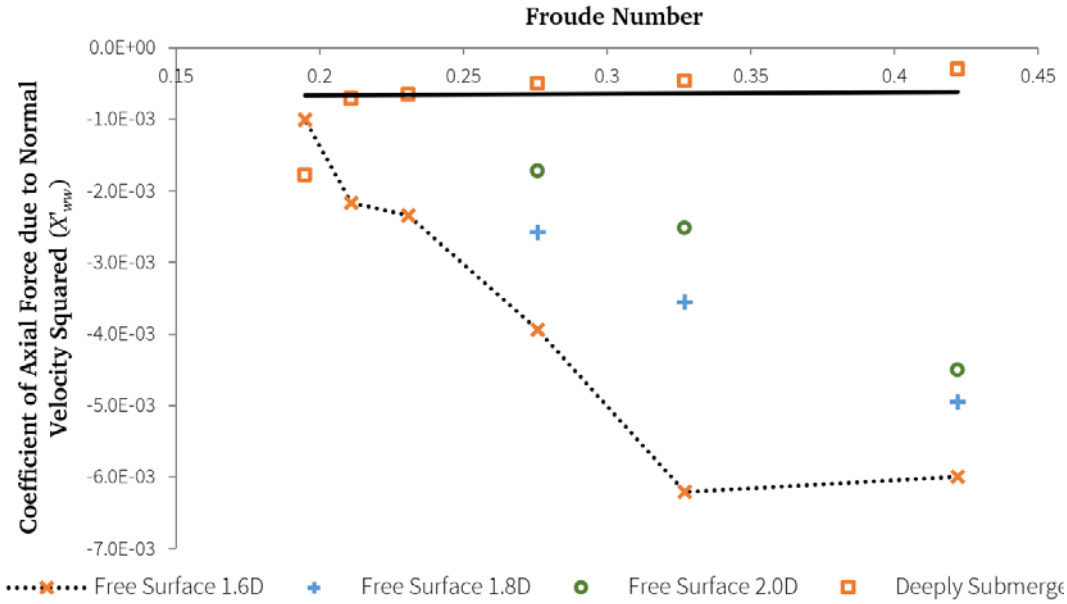

Figure 4-37 SUBOFF w/ Sail, X'_{ww} as a function of Fr_L and $H^\star$

General progression of 1.6D submergence series indicated. Trendline shown through DS cases.

The small scale of the effects noted in X'_w and X'_{ww}, is illustrated in the effects of a 6° bow down trim at a Froude Length Number of 0.250. The proportion of axial force calculated using equation 4-21 for each component under these conditions is shown in Table 4-12.

Table 4-12 Components of Axial Force at Fr_L 0.250, H* 1.6, Trim -6°

$X'_\star u'u'$	$X'_w u'w'$	$X'_{ww} w'w'$
-0.00061	*-0.00003*	*-0.00003*
90.6%	5.1%	4.3%

Although higher rates of cross flow may be experienced in the deeply submerged case, it is unlikely near the surface. Thus, for the range of Froude length numbers between 0.200 and 0.250, X'_{ww} is assessed to be of minimal significance.

4.7 Pitch Moment due to Constant Depth Motion at an Angle of Trim

Given an imposed moment M that leads to the conditions where a model maintains a steady speed, angle of trim and submergence:

$$u = U_0 cos\theta; \dot{u} = 0 \tag{4.22}$$

$$w = U_0 sin\theta; \dot{w} = 0 \tag{4.23}$$

$$q = 0; \dot{q} = 0 \tag{4.24}$$

Equation 3.16 reduces to:

$$M' = M'_w\, cos\theta sin\theta + M'_\star\, cos^2\theta \; + M'_{|w|}\, cos\theta|sin\theta| + M'_{w|w|}\, sin\theta|sin\theta| \; + M'_{ww}\, sin^2\theta \tag{4.25}$$

Allowing for the influence of the free surface:

$$M'(\boldsymbol{\eta}) = M'_\star\,(\boldsymbol{\eta})cos^2\theta + M'_w(\boldsymbol{\eta})\, cos\theta sin\theta + M'_{|w|}(\boldsymbol{\eta})\, cos\theta|sin\theta|$$

$$+M'_{w|w|}\,(\boldsymbol{\eta})\, sin\theta|sin\theta| \; + M'_{ww}(\boldsymbol{\eta})\, sin^2\theta \tag{4.26}$$

4.7.1 Coefficient Evaluation

Utilising the detailed series of simulations at different angles of trim that was conducted at a submergence of $1.6D$ / Fr_L 0.422, the results obtained for the non-dimensional pitch moment are plotted against angle of trim in Figure 4-38:

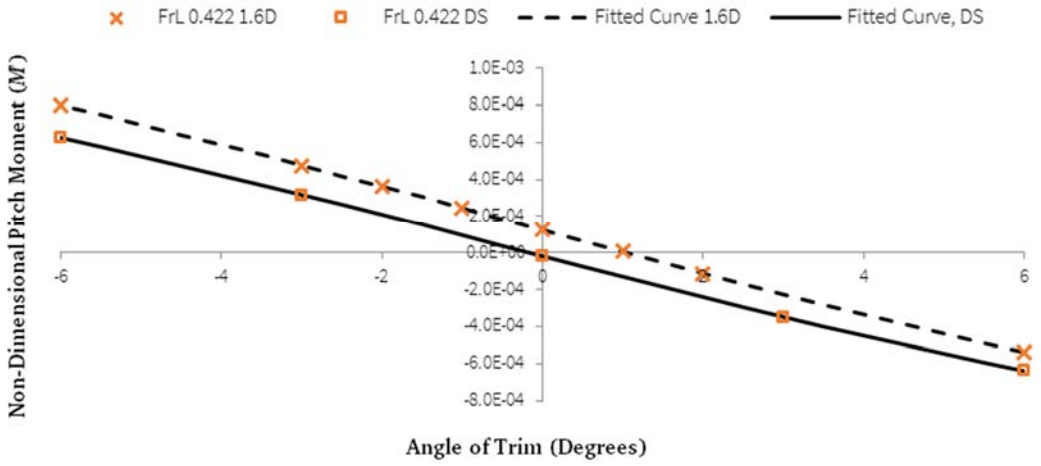

Figure 4-38 Pitch Moment as a function of Angle of Trim, Fr_L 0.422

The curves drawn have been fitted utilising Equation 4.26 and a least squares method. The fit is very good, and indeed, in the deeply submerged case where only five different trims were assessed, the fit is exact as there are five degrees of freedom in Equation 4.26.

In Equation 4.26, there are two pairs of coefficients that utilise an absolute value function to provide for asymmetry in the response. A quick comparison was undertaken to ascertain the degree of asymmetry present. It was found that the

values for $M'_{|w|}$ were typically between 5 and 10% the value of M'_w, while the values for M'_{ww} were typically 20% the value of $M'_{w|w|}$. The effects of both are likely to be small. On this basis, it was chosen to simplify the equation being used by dropping the (smaller) $M'_{|w|}$ term, leading to:

$$M'(\boldsymbol{\eta}) = M'_{\star}(\boldsymbol{\eta})cos^2\theta + M'_w(\boldsymbol{\eta})\, cos\theta sin\theta + M'_{w|w|}(\boldsymbol{\eta})\, sin\theta|sin\theta| + M'_{ww}(\boldsymbol{\eta})\, sin^2\theta \qquad (4.27)$$

All of the following coefficient analysis are completed by least squares fitting the data available at each speed and depth to Equation 4.27.

4.7.2 $M'_{\star}$ – Coefficient of Pitch Moment as a Function of u^2

$M'_{\star}$ is plotted in Figure 4-39 across a range of Froude Numbers and at different depths of submergence. The greater number of results for the zero-degree cases obtained were utilised to sketch curves which provide the results with a degree of context.

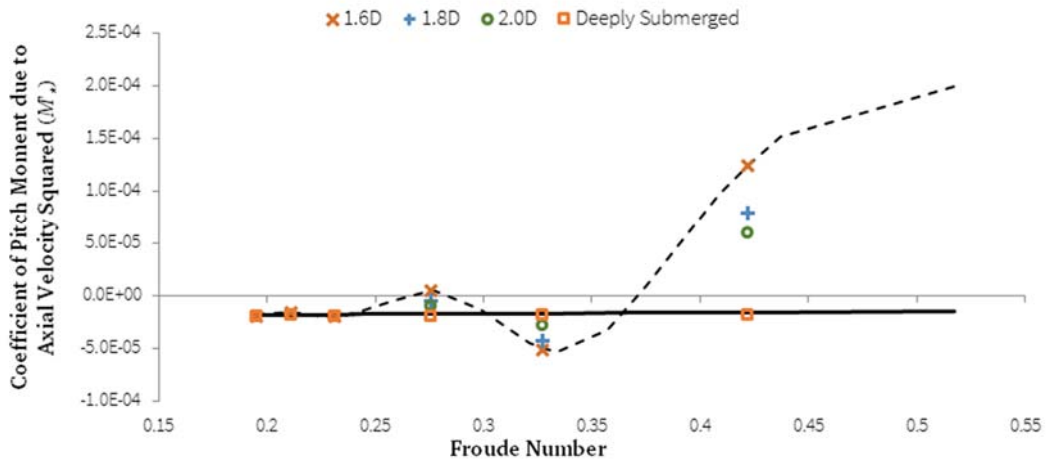

Figure 4-39 SUBOFF w/ Sail, $M'_{\star}$ as a function of Fr_L and $H^{\star}$

As with the results for $X'_{\star}$, these show a negligible difference from the deeply submerged case at Froude Numbers below Fr_L 0.250. At Froude Numbers higher than this, substantial pitch moments are imparted to the vessel that vary in sign and magnitude. Given the nominal sensitivity of 0.889 for $M'_{\star}$, the coefficient becomes of minor significance only above Fr_L 0.250, and then of major significance above Fr_L 0.380.

4.7.3 M'_w – Coefficient of Pitch Moment as a Function of uw

In Figure 4-40, the results obtained for M'_w are plotted across the range of Froude Numbers simulated.

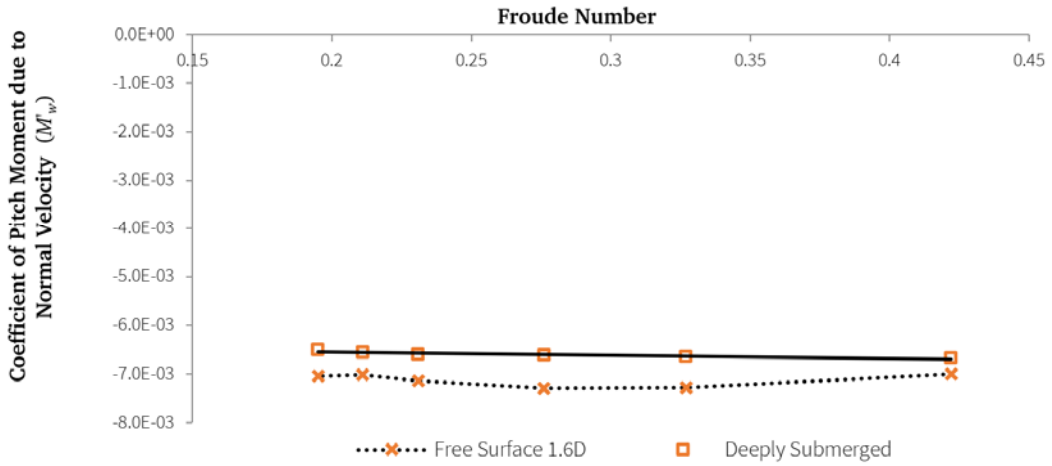

Figure 4-40 SUBOFF w/ Sail, M'_w as a function of Fr_L and $H^\star$

In general, there is a small (maximum 10.3%) but consistent increase in the value of M'_w when at a submergence of $1.6D$. With a nominal sensitivity of 0.979 (see Table 3-1), the variation of M'_w has minor significance throughout the range tested.

4.7.4 $M'_{w|w|}, M'_{ww}$ – Coefficients of Pitch Moment as a Function of $w|w|$ and w^2

The results for $M'_{w|w|}$ and M'_{ww} are shown in Figure 4-41 and Figure 4-42 respectively, plotted at the same vertical scale against Froude Number, in order to show the relative magnitude of each.

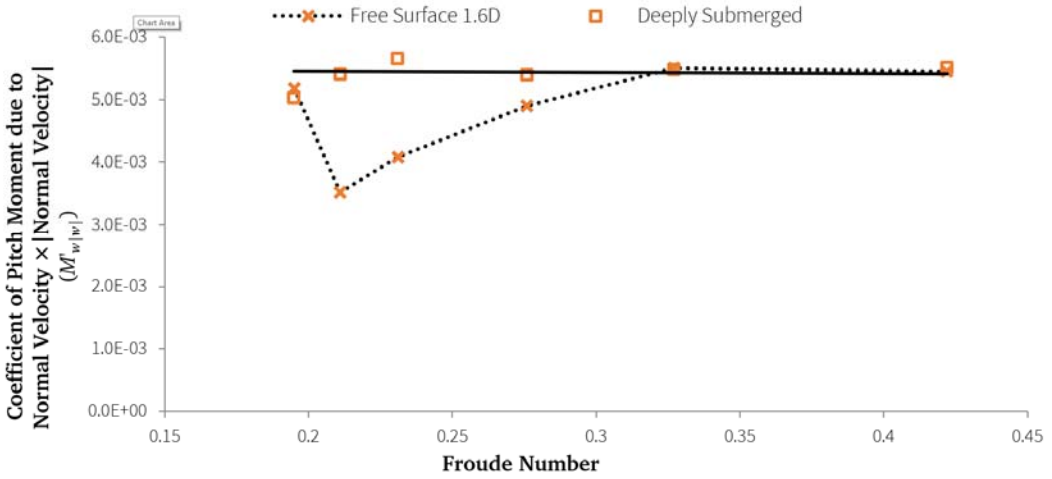

Figure 4-41 SUBOFF w/ Sail, $M'_{w|w|}$ as a function of Fr_L and $H^\star$

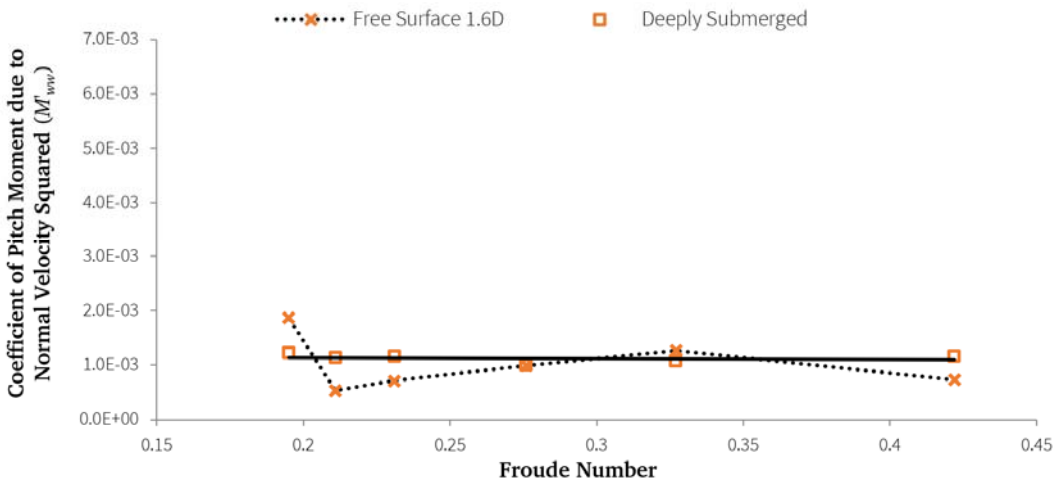

Figure 4-42 SUBOFF w/ Sail, M'_{ww} a function of Fr_L and H^*

Both coefficients $M'_{w|w|}$ and M'_{ww} show a drop in value for lower Fr_L, decreasing to ~65% of the deeply submerged value at Fr_L 0.211. This implies that each has a minor significance (0.32-0.45) to the overall equations of motion.

4.8 Normal Force due to Level Motion at an Angle of Trim, at Various Froude Numbers

Given an imposed force Z' that leads to the conditions where a model maintains a steady speed, angle of trim and submergence:

$$u = U_0 cos\theta; \dot{u} = 0 \tag{4.28}$$

$$w = U_0 sin\theta; \dot{w} = 0 \tag{4.29}$$

$$q = 0; \dot{q} = 0 \tag{4.30}$$

Equation 3.15 reduces to:

$$Z' = Z'_\star \, cos^2\theta + Z'_w \, cos\theta sin\theta + Z'_{|w|} cos\theta|sin\theta| + Z'_{ww} \, sin^2\theta + Z'_{w|w|} sin\theta|sin\theta| \tag{4.31}$$

Allowing for the influence of the free surface:

$$Z'(\boldsymbol{\eta}) = Z'_\star(\boldsymbol{\eta}) cos^2\theta + Z'_w(\boldsymbol{\eta}) \, cos\theta sin\theta + Z'_{|w|}(\boldsymbol{\eta}) cos\theta|sin\theta|$$

$$+Z'_{ww}(\boldsymbol{\eta}) sin^2\theta + Z'_{w|w|}(\boldsymbol{\eta}) sin\theta|sin\theta| \tag{4.32}$$

4.8.1 Coefficient Evaluation

As was the case for pitch moment, the inclusion of two different terms to adequately describe the asymmetry in the normal force between trim up and trim down was assessed. Equations 4.33 and 4.34 are produced by dropping the terms $Z'_{|w|}$ and Z'_{ww}respectively from Equation 4.32.

$$Z'(\boldsymbol{\eta}) = Z'_\star(\boldsymbol{\eta}) \cos^2\theta + Z'_w(\boldsymbol{\eta}) \, cos\theta sin\theta +$$

$$+Z'_{ww}(\boldsymbol{\eta})sin^2\theta + Z'_{w|w|}(\boldsymbol{\eta})sin\theta|sin\theta| \quad (4.33)$$

$$Z'(\boldsymbol{\eta}) = Z'_{\star}(\boldsymbol{\eta})cos^2\theta + Z'_{w}(\boldsymbol{\eta})\,cos\theta sin\theta + Z'_{|w|}(\boldsymbol{\eta})cos\theta|sin\theta|$$

$$+Z'_{w|w|}(\boldsymbol{\eta})sin\theta|sin\theta| \quad (4.34)$$

Utilising the detailed series of simulations at different angles of trim that was conducted at a submergence of $1.6D$ / Fr_L 0.422, the results obtained for the non-dimensional normal force are plotted against angle of trim as Figure 4-43 and Figure 4-44, with the curves fitted to Equations 4.33 and 4.34 respectively:

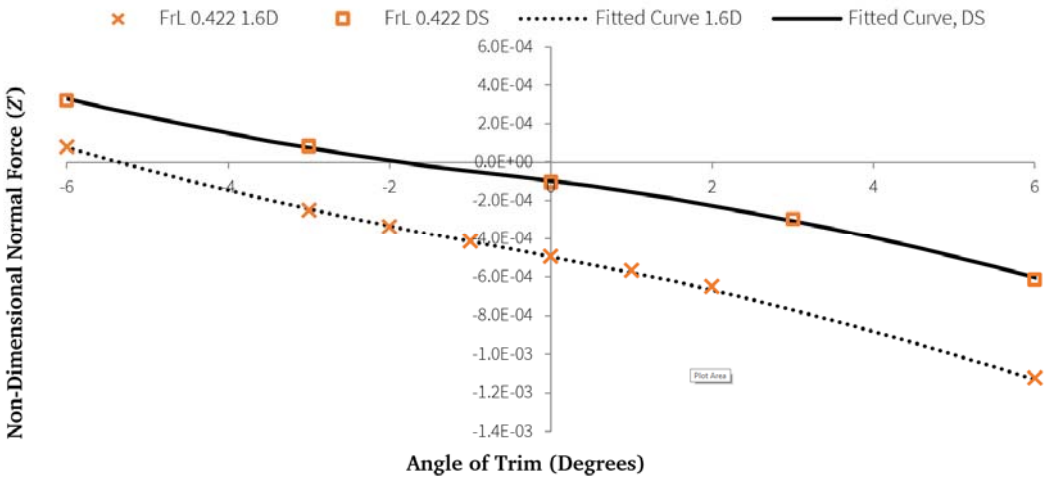

Figure 4-43 Z' as a function of Trim Angle, Fr_L 0.422
Fitted to Equation 4.33

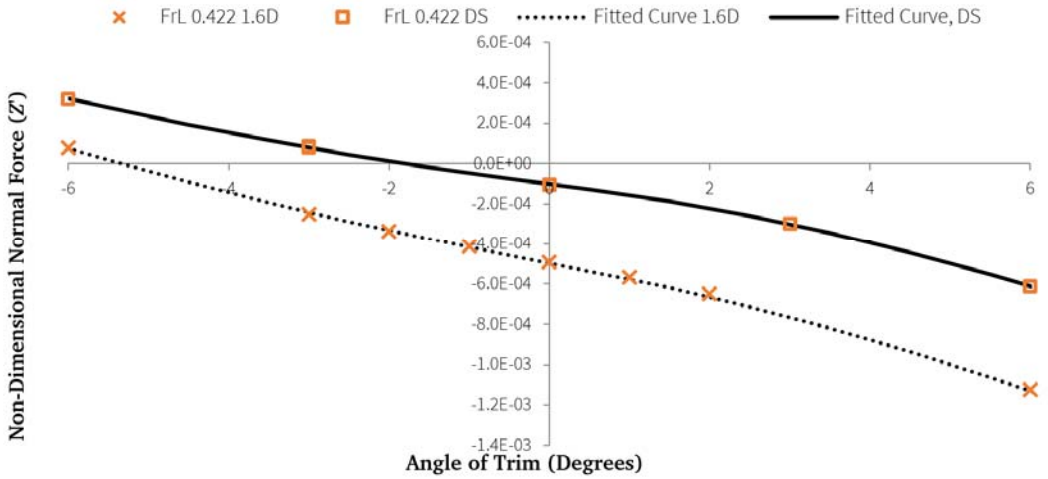

Figure 4-44 Z' as a function of Trim Angle, Fr_L 0.422
Fitted to Equation 4.34

Both equations produce visually acceptable results, and the total residual error in the fit is also quite similar. For consistency with the results for pitch moment, it was decided that the $Z'_{|w|}$ term would be eliminated; all Figures from here on are derived using a least squares fit of the available data to Equation 4.33.

4.8.2 $Z'_\star$ – Coefficient of Normal Force as a Function of u^2

$Z'_\star$ is plotted in Figure 4-45 below across a range of Froude Numbers and at different depths of submergence. The greater number of results for the zero degree cases were utilised to sketch a more accurate curve which provide the results with a degree of context.

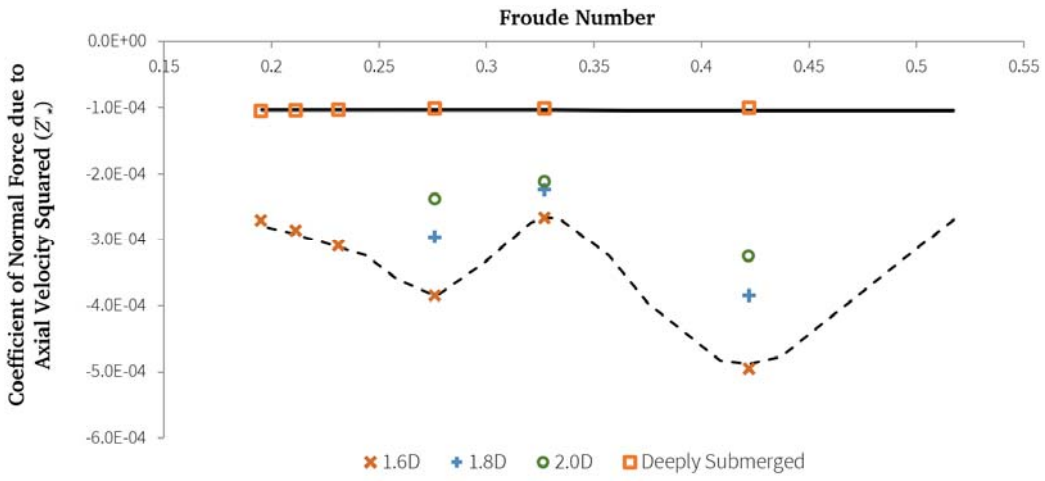

Figure 4-45 SUBOFF w/ Sail, $Z'_\star$ as a function of $H^\star$ and Fr_L

The change in normal force due to the near surface is large and sustained over the speed range of interest between Fr_L 0.200 and Fr_L 0.250, and the shape of the plot suggests that it will remain so at lower Froude Length Number. The sensitivity of the equations of motion to $Z'_\star$ is 1.203, resulting in a significance of between 2.5 and 3.0 across the range of interest. It will be necessary to treat $Z'_\star$ as $Z'_\star(\boldsymbol{\eta})$.

4.8.3 Z'_w – Coefficient of Normal Force as a Function of uw

In Figure 4-46, the results obtained for Z'_w are plotted across the range of Froude Numbers simulated:

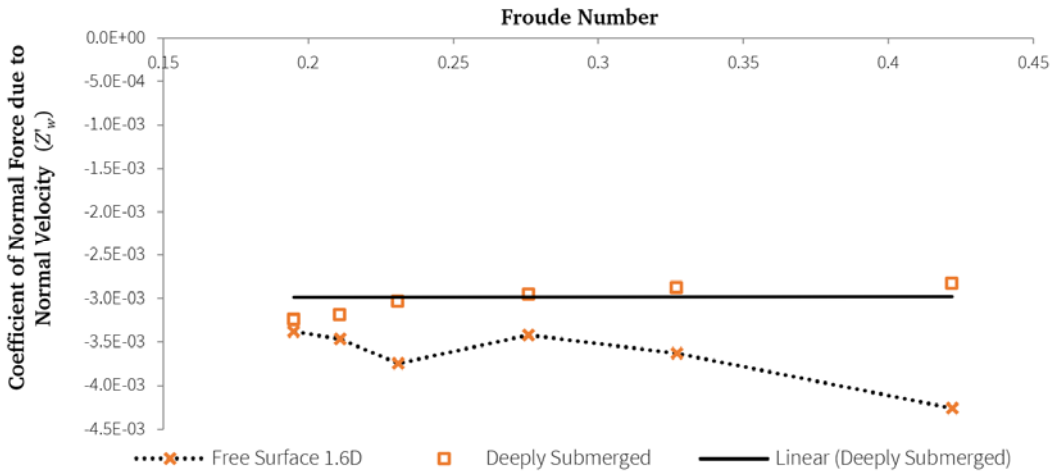

Figure 4-46 SUBOFF w/ Sail, Z'_w as a function of $H^\star$ and Fr_L

Similarly to M'_w, the additional force due to being in the near surface is a small fraction of the deeply submerged force — in this case increasing from approximately 0 to around 20% within the region of interest — but again a significant component in terms of the overall value for Z'. With a nominal sensitivity of 1.290 obtained from Table 3-1, this coefficient will have minor significance (up to 0.35).

A degree of variability (~10%) in the coefficient values obtained in the deeply submerged case is noticeable in Figures 4-46 through 4-48. This suggests there a degree of uncertainty regarding these figures in both the deep and near surface cases for these coefficients.

4.8.4 $Z'_{w|w|}, Z'_{ww}$ – Coefficients of Normal Force as a Function of $w|w|$ and w^2

$Z'_{w|w|}$ and Z'_{ww} are show in Figure 4-47 and Figure 4-48 respectively, plotted at the same vertical scale against Froude Number, in order to show the relative magnitude of each.

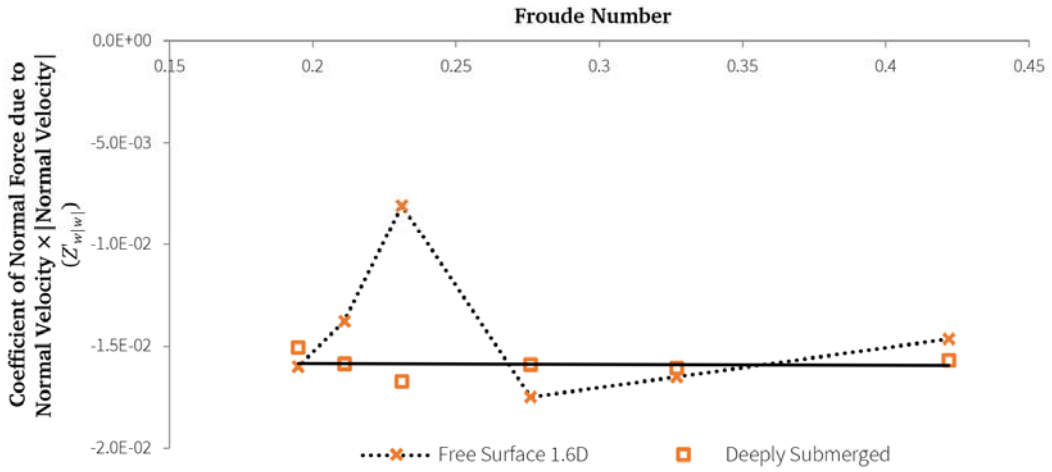

Figure 4-47 SUBOFF w/ Sail, $Z'_{w|w|}$ as a function of H^* and Fr_L

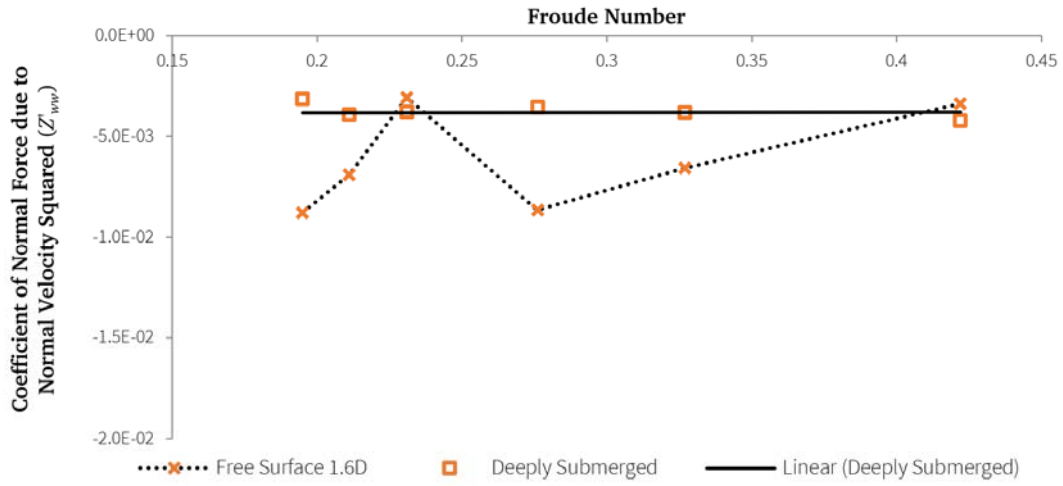

Figure 4-48 SUBOFF w/ Sail, Z'_{ww} as a function of H^* and Fr_L

Both coefficients are more erratic than the corresponding terms in pitch moment, with substantial variance across the range of interest; both terms should be treated as being of primary significance in modelling near surface effects.

4.9 Summary

4.9.1 Significance of Coefficients

Modelling of the SUBOFF hull form, with and without a sail appended, was undertaken, verified and validated against known data from physical model experiments. A preliminary series of tests was conducted at level trim under steady conditions, for a range of Froude Length Numbers and different submergences. This series showed that the change in axial force, normal force, and pitch moment form smooth curves with Froude Length Number, and vary exponentially with submergence. Finally, an extended series of tests was conducted across a larger range of Froude Length Number, and including variation in trim. The results of these tests were utilised to plot the effect of the near surface at different Froude Length Number across the set of velocity based vertical plane coefficients. These results were combined with the nominal sensitivity of the equations of motion to each coefficient to determine for which coefficients the near surface effects were significant to model, which are of a more minor significance, and which can be neglected in most circumstances. These are summarised in Table 4-13 below.

Table 4-13 Relative Significance of Various Coefficients

Primary Significance (> 0.5)
$Z'_{\star}\ Z'_{ww}\ Z'_{w\|w\|}$
Minor Significance (0.1 - 0.5)
$M'_{w}\ M'_{w\|w\|}\ M'_{ww}\ Z'_{\dot{w}}$
Conditional Significance (above $Fr_L > 0.25$)
$X'_{\star}\ M'_{\star}$
Minimal Significance (< 0.1)
$X'_{w}\ \ X'_{ww}$

4.9.2 Considerations regarding $Z'_{\dot{w}}$, $M'_{\dot{w}}$ and trim

Under the assumption of steady state conditions, both $Z'_{\dot{w}}$ and $M'_{\dot{w}}$ only occur near the surface when there is an angle of trim. However, in order to evaluate the acceleration coefficients $Z'_{\dot{w}}$ and $M'_{\dot{w}}$, the steady state condition must inherently be set aside in order to have acceleration occur. As soon as an acceleration $\dot{\boldsymbol{w}}' \neq 0$ occurs over some short time period, $\boldsymbol{w}'$ now has a magnitude that is independent of its angle of trim. It cannot reasonably be assumed that either $Z'_{\dot{w}}$ or $M'_{\dot{w}}$, due to some small rate of motion in the z-axis is going to be the same as the $Z'_{\dot{w}}$ or $M'_{\dot{w}}$, due to a steady rate of trim. A steady rate of trim establishes a change in the wave profile over the vessel, and thus also in the flow and pressure around the vessel; this does not occur in the same manner with a small z-axis motion.

Thus the $Z'_{\dot{w}}$ and $M'_{\dot{w}}$ values determined above as a function of $\boldsymbol{\eta}$, while correct for the conditions under which they were assessed, are actually the combination of two

distinct coefficients in the quasi-steady state required to assess the acceleration coefficients. One of these coefficients in each case is time-invariant under the assumptions of quasi steady motion and is perhaps best referred to as Z'_θ or M'_θ — delineating their correspondence to the angle of trim relative to the surface. The other coefficient in each case is dependent upon there being a small but non-zero velocity for some non-zero time period, such that the actual change in $\boldsymbol{\eta}$ is negligible.

Further to this, it is the velocity dependant Z'_w and M'_w that are more similar in nature to the Z'_w and M'_w utilised to describe deeply submerged operations than the position dependant Z'_θ and M'_θ. As such it would be ideal to retain the symbols Z'_w and M'_w for that component. Note that these components do remain sensitive to submergence and Froude Number. Under quasi-steady conditions, limited to the vertical plane, the relationships can be stated:

$$Z'_w(Fr_L, H^\star) = Z'_{w,\theta}(\boldsymbol{\eta}) - Z'_\theta(Fr_L, H^\star, \theta) \tag{4.35}$$

$$M'_w(Fr_L, H^\star) = M'_{w,\theta}(\boldsymbol{\eta}) - M'_\theta(Fr_L, H^\star, \theta) \tag{4.36}$$

That is – the values examined above as Z'_w and M'_w in steady state conditions contain, when that condition is abandoned for the quasi-steady constraints, two separable components one of which is dependent upon θ, and the other which is not.

In Chapter 6, values for $Z'_w(Fr_L, H^\star)$ and $\mathrm{M}'_w(Fr_L, H^\star)$ will be determined utilising a quasi-steady state methodology. These values through that process can then be subtracted out of those identified in this chapter to provide the coefficients due to trim relative to the surface $Z'_{w,\theta}(\boldsymbol{\eta})$, $M'_{w,\theta}(\boldsymbol{\eta})$ if those are required. However, in order to have confidence in that data, the general technique to be utilised is validated in Chapter 5.

5. VALIDATION OF HORIZONTAL PLANAR MOTION

This chapter examines the capacity of CFX to model the forces and moments exerted upon both unappended and appended submarine models undergoing pure sway motion in a horizontal planar motion, in both the deeply submerged and near surface conditions. The derived coefficients are compared to published experimental data, as well as the values obtained in Chapter 4.

5.1 Objectives and Methodology

- Validate CFD against accepted experimental results for Pure Sway motion in the deeply submerged case.

5.2 Theory

In a pure sway test, the experimental model is moved sinusoidally in the y-axis. There is no rotation of the model. The forward velocity is held constant. The motion is characterised by the non-dimensional amplitude $A^\star$ and the non-dimensional frequency ω', which expresses the frequency of oscillation in terms of the oscillations per vessel length travelled.

> Note: Using $A^\star = \frac{A}{D}$ to describe the scale of motion provides for consistency with the usage of $H^\star = \frac{H}{D}$. In both cases, D is a more logical non-dimensionalisation factor than L. However it is recognised that this introduces some complexity when interacting with the prime notation utilised elsewhere. A' is thus utilised in equations where $A^\star \frac{D}{L}$ would otherwise have to be written.

For clarity:

$$A^\star = \frac{A}{D} = A' \frac{L}{D} \tag{5.1}$$

$$\omega' = \frac{\omega L}{U} \tag{5.2}$$

where A is the amplitude of oscillation and ω is the frequency.

Under these conditions, the position of the model on the global Y-axis can be written:

$$\boldsymbol{y'} = \frac{y}{L} = A' \, sin(\omega' \, t') \tag{5.3}$$

The velocity along that axis:

$$\boldsymbol{v'} = \frac{v}{U} = A'\omega' \, cos(\omega' \, t') \tag{5.4}$$

The acceleration along that axis:

$$\dot{\boldsymbol{v}}' = \frac{\dot{v}L}{U} = -A'\omega'^2 \, sin(\omega' \, t') \tag{5.5}$$

The velocity of the model in the x-direction is assumed, for small $A^\star$:

$$\boldsymbol{u'} = \frac{\boldsymbol{u}}{U} = 1 \tag{5.6}$$

All other accelerations and velocities are zero, and weight and buoyancy are equal. The orientation of the model x-axis remains aligned with the global X-axis.

Under these conditions, the equation for lateral force reduces to:

$$Y'(t) = (Y'_{\dot{v}} - m')\dot{\boldsymbol{v}}' + Y'_{\star}\boldsymbol{u}'^2 + Y'_{v}\,\boldsymbol{u}'\boldsymbol{v}' + Y'_{v|v|}\,\boldsymbol{v}'|\boldsymbol{v}'| \qquad (5.7)$$

As the vessel is symmetrical about the zx-plane, $Y'_{\star}u'^2 = 0$. Also, as the lateral velocity $A'\omega'$ is small, the effect of the $Y'_{v|v|}\boldsymbol{v}|\boldsymbol{v}|$ and $N'_{v|v|}\boldsymbol{v}|\boldsymbol{v}|$ terms remain small and may be neglected.

Taking these notes into consideration and substituting in:

$$Y'(t) = (Y'_{\dot{v}} - m')A'\omega'^2\,sin(\omega'\,t') + Y'_{v}\boldsymbol{u}'A'\omega'\,cos(\omega'\,t') \qquad (5.8)$$

Similarly, for Yaw Moment:

$$N'(t) = (N'_{\dot{v}} - m'x'_G)A'\omega'^2\,sin(\omega'\,t') + N'_{v}\boldsymbol{u}'A'\omega'\,cos(\omega'\,t') \qquad (5.9)$$

5.3 Reference Physical Model Test Data

Roddy (1990) reports that a series of pure sway reference model tests that were conducted with their 4.356m model in the deeply submerged condition. Detailed results for the VPMM tests conducted to establish the values for $Y'_{\dot{v}}$ and $N'_{\dot{v}}$ (Feldman, 1995) do not appear to have been published. Final calculations of the resultant coefficients are provided and form an important comparison point. Values derived for Y_{v}' and N_{v}' are claimed to be accurate within 5% and those for $Y'_{\dot{v}}$ and $N_{\dot{v}}'$ within 7%. The relevant results are copied below in Table 5-1:

Table 5-1 Coefficients for Relevant Configurations Roddy (1990)

Item	Config 3 Bare Hull	Config 4 Sail Appended
Y'_{v}	-0.005948	-0.023008
$Y'_{\dot{v}}$	-0.013270	-0.015042
N'_{v}	-0.012795	-0.015534
$N'_{\dot{v}}$	-0.000202	-0.000008

The experimental values for $Y'_{\dot{v}}$ and $N'_{\dot{v}}$ were determined by oscillation at frequencies of 1.12 and 2.2 radians per second with *zero* forward velocity.

5.4 CFD Modelling

The existing CFD model developed in Chapter 4 has been modified slightly for use in this experiment. As motion in the y-axis results in asymmetry in the zx-plane, the mesh has been reflected across this centreplane and the symmetry boundary removed. Additionally, a mesh configured without the sail (See Figure 5-1) has been constructed by a process of simplification, in order to assess the performance of the CFD against more than a single data point. Given that these processes consisted of a

reflection and a simplification, the mesh independence study and validation detailed in Chapter 4 were not repeated for this configuration.

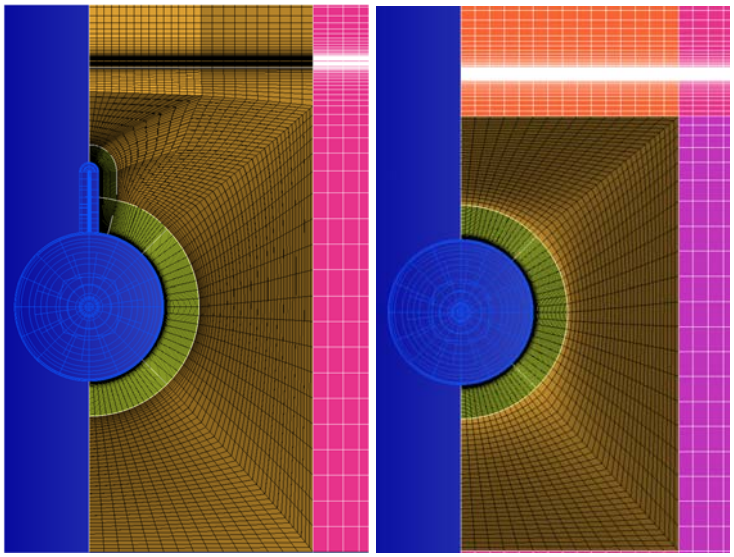

Figure 5-1 Mesh Cross-section showing Simplification of Existing Mesh (Half Mesh Shown)

a) Mesh with Sail b) Mesh without Sail

5.4.1 Deeply Submerged HPMM Simulation

In order to compare numerical predictions to the results measured in the deeply submerged experiments, pure sway simulations have been conducted at zero forward velocity. In addition, as the results are sensitive to oscillation frequency, numerical simulation was conducted at the two distinct frequencies cited in Roddy (1990).

Series 5-1 (4 cases)

Reynolds Number	N/A
Frequency (rad.s^{-1})	1.12, 2.20
Configurations	Bare Hull, Sail Appended
Submergence	Deep

These cases were run until the initial conditions had dissipated and a steady periodic response was established, typically requiring 8-10 seconds of simulated time.

In order to conduct these simulations in the time domain, an exploration of the effect of timestep on accuracy and stability was conducted. A simulation of a submarine in cross flow was conducted with the time step adjusted each step such that it represented 1/48th of the time remaining until 2 seconds of simulated time had passed. After the initial instability, the lateral force trended towards a fixed value, before becoming increasingly unstable as the timesteps reduced further. Figure 5-2 illustrates this process, showing the effect of time step frequency upon the resultant force. A fixed timestep of 1/96th of a second was selected in order to balance speed, solution stability (and ease of creating 1/24th second frames for visualisation). Each

timestep was iterated between 2 and 5 times, to achieve a residual RMS convergence of less than 10^{-4}.

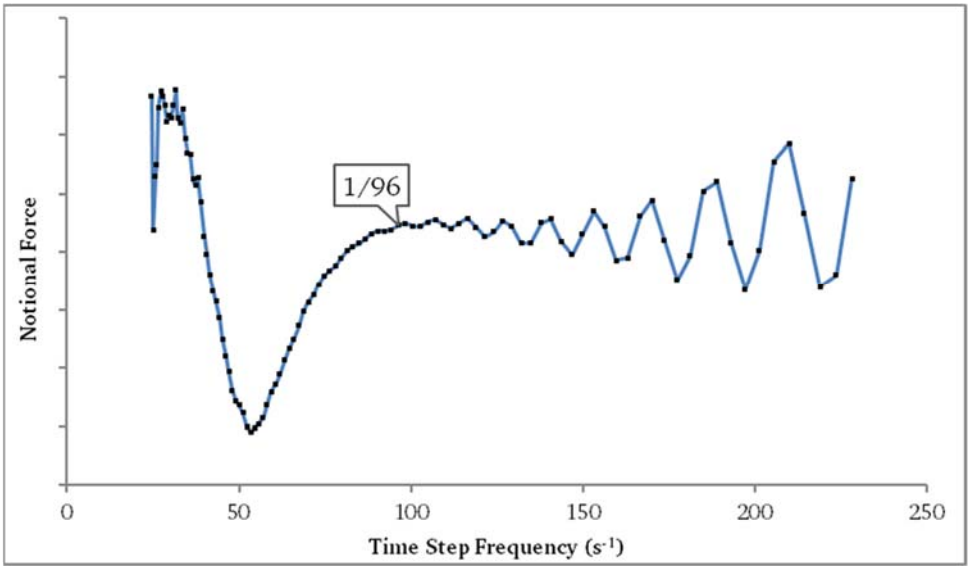

Figure 5-2 Decay in Time Domain Solution Stability with Decreasing Timestep

Results for the forces and moments modelled were collated and analysed for the final full period of motion, and are presented below.

5.5 Results

5.5.1 Validation for Bare Hull

Roddy (1990) indicates that the PMM frequencies utilised were 1.112 rad.s^{-1} and 2.220 rad.s^{-1}. These tests were conducted at zero forward velocity. Simulations were conducted at both frequencies, and the results are tabulated in Table 5-2.

Table 5-2 Bare Hull, Running Deeply Submerged, Comparison against Roddy (1990)

Source	Method	Configuration	$H_\star$	Re	ω	A'	$Y'_{\dot{v}}$	$N'_{\dot{v}}$
Roddy	Experimental	Bare Hull	Deep	0.0	-	-	-0.013270	0.000202
Polis	Numerical	Bare Hull	Deep	0.0	2.200	0.02296	-0.015847	0.000013
						Difference:	0.002577	0.000189
Polis	Numerical	Bare Hull	Deep	0.0	1.112	0.02296	-0.015873	0.000013
						Difference:	0.002603	0.000189

5.5.2 Validation with Sail Appended

Roddy (1990) indicates that the PMM frequencies utilised were 1.112 rad.s^{-1} and 2.220 rad.s^{-1}. A simulation was conducted at 1.257 rad.s^{-1}, and the results are tabulated in Table 5-3.

Table 5-3 Sail Appended, Running Deeply Submerged, Comparison against Roddy (1990)

Source	Method	Configuration	$H_\star$	Re	ω	A'	$Y'_{\dot{v}}$	$N'_{\dot{v}}$
Roddy	Experimental	Sail Appended	Deep	0.0	-	-	-0.015042	0.000008
Polis	Numerical	Sail Appended	Deep	0.0	1.257	0.02296	-0.016488	0.000225
						Difference:	0.001446	-0.000217

These results suggest the simulation is slightly underestimating the effect of appending the sail to the hull when compared to Roddy's figures, and in general the estimates for are between 10 and 15% above those measured.

5.6 Summary

SUBOFF was modelled in Pure Sway motion in order to validate the performance of the CFD arrangement to be utilised in Chapter 6. The capacity of CFX to model the forces and moments exerted upon both unappended and appended submarine models undergoing pure sway motion in a horizontal planar motion, in both the deeply submerged and near surface conditions was demonstrated.

This validation is leveraged in Chapter 6 to describe and assess two novel methodologies for the assessment of coefficients of motion for a submarine operating near the surface.

6. PLANAR MOTION METHODS FOR ANALYSIS NEAR A FREE SURFACE

6.1 Objectives and Methodology

This chapter describes two novel methodologies by which additional manoeuvring coefficients for a submarine near the free surface can be obtained. The intent is to compare possible methodologies to discern the effect of the free surface on those coefficients. These methods are validated against established techniques in deep water and then utilised to determine the value of the acceleration coefficients $M_{\dot{w}}$ and $Z_{\dot{w}}$ for the SUBOFF model at a submergence of $1.65D$. In addition, values for M_w and Z_w are derived for the level trim condition, in order that the effects of trim near the free surface can be separated from the effects of flow in the z-axis near the free surface. Consideration of the sensitivity of the manoeuvring model to variation in these manoeuvring coefficients is then given in order to assess the significance that should be placed upon the evaluation of these coefficients for modelling submarine motion in the near surface region, and the rate of decay with depth tested.

In order to determine the value of $M_{\dot{w}}$ or $Z_{\dot{w}}$ in the deeply submerged state, a pure heave experiment could be carried out. This would normally have an amplitude in the order of the diameter of the submarine, and potentially substantially greater. However, in the near surface region, there is a measurable change with depth in the forces and moment exerted on a moving submarine. Given a motion in the order of the diameter of the submarine induces a change in submergence of that magnitude, this introduces a number of confounding elements into the response being measured. While the change in depth itself *may* be able to be accounted for once the nature of the variation of each coefficient with depth is established, the motion involved would also significantly alter the form of the wavetrain produced, further disguising any results.

The first proposed methodology for resolving this conundrum, Fractional Planar Motion (FPM), is a variation on the established PMM testing for submarines, where the amplitude of motion is reduced to a small fraction of the diameter of the submarine to minimise the effects of change of depth. The assumption is that the whole manoeuvre can be conducted over such a small depth change that the coefficients remain constant during the manoeuvre.

The second methodology — Sudden Linear Acceleration (SLA) — provides a rapid measure of the acceleration coefficient utilising linear acceleration from a steady state condition. These methodologies are outlined in Sections 6.2 and 6.3 respectively. Section 6.4 assesses the two methods in comparison to each other, and Section 6.5 details the application of FPM in the determination of the coefficients $M_w, M_{\dot{w}}, Z_w$ and $Z_{\dot{w}}$ for the bare hull SUBOFF configuration, and the change in these coefficients with depth.

6.2 Fractional Planar Motion

Fractional Planar Motion is the numerical modelling of the oscillation of a submarine, wherein the motion is limited in amplitude to a small fraction of the diameter of the submarine. This prescribed motion is specifically intended to address the issues involved in the assessment of coefficients of motion in the near surface, and to do so by taking advantage of the specific characteristics of numerical modelling. In the computational environment, signal noise is substantially reduced, allowing very small forces and moments to be measured distinctly. Position may be controlled to the limits of machine precision; imposed forces are effectively unlimited, with no mechanical flexure; no compromises are required to 'mount' the model; and the results can be obtained without blockage effects. The result is that far smaller amplitude motions can be utilised in numerical modelling to obtain an outcome than would be feasible utilising a physical model.

Although this concept is applicable to all oscillating PMM type motions (Pure Sway, Pure Yaw, Pure Heave, Pure Pitch), this thesis will focus upon Pure Heave, in line with the general thrust of this work.

Pure Heave motion is generally conducted deeply submerged at a fixed forward velocity with a sinusoidal oscillation in the vertical axis. In this instance, only the case where the submarine x-axis is aligned with the global X-axis is considered. For small values of $\boldsymbol{w}$, the velocity U is simply the axial velocity $\boldsymbol{u}$, and higher order terms in $\boldsymbol{w}$ can be neglected. Thus, as Equation 6.1:

$$\boldsymbol{u}' = \frac{\boldsymbol{u}}{U} = 1; \boldsymbol{w}'(t) = \frac{\boldsymbol{w}}{U} = A'\omega' \cos(\omega' t'); \boldsymbol{v}' = \boldsymbol{q}' = \boldsymbol{r}' = 0 \qquad (6.1)$$

> Note: As per Chapter 5, discussion of amplitude in the text will refer to amplitude as a proportion of diameter ($A^\star$) as this reference is more useful in characterising similar motion across different submarines, and consistent with the practice of referring to submergence as $H^\star$. However, due to the non-dimensionalisation scheme, non-dimensionalisation by length (A') is used in the equations. The conversion is as follows:

$$A^\star = \frac{A}{D} = A'\frac{L}{D} \qquad (6.2)$$

Allowing also that the control vector $\boldsymbol{\tau} = 0$, the equations of motion for normal force and pitch moment respectively reduce to:

$$\boldsymbol{Z}'(\boldsymbol{t}) = Z'_{\star}\boldsymbol{u}'^2 + Z'_{w}\boldsymbol{u}'\boldsymbol{w}' + Z'_{w|w|}\boldsymbol{w}'|\boldsymbol{w}|' + (Z'_{\dot{w}} - \boldsymbol{m}')\dot{\boldsymbol{w}}' \qquad (6.3)$$

$$\boldsymbol{M}'(\boldsymbol{t}) = M'_{\star}\boldsymbol{u}'^2 + M_{w}\boldsymbol{u}'\boldsymbol{w}' + M'_{w|w|}\boldsymbol{w}'|\boldsymbol{w}|' + (M'_{\dot{w}} - \boldsymbol{m}'x_G)\dot{\boldsymbol{w}}' \qquad (6.4)$$

These are the same equations except oriented in the vertical plane as those used in Chapter 5 (Equations 5.8, 5.9). In order to consider the use of Fractional Planar Motion for analysis in the near surface region, it must first be shown that doing so in

the deeply submerged region results in minimal differences from the same simulations conducted at more commonly accepted amplitudes.

To show this, a series of numerical simulations was conducted using SUBOFF in the bare hull configuration. Each simulation was conducted at otherwise identical conditions, but $A^{\star}$ was varied from 0.8 to 0.0125 in four geometric steps. Values for $Z'_w, M'_w, Z'_{\dot{w}}$ and $M'_{\dot{w}}$ were obtained by fitting curves to the functions above, noting that in this instance the asymmetric terms were zero due to symmetry. The results of these simulations are presented in Figure 6-1 and Figure 6-2 and tabulated in Table 6-1. Note that in these figures the x-axis is logarithmic in order to appropriately display the results of the geometric progression.

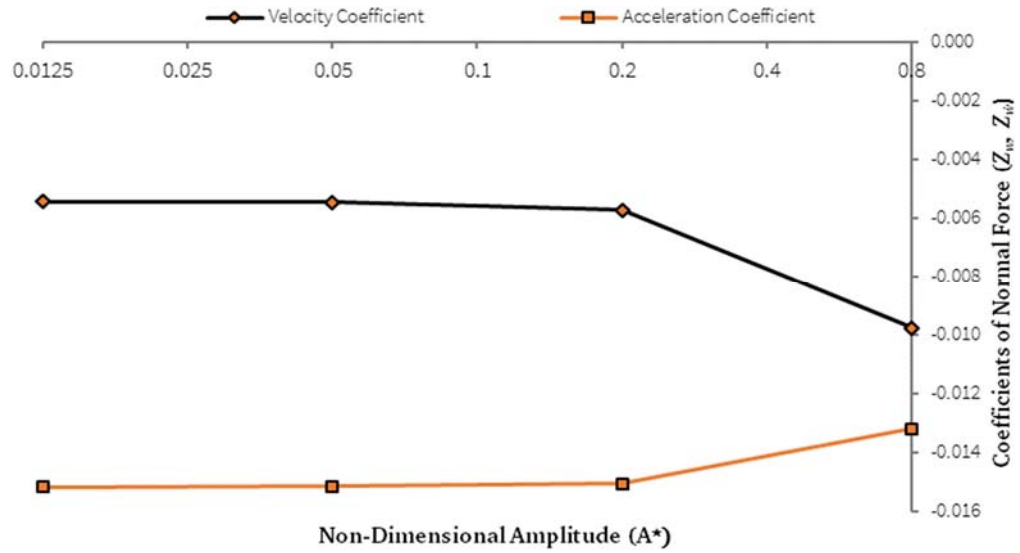

Figure 6-1 Log-Linear plot of Normal Force Coefficients as a function of Amplitude, Deeply Submerged

All tests Re=1.6×10^7, Deeply submerged, ω' =0.5, SUBOFF in Bare Hull Configuration

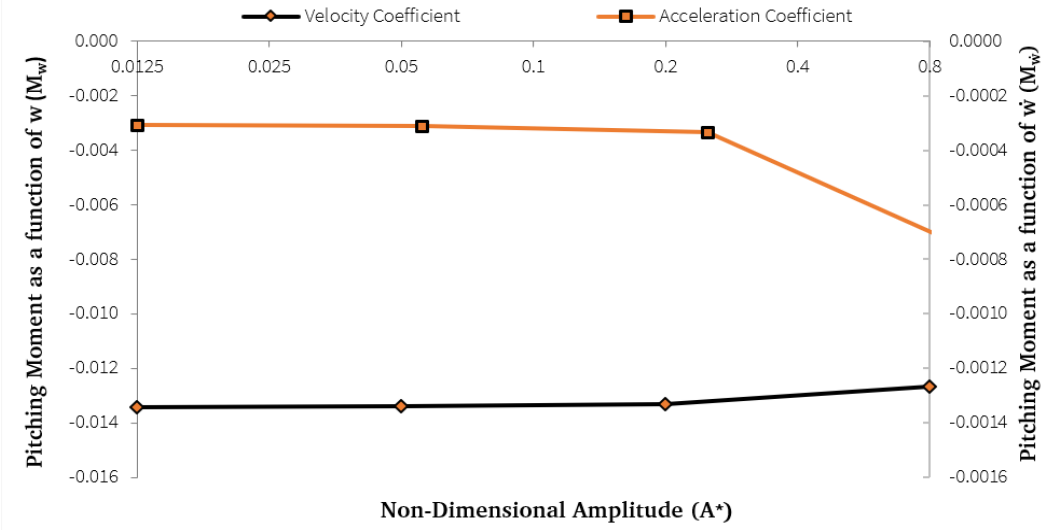

Figure 6-2 Log-Linear plot of Pitch Moment Coefficients as a function of Amplitude, Deeply Submerged

All tests Re=1.6×10^7, Deeply submerged, ω' =0.5, SUBOFF in Bare Hull Configuration

All four coefficients show little change over the range $0.0125 \leq A^{\star} \leq 0.2$. However, for values of $A^{\star}$ greater than 0.2, the coefficients become functions of $A^{\star}$. Closer inspection of the results indicates that there is also a marked increase in the higher order terms for these values of $A^{\star}$, due to the large angle of attack resulting in a high degree of nonlinearity.

Table 6-1 Manoeuvring Coefficients at various Amplitudes

$A^{\star}$	Z'_w	$Z'_{\dot{w}}$	M'_w	$M'_{\dot{w}}$
0.0125	-0.005435	-0.015162	-0.013408	-0.000307
0.050	-0.005467	-0.015157	-0.013397	-0.000311
0.20	-0.005728	-0.015065	-0.013324	-0.000334
0.8	-0.009775	-0.013193	-0.012672	-0.000801

In summary, in the deeply submerged case, each of the coefficients examined behaves in a stable and predictable manner as amplitude is reduced, with little variation found except where high angle of attack introduces substantial higher order effects. Note that were ω' not held constant, but rather reduced with increasing amplitude, high angle of attack effects could be avoided.

6.2.1 Effect of variation of Oscillation Frequency when Deeply Submerged

As noted in Chapter 2, there is a well described relationship between the non-dimensionalised oscillation frequency and the various coefficients of motion for a submarine. Typically, as ω' is reduced below 1.0, the coefficients tend towards a 'zero frequency' value.

In order to show that this relation holds under conditions of fractional amplitude, a series of numerical simulations was conducted using SUBOFF in the bare hull configuration. Each simulation was conducted at otherwise identical conditions, but ω' was varied from 0.625 to 1.6 in four geometric steps. Values for $Z'_w, M'_w, Z'_{\dot{w}}$ and $M'_{\dot{w}}$ were obtained by fitting curves to the functions above, noting that in this instance the asymmetric terms were zero due to symmetry. The results of these simulations are presented in Figure 6-3 and Figure 6-4, and tabulated in Table 6-2.

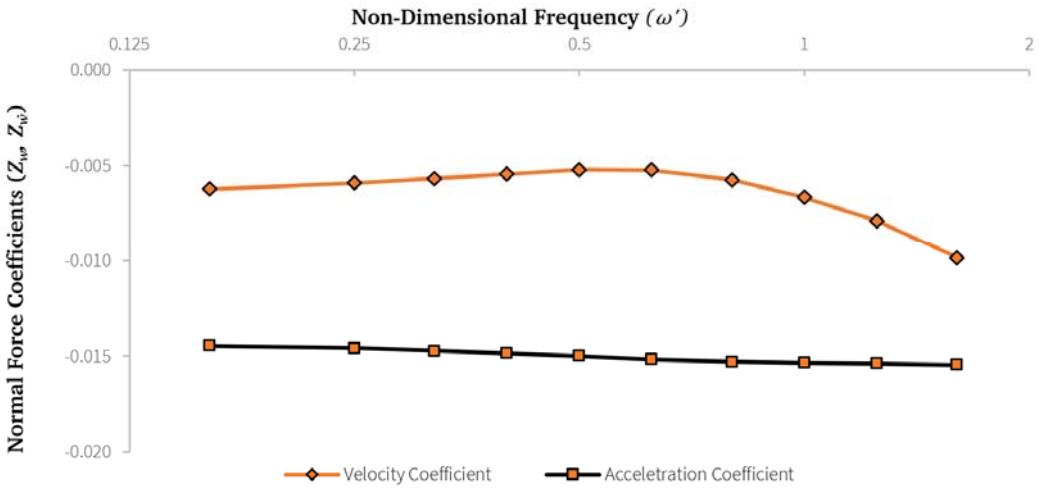

Figure 6-3 Log-Linear plot of Normal Force Coefficients as a function of Frequency, Deeply Submerged

All tests Re=1.6×10^7, Deeply submerged, $A^\star = 0.0625$, SUBOFF in Bare Hull Configuration

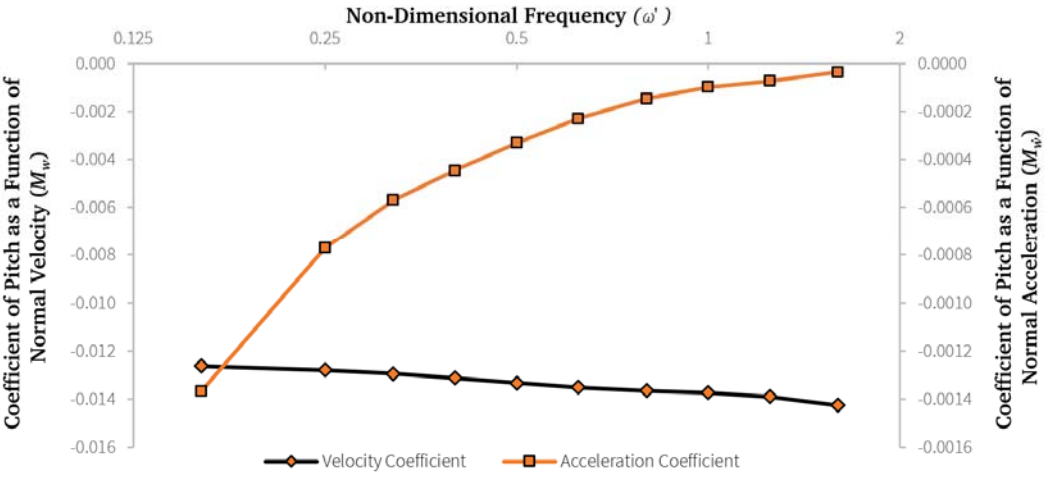

Figure 6-4 Log-Linear plot of Pitch Moment Coefficients as a function of Frequency, Deeply Submerged

All tests Re=1.6×10^7, Deeply submerged, $A^\star = 0.0625$, SUBOFF in Bare Hull Configuration

Table 6-2 Manoeuvring Coefficients at Different Frequencies

ω'	Z'_w	$Z'_{\dot{w}}$	M'_w	$M'_{\dot{w}}$
0.160	-0.006239	-0.014452	-0.012619	-0.001367
0.250	-0.005922	-0.014576	-0.012793	-0.000772
0.32	-0.005675	-0.014722	-0.012937	-0.000570
0.40	-0.005442	-0.014848	-0.013118	-0.000447
0.50	-0.005219	-0.015001	-0.013323	-0.000331
0.63	-0.005228	-0.015164	-0.013509	-0.000230
0.80	-0.005751	-0.015296	-0.013643	-0.000147
1.00	-0.006672	-0.015357	-0.013738	-0.000099
1.25	-0.007895	-0.015377	-0.013900	-0.000074
1.6	-0.009858	-0.015450	-0.014254	-0.000037

Three coefficients ($Z'_w, Z'_{\dot{w}}$ and M'_w) show a gradual approach to a 'zero frequency coefficient' where $\omega' \leq 0.5$. The values for $M'_{\dot{w}}$ show an unexpected failure to converge to a constant value with decrease in frequency, which makes establishment of a zero-frequency value somewhat challenging, suggesting this may require some further study in the deep case.

6.2.2 Near Surface Considerations

In the near surface region, all the coefficients above are necessarily considered functions of submergence. Equations 6.3, 6.4 must thus be rewritten as:

$$\boldsymbol{Z'(t)} = Z'_{\star}(H^{\star})\boldsymbol{u'^2} + Z'_{w}(H^{\star})\boldsymbol{u'w'} + Z'_{w|w|}(H^{\star})\boldsymbol{w'|w|'} + (Z'_{\dot{w}}(H^{\star}) - \boldsymbol{m'})\dot{\boldsymbol{w}}' \quad (6.5)$$

$$\boldsymbol{M'(t)} = M'_{\star}(H^{\star})\,\boldsymbol{u'^2} + M_{w}(H^{\star})\boldsymbol{u'w'} + M'_{w|w|}(H^{\star})\boldsymbol{w'|w|'} + (M'_{\dot{w}}(H^{\star}) - \boldsymbol{m'}x_G)\dot{\boldsymbol{w}}' \quad (6.6)$$

The result of this is a substantial increase in complexity. For any change in $H^{\star}$, use of these equations requires a prior understanding of how each coefficient is a function of $H^{\star}$. However, if as proposed in FPM, the change in $H^{\star}$ is small, then the change in each coefficient can be neglected. This then allows determination of each coefficient at different $H^{\star}$ to determine the relevant function of the coefficient value with $H^{\star}$.

In Chapter 4, it was found that for a submarine operating at some depth $H^{\star}$ and speed Fr, the steady state coefficient functions $Z'_{\star}(H^{\star}, Fr_L)$ and $M'_{\star}(H^{\star}, Fr_L)$ can be approximated by the forms:

$$Z'_{\star}(H^{\star}, Fr_L) = Z'_{\star} + e^{-k_z H^{\star}} Z'_{\zeta}(Fr_L) \quad (6.7)$$

$$M'_{\star}(H^{\star}, Fr_L) = M'_{\star} + e^{-k_m H^{\star}} M'_{\zeta}(Fr_L) \quad (6.8)$$

where k_z, k_m are some decay constants to be determined, $Z_{\star}, M_{\star}$ are the coefficients deeply submerged, and $Z_{\zeta}(Fr)$ and $M_{\zeta}(Fr)$ are coefficients due to the proximity of the free surface at a given Froude Length Number.

FPM offers the potential to determine similar usable approximations for each of the other coefficients.

In order to derive such data then it needs to be demonstrated in this Section that:

- The effect of reduction in amplitude in the near surface shows a trend towards a fixed value for each coefficient;
- The effect of small amplitude oscillations on the free surface are minimal and may be neglected;
- The frequency of oscillation in the near surface has a similar degree of effect upon the results as it does in the deep condition and can be accounted for in the same manner.

Unless noted otherwise, all simulations in this Section were conducted at Re 1.6×10^7. Where conducted near the free surface, submergence is $1.65D$.

6.2.3 Effect of reduction in Amplitude in the Near Surface Region

In order to examine the effects of a reduction in amplitude in the presence of a nearby free surface, a geometric series of runs was conducted, scaling the amplitude from $D/16$ through to $D/80$. The results of these simulations for the Z coefficients are presented in Figure 6-5, and for the M coefficients in Figure 6-6.

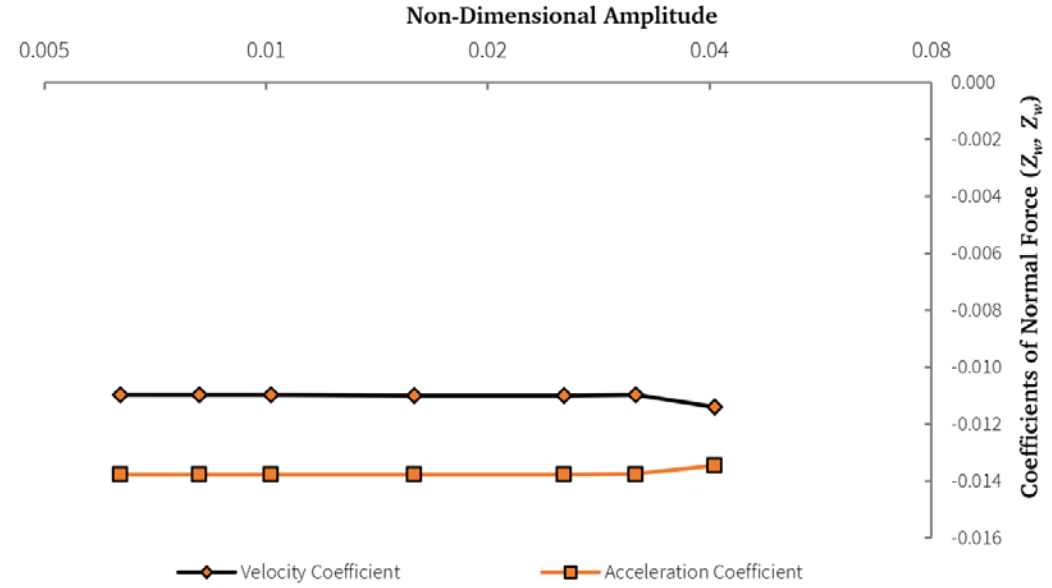

Figure 6-5 Log-Linear plot of Normal Force Coefficients as a function of Amplitude, Near Surface

All tests Fr_L =0.512, $H^\star$ =1.65, ω' =0.5, SUBOFF in Bare Hull Configuration.

These were conducted using the bare hull configuration of SUBOFF at a constant non-dimensional oscillation frequency of 0.5 and a submergence of 1.65D. The results show that both the velocity and acceleration coefficients for normal force are independent of amplitude for $A^\star < 0.031$.

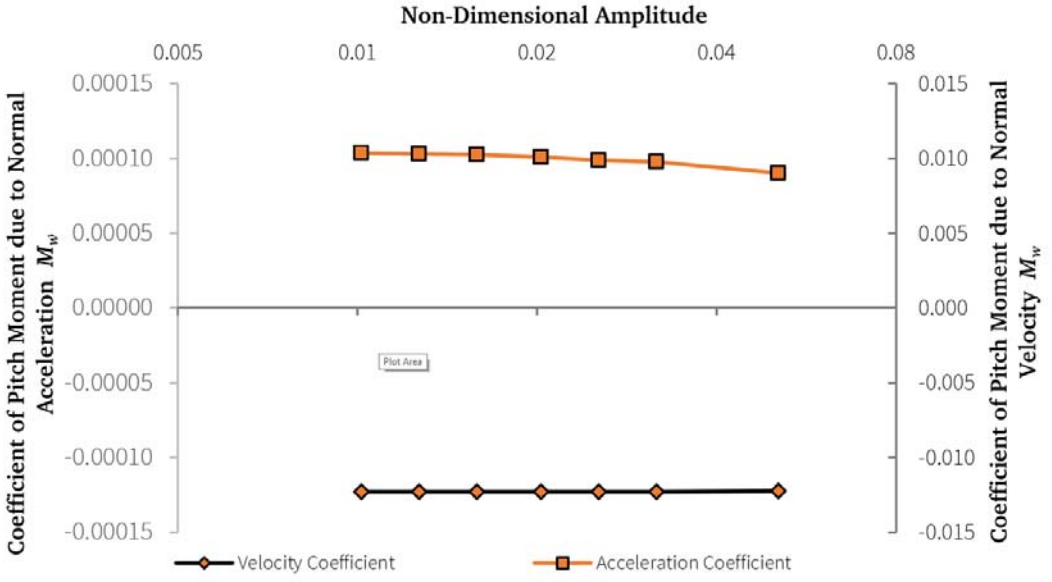

Figure 6-6 Log-Linear plot of Pitch Coefficients as a function of Amplitude, Near Surface

All tests Fr_L =0.512, $H^\star$ =1.65, ω' =0.5, SUBOFF in Bare Hull Configuration

The results show that both the velocity and acceleration coefficients for pitch moment are near independent of amplitude towards for $A^{\star} < 0.05$. This is notably different than the results obtained in the deep case.

6.2.4 Effect of small amplitude oscillations upon the free surface

To examine the effect of small scale oscillations on the free surface, a centreline wave cut is taken at the same point in the cycle from the geometric series of oscillations used in Section 1 (see Figure 6-7):

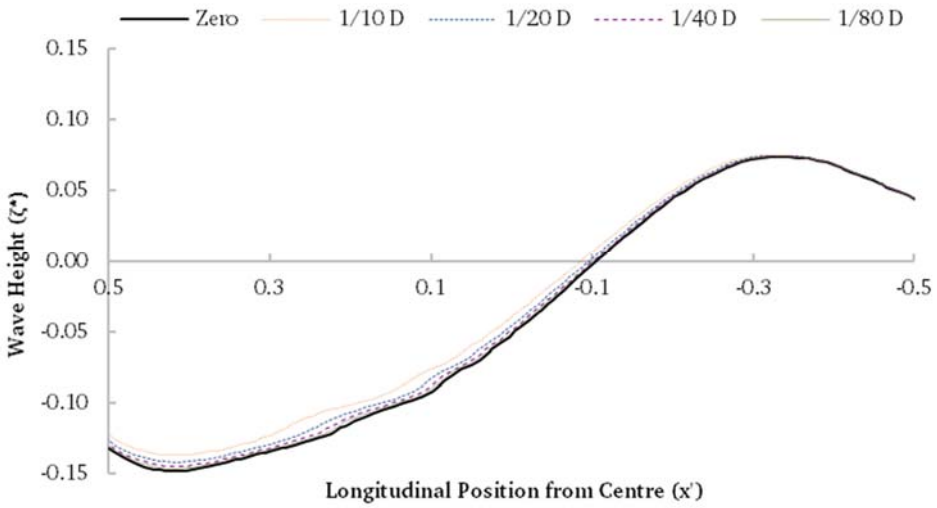

Figure 6-7 Wave Profile at Different Amplitudes of Oscillation

Fr_L =0.512, $H^{\star}$ =1.65, ω' =0.5, SUBOFF in Bare Hull Configuration

As the amplitude of oscillatory motion decreases, the variation in the wave profile above the submarine decreases. In terms of the difference from the static wave profile each case produces the same basic form and the scale of the response is approximately proportional to the amplitude of oscillation, with some longitudinal shift of the peaks and troughs occurring (see Figure 6-8).

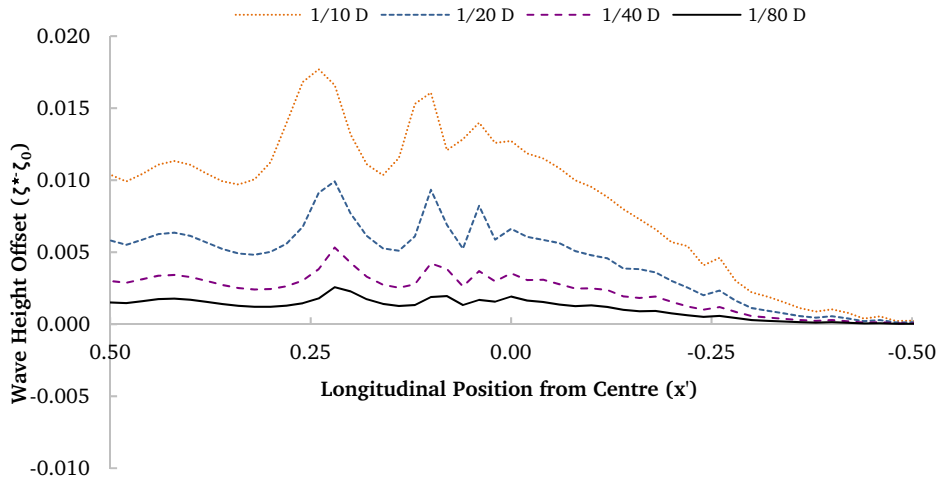

Figure 6-8 Wave Profile Offset at different Amplitudes of Oscillation

Fr_L =0.512, $H^{\star}$ =1.65, ω' =0.5, SUBOFF in Bare Hull Configuration

In all cases the change in wave profile is small, peaking at approximately 1/5th the amplitude of oscillation, and typically approximately 1/10th across the aftward 2/3rds of the vessel. Thus, the effect of small amplitude oscillations on the free surface is found minimal and hereafter neglected.

6.2.5 Significance of oscillation frequency in the near surface

In order to assess the effect of oscillation frequency, a geometric series of cases was conducted at non-dimensional frequencies between 0.5 and 8.0. Each of these was conducted with an amplitude of oscillation of $D/80$. The results for the normal force coefficients are presented below as Figure 6-9, and for pitch moment coefficients as Figure 6-10.

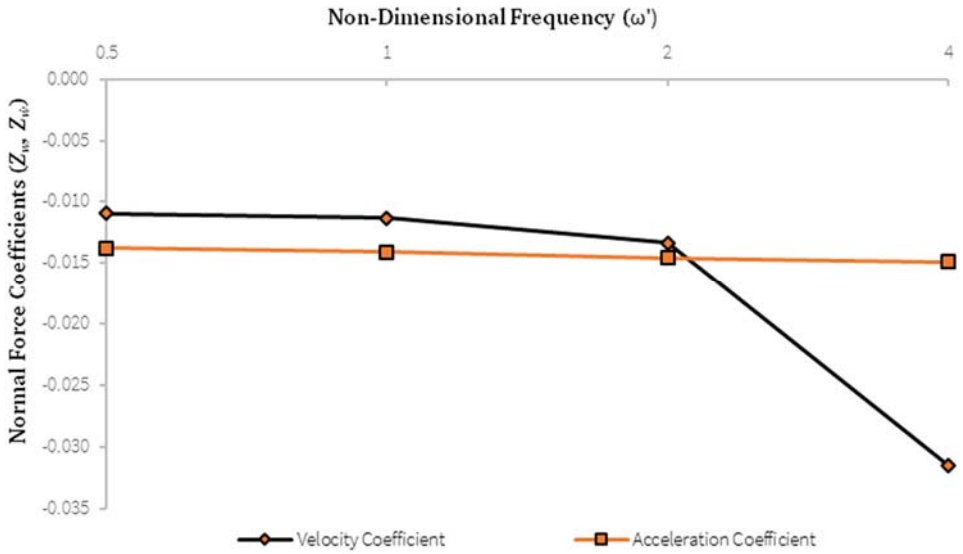

Figure 6-9 Log-Linear plot of Effect of Oscillation Frequency on Normal Force Coefficients Near the Surface

All tests Fr_L 0.512, H^* 1.65, A^* 1/80, SUBOFF in Bare Hull Configuration

For the force coefficients, the velocity coefficient is substantially more sensitive to an increase in non-dimensional frequency. As the non-dimensional frequency increases, the acceleration term dominates, and the flow field becomes more affected by prior motions. For non-dimensional frequency values of <1.0, coefficients can be extrapolated to the zero-frequency value.

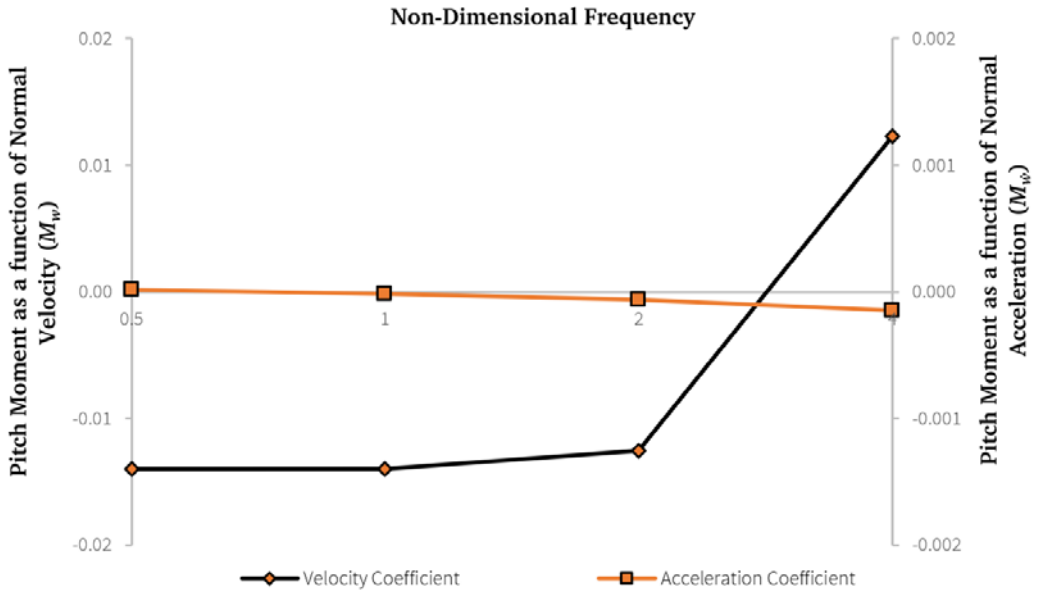

Figure 6-10 Log-Linear plot of Effect of Oscillation Frequency on Pitch Moment Coefficients Near the Surface

All tests Fr_L 0.512, H^* 1.65, A^* 1/80, SUBOFF in Bare Hull Configuration

The same pattern can be seen in the moment coefficients. In both cases, the frequency of oscillation in the near surface has a similar effect upon the results as can typically be found for testing in the deep condition and can be accounted for in the same manner.

6.3 Sudden Linear Acceleration

The second proposed approach to resolving the coefficients in the near surface region is to simulate the instantaneous application of a specified constant acceleration to a submarine in a steady state. This method has the advantage that the simulation time required in order to obtain a result is reduced by approximately an order of magnitude when compared to FPM: there is no need to wait until a steady response to the sinusoidal motion has been obtained, merely until the transient response to acceleration is resolved and enough data points have been obtained in order to predict an initial response at the time the acceleration commenced.

Section 6.3.1 discusses the normal force and pitch moments that result from sudden acceleration in the deeply submerged region. These results are then compared with those obtained by other methods in Section 6.3.2.

In order to characterise this response in the near surface region:

- Section 6.3.3 shows the coefficients are largely independent of the magnitude of the acceleration;
- Section 6.3.4 shows the coefficients are independent of the direction of acceleration;
- Section 6.3.5 compares the results obtained by the two methodologies presented in the near surface region.

6.3.1 Characteristics of numerical response in Heave

SUBOFF was simulated in its bare hull configuration at level trim, a constant speed of Fr_L 0.512, at a constant submergence of 1.65D. After convergence was achieved, a constant acceleration was imposed upon it normal to the direction of motion. The forces at each timestep over a period sufficient to move a distance $D/80$ were recorded. The results are presented in Figure 6-11. Results for pitch moment will follow after some discussion.

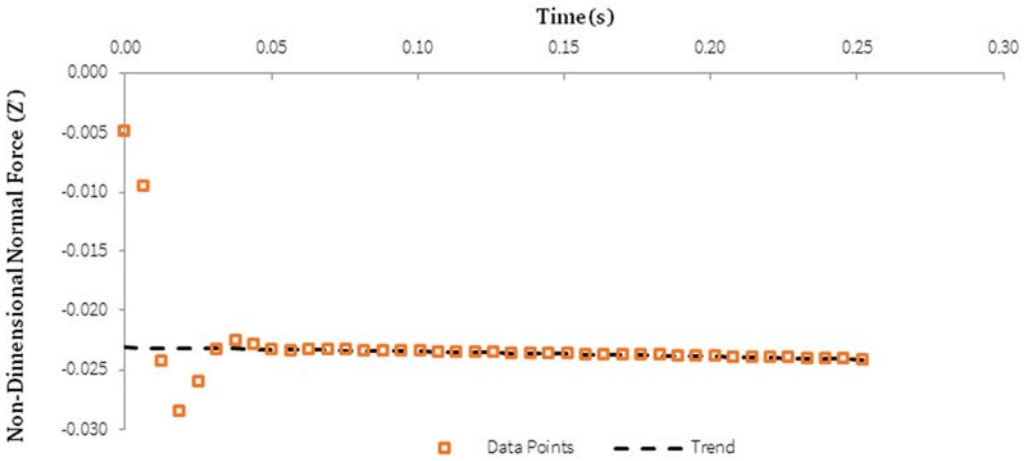

Figure 6-11 Typical Normal Force after a Sudden Change in Acceleration (First 20 timesteps)

Fr_L =0.512, H^* =1.65, $\dot{\boldsymbol{w}}'$ =0.0762, SUBOFF in Bare Hull Configuration

In this example, at $t = 0$, the non-dimensional acceleration is changed from 0 to 0.0762. As noted in Section 1, for small values of $\boldsymbol{w}'$ the deeply submerged the expected response is governed by Equations 6.9 and 6.10:

$$Z'(t) - Z'_{\star}\boldsymbol{u}'^2 = Z'_{w}\boldsymbol{u}'\boldsymbol{w}' + Z'_{w|w|}\boldsymbol{w}'|\boldsymbol{w}|' + (Z'_{\dot{w}} - \boldsymbol{m}')\dot{\boldsymbol{w}}' \tag{6.9}$$

$$M'(t) - M'_{\star}\,\boldsymbol{u}'^2 = M'_{w}\boldsymbol{u}'\boldsymbol{w}' + M'_{w|w|}\boldsymbol{w}'|\boldsymbol{w}'| + (M'_{\dot{w}} + x'_{G}\boldsymbol{m}')\dot{\boldsymbol{w}}' \tag{6.10}$$

Note that the values for $Z'_{\star}\boldsymbol{u}'^2$ and $M'_{\star}\boldsymbol{u}'^2$ are obtained from the steady state condition (where $\boldsymbol{w} = 0$; $\dot{\boldsymbol{w}} = 0$) immediately prior to acceleration commencing and are thus transferred to the left hand side of this equation to leave only the response to the acceleration. At some short time $t = \epsilon$ after the acceleration commences, $\boldsymbol{w}$ remains small while $\dot{\boldsymbol{w}}$ assumes its full value.

At $t = \epsilon,\ \boldsymbol{w}' \approx 0.0, u' = 1$:

$$Z'(\epsilon) - Z'_{\star}\boldsymbol{u}'^2 = (Z'_{\dot{w}} - \boldsymbol{m}')\dot{\boldsymbol{w}}' \tag{6.11}$$

$$M'(\epsilon) - M'_{\star}\,\boldsymbol{u}'^2 = (M'_{\dot{w}} + x'_{G}\boldsymbol{m}')\dot{\boldsymbol{w}}' \tag{6.12}$$

From which, in ideal circumstances, $Z'_{\dot{w}}$ and $M'_{\dot{w}}$ could both be derived directly. However, a temporary numerical oscillatory response to the change in acceleration occurs, obscuring this data point. This oscillatory response becomes negligible after 8-10 steps.

Allowing $Z'_\star = 0, M'_\star = 0$ in this instance due to xy-plane symmetry, that $\boldsymbol{m}' = 0$ as only the hydrodynamic force is modelled in the numerical solution, and $\boldsymbol{w}' = (\dot{\boldsymbol{w}}' t')$, Equations 6.11 and 6.12 are reduced to:

$$Z'(t) = Z'_{w}\dot{\boldsymbol{w}}' t' + Z'_{\dot{w}}\dot{\boldsymbol{w}}',\ Z'(0) = Z'_{\dot{w}}\dot{\boldsymbol{w}}' \qquad (6.13)$$

$$M'(t) = M'_{w}\dot{\boldsymbol{w}}' t' + M'_{\dot{w}}\dot{\boldsymbol{w}}',\ M'(0) = M'_{\dot{w}}\dot{\boldsymbol{w}}' \qquad (6.14)$$

Note that where xy-symmetry does not hold, values for $Z'_\star \boldsymbol{u}'^2$ and $M'_\star\, \boldsymbol{u}'^2$ can be determined directly from the steady state condition prior to acceleration commencing, then deducted from the measured force as per Equations 6.11 and 6.12.

To establish $Z'_{\dot{w}}$ and $M'_{\dot{w}}$, curves are least-square fitted to points 10 through 40 (see 'Trend' curves in Figure 6-12, Figure 6-13) using Equations 6.9 and 6.10, and then extrapolated back to t=0. The quadratic coefficient of these curves yields the value for $Z'_{w|w|}$ and $M'_{w|w|}$; the linear coefficient yields Z'_{w} and M'_{w} ; and the value at $t = 0$ yields $Z'_{\dot{w}}$ and $M'_{\dot{w}}$.

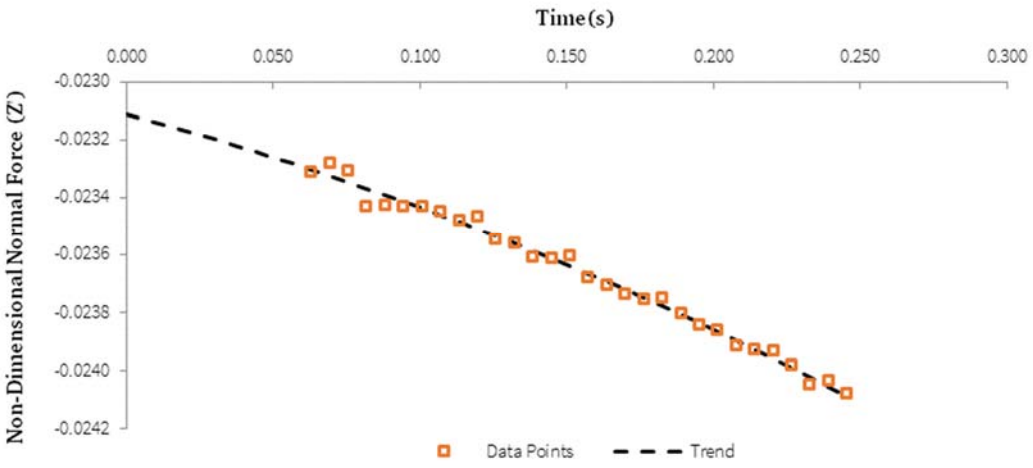

Figure 6-12 Response of Normal Force to Sudden Acceleration, After Initial Oscillation

Note: chart shows a subset of information in Figure 6-11 at markedly increased vertical scale

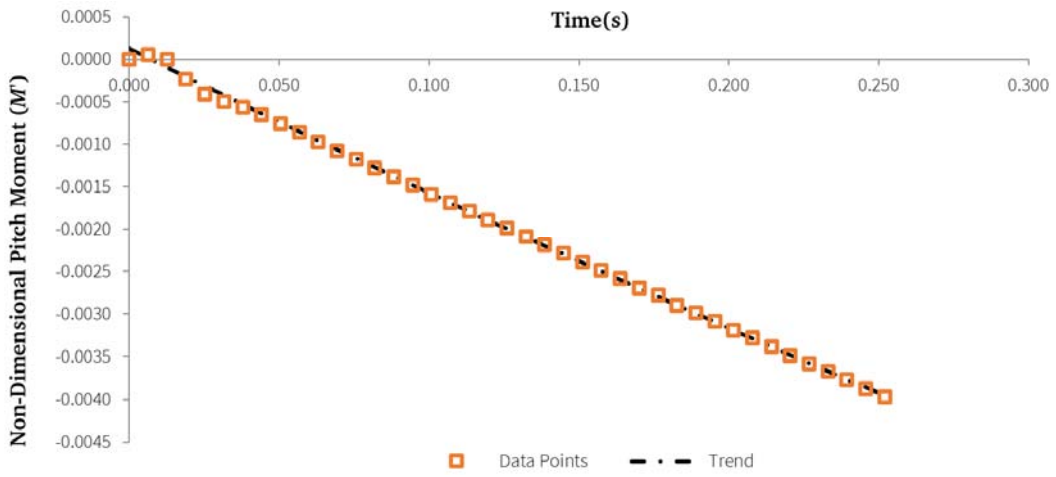

Figure 6-13 Typical Pitch Moment after Sudden Change in Acceleration (First 20 timesteps)

Fr_L =0.512, $H^\star$ =1.65, $\dot{\boldsymbol{w}}'$ =0.0762, SUBOFF in Bare Hull Configuration

It is immediately clear from the slope of the curves in Figures 6-11 and 6-13 that the relative scale of M'_w and $M'_{\dot{w}}$ are quite different than Z'_w and $Z'_{\dot{w}}$ The shift found for acceleration is quite small compared to the slope of the curve, and the initial decaying oscillatory response is of smaller relative scale. This is consistent with the experimental data from Roddy (1990).

Thus it is found that values of $Z'_\star$ and $M'_\star$ can be established from the steady state period prior to acceleration occurring, and values are obtained for Z'_w and M'_w through the process of curve fitting for extrapolation.

6.3.2 Effect of Acceleration Magnitude, Deeply Submerged

To compare the results found under different values of acceleration, simulations were carried out with the z-axis acceleration ($\dot{\boldsymbol{w}}'$) set instantaneously to 0.0381, 0.0762, and 0.1524 after an initial convergence period. Each acceleration continued until a change in depth of $D/80$ had occurred. Results are plotted below as Figure 6-14 and Figure 6-15, showing the results for force and moment respectively.

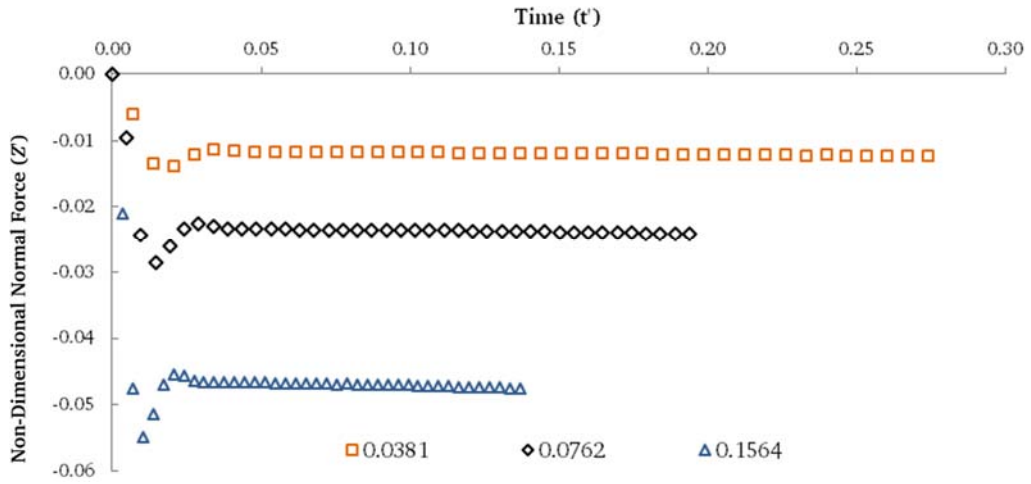

Figure 6-14 Normal Force Coefficient as a function of Time at Different Accelerations

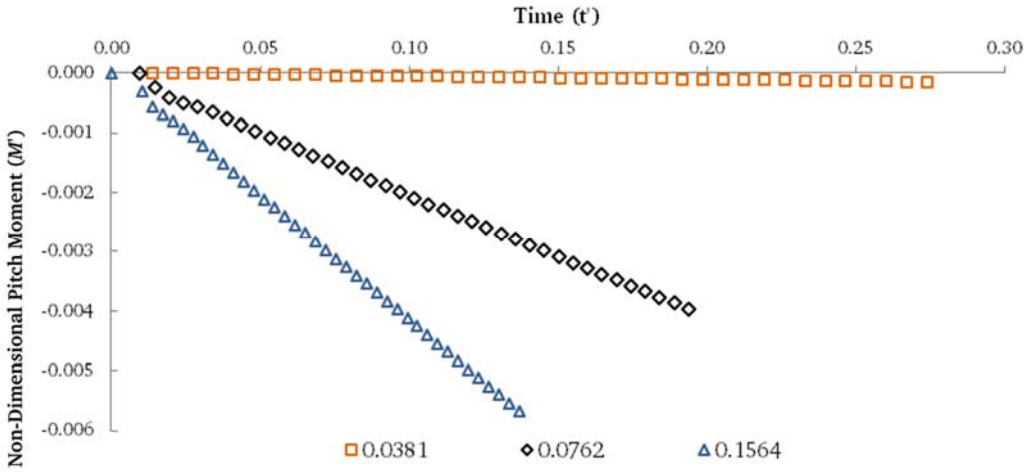

Figure 6-15 Pitch Coefficient as a function of Time at Different Accelerations

As noted in Section 6.3.1, there is a period after the acceleration begins in which the signal is obscured by the rate at which the numerical modelling adapts to the new state. Utilising the method outlined in Section 6.3.1, the values for force are projected to zero normal velocity, and the coefficient of acceleration determined for each case (See Table 6-3)

Table 6-3 Coefficients of Acceleration at Different Magnitudes of Acceleration

Acceleration		Coeff.	Coeff.
$\dot{w}$	$\dot{w}'$	$Z'_{\dot{w}}$	$M'_{\dot{w}}$
0.1	0.03884	-0.015678	0.000041
0.2	0.07768	-0.015664	0.000067
0.4	0.15536	-0.015660	0.000099

Variation in the predicted value of $Z'_{\dot{w}}$ is approximately 0.1%, indicating that the acceleration coefficients for $\dot{\boldsymbol{w}}$ are largely independent of the acceleration magnitude.

Variation in the predicted value of $M'_{\dot{w}}$ is higher, both in a relative and absolute sense. This is, however, to be expected as the value of $M'_{\dot{w}}$ is determined by the same

forces that develop $Z'_{\dot{w}}$, but with the portions both fore and aft of the centre of action being differenced from each other rather than combined. In this instance, error of a slightly higher absolute magnitude can be expected, leading directly to the large relative error in this case. With that taken into consideration, the value of $M'_{\dot{w}}$ can also be considered largely independent of the magnitude of acceleration, although less so than for $Z'_{\dot{w}}$.

6.3.3 Directional Considerations

To confirm that the direction of acceleration is not significant, two near surface cases were run that were identical except for the direction of acceleration. Results are plotted against non-dimensionalised time as Figure 6-16:

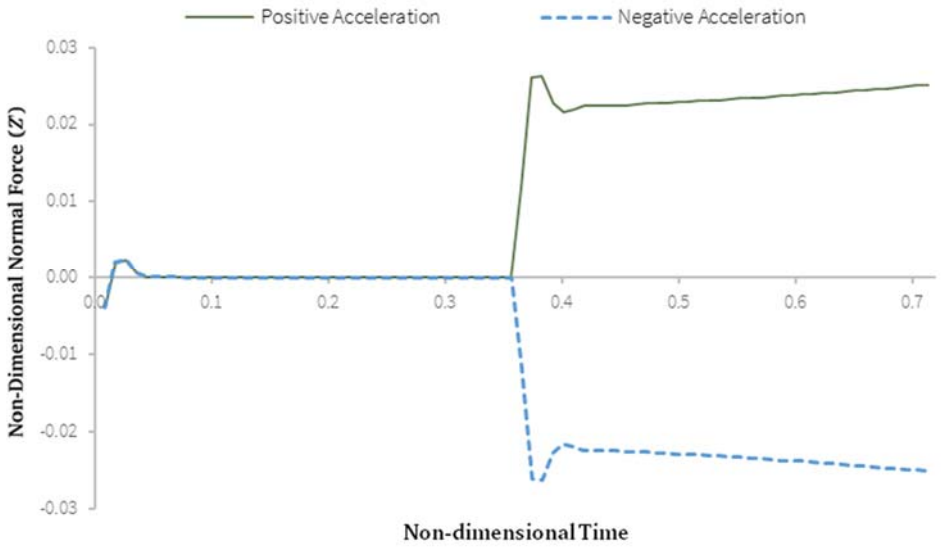

Figure 6-16 Response to Sudden Acceleration, Different Directions

Fr_L =0.512, H^* =1.65, $\dot{\boldsymbol{w}}'$ =±0.0768, A^* = 0.025, SUBOFF in Bare Hull Configuration

The results appear similar except for their sign. To compare these more closely, the absolute value of the results for negative acceleration are plotted against the results for positive acceleration in Figure 6-17.

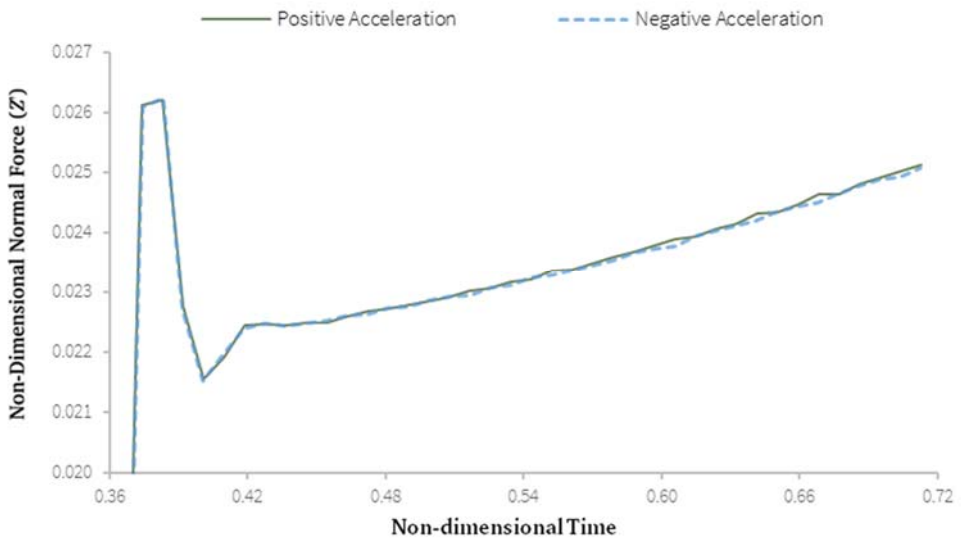

Figure 6-17 Absolute Response to Sudden Acceleration, Different Directions

Fr_L =0.512, $H^\star$ =1.65, $\dot{\boldsymbol{w}}'$ =±0.0768, $A^\star$ = 0.025, SUBOFF in Bare Hull Configuration

Figure 6-17 shows negligible differences between the two cases. Thus, even near the surface, the acceleration coefficient is shown to be independent of direction. This is a useful outcome as compressing the mesh upwards towards the surface is more liable to simulation failure due to mesh tearing than moving downwards is. This also indicates that the variation in the asymmetric terms will take the same form as their symmetric counterparts.

6.3.4 Comparison in Deeply Submerged Case to FPM results

To compare results between the two methods, two tests were conducted with Re 1.6×10^7 in the deeply submerged condition. The oscillation was conducted at a non-dimensional frequency (ω') of 0.5, with an amplitude ($A^\star$) of 0.0125. The linear acceleration was conducted at a non-dimensionalised acceleration of 0.0762 over a distance of $0.0125D$. Results are summarised in Table 6-3.

Table 6-4 Fractional Planar Motion compared to Sudden Linear Acceleration (Deep)

FPM	$A^\star$	ω'	Z'_w	$Z'_{\dot{w}}$	M'_w	$M'_{\dot{w}}$
	1/80 D	0.500	-0.005435	-0.015162	-0.013409	-0.000307
SLA	$\boldsymbol{w}'$	$\boldsymbol{z}'$	Z'_w	$Z'_{\dot{w}}$	M'_w	$M'_{\dot{w}}$
	0.07620	0.001	-0.004654	-0.016577	-0.014602	-0.000027

The SLA method produces a value 14% lower than the FPM for Z'_w, 9.3% higher for $Z'_{\dot{w}}$, and 8.9% higher for M'_w. The value for $M'_{\dot{w}}$ is 11 times larger, reflecting the issues noted earlier regarding absolute error in the near zero region.

Given that the FPM results have been shown to be near equivalents of the value obtained utilising conventional amplitudes of motion in the deep case, this amount and variation in sign of difference across all coefficients casts some doubt upon the values obtained utilising SLA. While SLA is much quicker to run, it is important to obtain values that are validated. Furthermore, when SLA is conducted in the near surface, the values obtained for Z'_w and M'_w are conflated with the change that occurs in $Z'_\star$ and $M'_\star$ over the distance travelled. Nor are the changes in $Z'_\star$ and $M'_\star$ easily discernible, as both are time dependant; the surface takes some time to establish a new profile for the change in depth.

As such it was elected to undertake the assessment of change in the coefficients with depth utilising the FPM method alone. While further work could lead to reliable outcomes in the deep case, the concerns with conflation in the near surface made the method less well suited to the purposes in mind.

6.4 Variation of coefficients ($Z'_{\dot{w}}, M'_{\dot{w}}, Z'_w$ and M'_w) as a function of depth

6.4.1 SUBOFF Barehull

Having derived a value for the deeply submerged coefficients, a simulation was conducted with the intent of establishing the values of all four coefficients across a series of depth. This, along with the deeply submerged value, allows calculation of the rate of decay towards the deeply submerged value.

A sinusoidal oscillation with an amplitude of $0.0125D$ was superimposed on a gradual progression from a submergence of $1.6D$ to $1.9D$, with discrete steps of $0.025D$. At each submergence step, time was allowed for the wave profile to propagate fully along the vessel, so that the forces and moments would be quasi-static for that depth. Once a full oscillation had been conducted in that quasi-steady state, a linear transition to the new depth over the period of half a cycle was conducted, and the process repeated for each depth.

The results of this simulation for normal force and pitch moment have been plotted against submergence in Figure 6-17 and Figure 6-18 respectively, and then tabulated in Table 6-5.

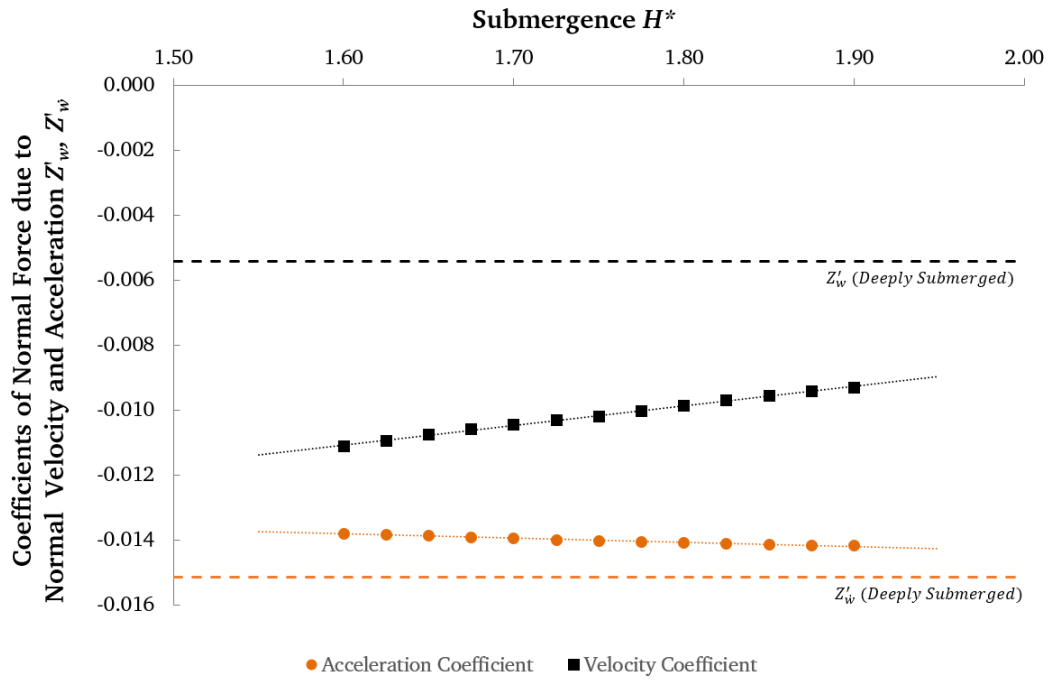

Figure 6-18 Coefficients of Normal Force as a function of Submergence

Fr_L =0.512, A^* =0.0125, $\omega' = 0.5$, SUBOFF in Bare Hull Configuration

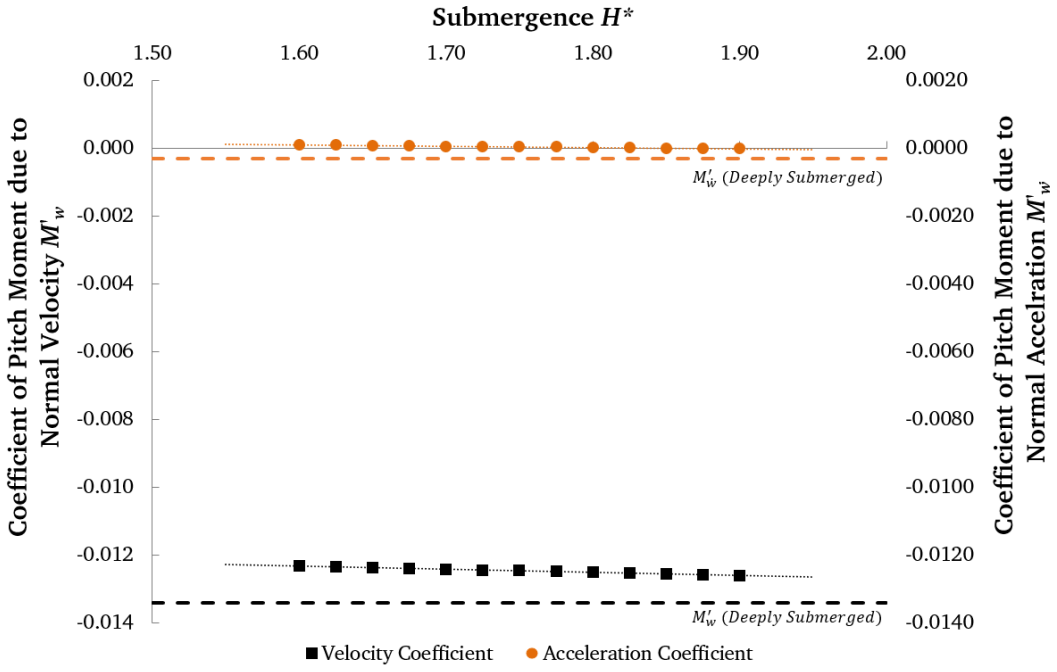

Figure 6-19 Coefficients of Pitch Moment as a function of Submergence

Fr_L =0.512, A^* =0.0125, $\omega' = 0.5$, SUBOFF in Bare Hull Configuration

Table 6-5 Coefficients for Bare Hull SUBOFF as a function of Submergence

$H^\star$	$Z'_{\dot{w}}$	Z'_w	$M'_{\dot{w}}$	M'_w
1.600	-0.013810	-0.011123	0.000099	-0.012314
1.625	-0.013845	-0.010940	0.000088	-0.012347
1.650	-0.013879	-0.010757	0.000076	-0.012374
1.675	-0.013914	-0.010597	0.000065	-0.012398
1.700	-0.013953	-0.010449	0.000056	-0.012420
1.725	-0.013997	-0.010316	0.000049	-0.012438
1.750	-0.014042	-0.010204	0.000044	-0.012456
1.775	-0.014070	-0.010040	0.000034	-0.012479
1.800	-0.014094	-0.009876	0.000024	-0.012505
1.825	-0.014117	-0.009715	0.000013	-0.012530
1.850	-0.014143	-0.009561	0.000002	-0.012554
1.875	-0.014164	-0.009416	-0.000008	-0.012578
1.900	-0.014187	-0.009302	-0.000016	-0.012599

For each coefficient, a steady trend towards the deeply submerged value is observed. From this information, an approximate function for each coefficient can be derived. While it is evident that at some depth each of these coefficients will attain the deeply submerged value, this range of values has resulted in insufficient curvature to reasonably fit a curve to; the fit is just as good to a linear function.

For values of these coefficients, a function with simple fit to the data established within the range of $1.6D < H^\star < 1.9D$ is tabulated in Table 6-6:

Table 6-6 Coefficient Functions of Depth

Coefficient	Formula
$Z'_{\dot{w}}$	-1.2906E-03 $H^\star$ - 1.1758E-02
Z'_w	6.0233E-03 $H^\star$ - 2.0717E-02
$M'_{\dot{w}}$	-3.7391E-04 $H^\star$ + 6.9482E-04
M'_w	-9.2116E-04 $H^\star$ - 1.0849E-02

It is to be anticipated that similar studies at greater submergence would enable the fitting of functions that smoothly transition from the deeply submerged case to the near surface region.

6.5 Summary

Two novel methodologies for determination of acceleration coefficients — Fractional Planar Motion and Sudden Linear Acceleration — were described and assessed. Fractional Planar Motion involves the modelling of small scale motions of the submarine (a 'fraction' of the diameter) in order to minimise the effects of change in depth upon the forces measured. Sudden Linear Acceleration models the impact of a sudden acceleration upon a submarine body, from which coefficients of acceleration and velocity can be derived by back-extrapolation to the zero-acceleration point.

Through a series of investigations, it has been shown that for Fractional Planar Motion:

- The results for the velocity and acceleration coefficients obtained when deeply submerged when using very small amplitudes of oscillation (FPM), are of minimal difference to those obtained using conventional amplitudes of oscillation (Section 6.2.1);
- $Z'_w, M'_w, Z'_{\dot{w}}$ and $M'_{\dot{w}}$ are independent of amplitude in the near surface region when $A^\star < 0.03$. (Section 6.2.3)
- The effect of small amplitude oscillations on the free surface is minimal and may be neglected (Section 6.2.4);
- At low frequencies of oscillation, values obtained tend towards a 'zero frequency' value for each coefficient in both the deeply submerged case (Section 6.2.1) and the near surface case (Section 6.2.5)

These results imply that a single oscillatory test, of amplitude less than $D/32$ and non-dimensional oscillation frequency less than or equal to 0.5 is sufficient to determine the values of $Z'_w, M'_w, Z'_{\dot{w}}$ and $M'_{\dot{w}}$ in the near surface region.

Similarly, for Sudden Linear Acceleration:

- Values for $Z'_\star, M'_\star, Z'_w, M'_w, Z'_{w|w|}, M_{w|w|}, Z'_{\dot{w}}$ and $M'_{\dot{w}}$ are all able to be obtained from a single Sudden Linear Acceleration test through curve fitting back to the time acceleration commenced, once the initial instability is resolved (Section 6.3.1);
- $Z'_{\dot{w}}$ is independent of acceleration, while the changes in $M'_{\dot{w}}$ are small in absolute terms. (Section 6.3.2)
- The effect of the direction of acceleration near the free surface may be neglected (Section 6.3.3);
- Values obtained for Z'_w, M'_w and $Z'_{\dot{w}}$ using SLA are within 8-15% of those obtained using FPM. Values for $M'_{\dot{w}}$ are close in absolute terms. (Section 6.3.4)

These results imply that a single acceleration test, with a non-dimensional acceleration on the order of 0.1 is sufficient to approximate the values of $Z'_w, M'_w, Z'_{\dot{w}}$ and $M'_{\dot{w}}$. It should be noted that these tests are markedly faster to run than FPM tests

— more comparable to static cases — and as such these results suggest refinement of this approach in the deeply submerged condition may allow for rapid estimation of these coefficients. However, concerns remain regarding the confounding effect that change of depth may impose in the near surface region.

As such, the decision was made to move ahead with analysis of SUBOFF using FPM alone at this point. From the results obtained, it can be seen that below a submergence of $1.6D$, the largest change in the values from the deep condition of is in the order of 9% for $Z'_{\dot{w}}$, whereas $M'_{\dot{w}}$ undergoes a small absolute change, but one that includes a change in sign as depth increases. Given the sensitivity of the equations of motions to these two coefficients as per Table 3-1 (1.597, 1.010), both near surface changes in $Z'_{\dot{w}}$ and in $M'_{\dot{w}}$ should be treated as of minor significance as summarised in Table 6-7. It should be noted that the results for $M'_{\dot{w}}$ may vary in significance from vessel to vessel as the small absolute value of $M'_{\dot{w}}$in this instance may be compromising the assessment methodology.

Table 6-7 Significance of Coefficients

Minor Significance (0.1 - 0.5)
$Z'_{\dot{w}}$ $M'_{\dot{w}}$

7. CONCLUSIONS AND RECOMMENDATIONS

The operational profile of modern diesel submarines inherently and increasingly includes important mission components near the surface of the water. To optimise for operations in this region, it is necessary to be able to estimate beforehand the manoeuvring characteristics of a submarine when travelling near the surface. Coefficient based manoeuvring models for submarines operating deeply submerged have been utilised for more than 50 years and have well established general forms that are modified as needed for specific cases. Similarly, the changes in hydrodynamic force and moments that occur when a submarine is operating near the surface at speed have been studied experimentally since the 1930s, and numerically over the last two decades. However, the manner and degree to which many of the various manoeuvring coefficients change in the near surface region has been neglected. The work in the thesis identifies the most significant coefficients when modelling submarine motion and their sensitivity when operating near the free surface through validated CFD simulations.

7.1 Concluding Remarks

What changes occur in the manoeuvring forces acting on a submarine due to its own motion when operating near the ocean surface compared to operating deeply submerged?

In seeking answers to this question, this thesis has focussed on pure heave motion in the vertical plane, first in steady state conditions, and then quasi steady state conditions, with motions of an amplitude a mere fraction of the submarine's diameter.

In this thesis it has been demonstrated that in considering the manoeuvring of a submarine near the free surface, within the normal operating envelope it is most useful to model the effect of the free surface on the coefficient for normal force due to square of the axial velocity($Z'_\star$), and may be useful to model the effects of the coefficients for normal force due to normal velocity and acceleration ($Z'_w, Z'_{\dot{w}}$) and the coefficients of pitch moment due to normal velocity and acceleration ($M'_w, M'_{\dot{w}}$). For each of these coefficients, there is a combination of manoeuvring model sensitivity and degree of change in coefficient near the surface that justifies the greater effort required to model these changes.

The effects of being near the free surface on the coefficients for axial force and pitch moment due to the square of the axial velocity ($X'_\star$ and $M'_\star$) may be neglected in the normal operating envelope of a submarine. However, if operation near the surface at higher Froude Length Numbers (over 0.25) is important and frequent for a specific vessel, then it would prove useful to analyse and include these coefficients in the manoeuvring model. This distinction is made due to the significant changes in value that occur in the near surface region when the Froude Length Number is above 0.25.

The effects of the free surface upon other coefficients considered ($X'_w, X'_{ww}, Z'_{ww}, Z'_{w|w|}, M'_{ww}$ and $M'_{w|w|}$) is negligible, and these may be treated as equal to their deeply submerged values.

In order to assess the changes that occur in the vertical plane coefficients in the near surface region, a steady state approach at level trim was first utilised to assess values for $X'_\star, Z'_\star$ and $M'_\star$

as a function of Froude Length Number and Submergence. Then, steady state simulation at an angle of trim was utilised to determine degree to which X'_w, X'_{ww}, Z'_w, Z'_{ww}, $Z'_{w|w|}$, M'_w, M'_{ww} and $M'_{w|w|}$ were functions of the relationship between the submarine and the surface. However, this methodology presented two significant issues. Firstly, it did not provide values for the acceleration coefficients ($Z'_{\dot{w}}$ and $M'_{\dot{w}}$), both of which the manoeuvring model is sensitive to. Secondly, in the values obtained for the various coefficients of $\boldsymbol{w}$, two distinct effects — the effect of trim on the relationship to the surface, and the effect of the nearness of the surface on the flow in the z-axis of the submarine — were conflated.

In order to resolve these issues, two novel variations on existing approaches to deriving manoeuvring coefficients were proposed and tested. Fractional Planar Motion (FPM) utilises the specific properties of numerical modelling to reduce the amplitude of pure heave oscillation to allow its effective use in the near surface region. Sudden Linear Acceleration(SLA) also utilises the advantages of the numerical method to instantaneously impose a constant acceleration onto the submarine, allowing the measurement of acceleration coefficients without the need for separating in-phase and out of phase components inherent to oscillatory techniques.

FPM was found to produce results consistent with those obtained using more conventional amplitudes of oscillation in the deeply submerged case. These values are dependent upon the frequency of oscillation, however, as in the case for conventional PMM, values for a 'zero frequency' state can be projected from results obtained at a low enough frequency. Using FPM, values were found for $Z'_w, Z'_{\dot{w}}, M'_w$ and $M'_{\dot{w}}$ at a series of different submergences. From this, a relationship was established between submergence and each coefficient. These results can also be utilised to separate the different effects of a) trim relative the surface and b) flow in the submarine's z-axis when near the surface.

SLA was found to produce results that were not consistent with FPM, with some coefficients relatively overestimated and others underestimated. Further, it was found to be difficult to derive values for Z'_w and M'_w in the near surface region, as changes to other coefficients were conflated together. As such, despite the relative advantages of this method in terms of speed — approximately an order of magnitude faster than FPM — the use of FPM was favoured for the derivation of near surface coefficients.

7.2 Recommendations for Future Work

7.2.1 Assessment of rotational coefficients using Fractional Planar Motion

By utilising pure yaw motion rather than pure sway, the work in Chapter 6 can be extended to include the effects of the near surface on the coefficients of angular velocity and angular acceleration. Given that the coefficient model's greatest sensitivity is to M'_q , it is likely that there will be additional coefficients identified that are valuable to assess for near surface effect.

7.2.2 Determine effect on Control Vector due to operation in the Near Surface Region

Operation in the near surface region alters the angle of flow past control surfaces, in particular those in the horizontal plane. Sail mounted planes, given their relative proximity to the surface, are likely to be most affected. By modelling a submarine with its control planes, determine the scale of these effects and whether these changes need to be included in a near surface manoeuvring model.

7.2.3 Assessment of the effect of roll in the near surface

If roll is considered, the integration of near surface effects into a manoeuvring model becomes rather more complex. The more complex the model becomes, the more it becomes necessary to treat surface effects similar to the manner in which buoyancy / mass effects are treated, rather than simply as modifications to existing coefficients.

7.2.4 Sensitivity Study for Near Surface Coefficients

Conduct a coefficient sensitivity study for submarines operating in the near surface rather than estimating based on previous work.

7.2.5 Validation of near surface coefficient based manoeuvring model

Validate predictions of the manoeuvring of a submarine close to the surface by use of a free running model.

7.3 Final Statement

A novel method — Fractional Planar Motion — for the determination of both velocity and acceleration based manoeuvring coefficients in the near surface region has been demonstrated. Using this method, in combination with steady state simulations, the change in various manoeuvring coefficients due to operation in the near surface region in for a generic submarine model was measured. In combination with published measures of the sensitivity of the manoeuvring model to each coefficient, this information was used to assess the relative significance of adjusting each coefficient for the effect of a near surface.

With the evident extension of this method to modelling pure pitching motion, this will enable the evaluation of sufficient coefficients of motion in the near surface region to provide a first approximation of near surface motions.

BIBLIOGRAPHY

Abkowitz, M. A., (1969). *Stability and motion control of ocean vehicles*. Cambridge, Mass: M.I.T Press

Anderson, B., Campanella, G., and Walker, G.J., (1995). Development of a horizontal planar motion mechanism for determining hydrodynamic characteristics of underwater vehicles, *Proceedings of the 12th Australasian Fluid Mechanics Conference*. (1) 151-154. Sydney, Australia.

ANSYS (2015). *CFX Theory Guide*, Release 17, ANSYS Inc.

Atkins, W. (2003). *MARNET Best practice guidelines for marine applications of computational fluid dynamics*. MARNET.

Baker, C. (2004). *Estimating drag forces on submarine hulls*. (DRDC Report CR 2004-125). New Brunswick, Canada: Defence Research and Development Canada

Bishop, R. E. D., Burcher, R. K., & Price, W. G. (1973). Application of functional analysis to oscillatory ship model testing. *Proceedings of the Royal Society of London Series A-Mathematical and Physical Sciences*, 332(1588), 37-49. doi: DOI 10.1098/rspa.1973.0012

Bishop, R. E. D., Burcher, R. K., & Price, W. G. (1973). Directional stability analysis of a ship allowing for time history effects of the flow. *Proceedings of the Royal Society A: Mathematical, Physical and Engineering Sciences*, 335(1602), 341-354. doi: 10.1098/rspa.1973.0129

Bishop, R. E. D., & Parkinson, A. G. (1970). On the planar motion mechanism used in ship model testing. *Philosophical Transactions of the Royal Society A: Mathematical, Physical and Engineering Sciences*, 266(1171), 35-61. doi: 10.1098/rsta.1970.0002

Brownell, W.F., (1956). *A rotating arm and manoeuvring basin*. (DTMB Report 1053). Bethesda, USA: David Taylor Model Basin

Cauchy, A.-L. (1827). Mémoire sur la théorie de la propagation des ondes à la surface d'un fluide pesant d'une profondeur indéfinie, in mémoires présentés par divers savants à l'académie royale des sciences de l'institut de france. *Sciences Mathématiques et Physique*, 130.

Chorin, A. J. (1968). Numerical solution of the Navier-Stokes equations. *Mathematics of computation*, 22(104), 745-762.

Clarke, D. (2003). The foundations of steering and manoeuvring. *Proceedings of the IFAC conference on manoeuvering and controlling marine crafts*. IFAC, Girona, Spain.

Craik, A. D. D. (2004). The origins of water wave theory. *Annual Review of Fluid Mechanics*, 36, 1-28. doi: 10.1146/annurev.fluid.36.050802.122118

Craik, A. D. D. (2005). George gabriel stokes on water wave theory. *Annual Review of Fluid Mechanics*, 37, 23-42. doi: 10.1146/annurev.fluid.37.061903.175836

Crook, T. P. (1994). *An initial assessment of free surface effects on submerged bodies*. (Doctoral Thesis, Naval Postgraduate School, Monterey, California)

Crossland, P. (2013). Profiles of excess mass for a generic submarine operating under waves. *Proceedings of Pacific 2013 International Maritime Conference*. 210-219.

Dawson, E. (2014). *An investigation into the effects of submergence depth, speed and hull length-to-diameter ratio on the near-surface operation of conventional submarines*. (Master of Philosophy, University of Tasmania, Launceston, Tasmania)

Day, A. H., Clelland, D., & Doctors, L. J. (2009). Unsteady finite-depth effects during resistance tests on a ship model in a towing tank. *Journal of Marine Science and Technology*, 14(3), 387-397. doi: 10.1007/s00773-009-0057-2

de Barros, E. A., Pascoal, A., & de Sa, E. (2008). Investigation of a method for predicting AUV derivatives. *Ocean Engineering*, 35(16), 1627-1636. doi: 10.1016/j.oceaneng.2008.08.008

Doctors, L. J., Day, A. H., & Clelland, D. (2008). Unsteady effects during resistance tests on a ship model in a towing tank. *Journal of Ship Research*, 52(4), 263-273.

Eloot, K., & Vantorre, M. (2003). Development of a tabular manoeuvring model for hull forces applied to full and slender ships in shallow water. In *International Conference on Marine Simulation and Ship Maneuverability*, 3, 25-28.

Euler, L. (1761). Principia motus fluidorum. *Novi Commentarii Acad. Sci. Petropolitanae*, 6(1756/7), 271-311.

Feldman, J. (1979). *DTNSRDC revised standard submarine equations of motion*. (DTIC Document DTNSRDC/SPD-0393-09) Bethesda, Maryland: David Taylor Naval Ship Research and Development Center.

Feldman, J. (1987). *Straightline and rotating arm captive-model experiments to investigate the stability and control characteristics of submarines and other submerged vehicles*: (DTIC Document DTRC/SHD-0393-20). Bethesda, Maryland: David Taylor Research Center

Feldman, J. (1995). *Method of performing captive-model experiments to predict the stability and control characteristics of submarines*. (DTIC Document CRDKNSWC-HD-0393-25). Bethesda, Maryland: Naval Surface Warfare Center Carderock Division

Filon, L. N. G. (1926). The forces on a cylinder in a stream of viscous fluid. *Proceedings of the Royal Society of London. Series A, Containing Papers of a Mathematical and Physical Character*, 113(763), 7-27.

Fossen, T. I. (1994). *Guidance and control of ocean vehicles*. John Wiley & Sons Inc.

Furlong, M., Turnock, S. R., & Phillips, A. B. (2010). The use of computational fluid dynamics to aid cost-effective hydrodynamic design of autonomous underwater vehicles. *Proceedings of the Institution of Mechanical Engineers, Part M: Journal of Engineering for the Maritime Environment*, 224(4), 239-254. doi: 10.1243/14750902jeme199

Gertler, M. (1950). *Resistance experiments on a systematic series of streamlined bodies of revolution-for application to the design of high-speed submarines*: (DTMB Report C-297). Bethesda, Maryland: David Taylor Model Basin

Gertler, M. (1967). *The DTMB planar-motion-mechanism system*, (DTIC Document HML-TR-2523). Bethesda, Maryland: David Taylor Naval Ship Research and Development Center

Gertler, M., & Hagen, G. R. (1967). *Standard equations of motion for submarine simulation*. (DTIC Document. NSRDC-2510). Bethesda, Maryland: David Taylor Naval Ship Research and Development Center

Geez (2016), Law of the Wall, retrieved from: https://www.cfdonline.com/W/images/6/6a/Img_lawOfTheWall_whiteBG.png, on 17/2/2016

Gorski, J., Coleman, R.M., & Haussling, H.J. (1990). *Computation of incompressible flow around the DARPA SUBOFF bodies*. (DTIC Document DTRC-90/016). Bethesda, Maryland: David Taylor Research Center

Gourlay, T., & Dawson, E. (2015). A Havelock source panel method for near-surface submarines. *Journal of Marine Science and Application*, 14(3), 215-224.

Griffin, M. J. (2002). *Numerical prediction of the maneuvering characteristics of submarines operating near the free surface*. (Doctoral Thesis, Massachusetts Institute of Technology). Retrieved from http://hdl.handle.net/1721.1/8327

Groves, N. C., Huang, T. T., & Chang, M. S. (1989). *Geometric characteristics of DARPA SUBOFF models*. (DTIC Document DTRC/SHD-1298-01). Bethesda, Maryland: David Taylor Research Center

Havelock, T. (1917a). The initial wave resistance of a moving surface pressure. *Proceedings of the Royal Society of London. Series A, Containing Papers of a Mathematical and Physical Character*, 93(650), 240-253.

Havelock, T. (1917b). Some cases of wave motion due to a submerged obstacle. *Proceedings of the Royal Society of London. Series A, Containing Papers of a Mathematical and Physical Character*, 93(654), 520-532.

Havelock, T. (1919). Wave resistance: some cases of three-dimensional fluid motion. *Proceedings of the Royal Society of London. Series A, Containing Papers of a Mathematical and Physical Character*, 95(670), 354-365.

Havelock, T. (1928). The wave pattern of a doublet in a stream. *Proceedings of the Royal Society of London. Series A, Containing Papers of a Mathematical and Physical Character*, 121(788), 515-523.

Havelock, T. (1950). The forces on a submerged spheroid moving in a circular path. *Proceedings of the Royal Society of London A: Mathematical, Physical and Engineering Sciences*, 291(1066), 297-305. doi: 10.1098/rspa.1950.0061

Havelock, T. (1931). The wave resistance of an ellipsoid. *Proceedings of the Royal Society A: Mathematical, Physical and Engineering Sciences*, 132(820), 480-486. doi: 10.1098/rspa.1931.0113

Healey, A. J., & Lienard, D. (1993). Multivariable sliding mode control for autonomous diving and steering of unmanned underwater vehicles. *IEEE Journal Of Oceanic Engineering*, 18(3), 327-339.

Hellsten, A. (2004). *New two-equation turbulence model for aerodynamics applications.* (Doctoral Thesis, Helsinki University of Technology, Helsinki, Finland)

Hellsten, A., & Wallin, S. (2009). Explicit algebraic Reynolds stress and non-linear eddy-viscosity models. *International Journal of Computational Fluid Dynamics*, 23(4), 349-361.

Huang, T. T., Liu, H.-L., & Groves, N. C. (1989). *Experiments of the DARPA SUBOFF Program*. (DTIC Document DTRC/SHD-1298-02). Bethesda, Maryland: David Taylor Research Center

Imlay, F. H. (1961). *The complete expressions for added mass of a rigid body moving in an ideal fluid*. (DTIC Document DTMB-1528). Bethesda, Maryland: David Taylor Model Basin

Jensen, P. S., Chislett, M. S., & Romeling, J. U. (1993). DEN-MARK 1 - An innovative and flexible mathematical model for simulation of ship manoeuvrability. *Intl Conf on Marine Simulation & Ship Manoeuvrability*, 1, 219-227. Newfoundland, Canada.

Jones, W. P., & Launder, B. (1972). The prediction of laminarization with a two-equation model of turbulence. *International Journal Of Heat And Mass Transfer*, 15(2), 301-314

Joubert, P. (2004). *Some Aspects of Submarine Design Part 1. Hydrodynamics*. (Report DSTO-TR-1622). Melbourne, Australia: Defence Science and Technology Organisation

Joubert, P. (2006). *Some aspects of submarine design. Part 2. Shape of a submarine 2026*. (Report DSTO-TR-1920). Melbourne, Australia: Defence Science and Technology Organisation

Kelvin, W. (1871). The influence of wind on waves in water supposed frictionless. *Phil. Mag*, 42(4), 368-374

Kelvin, W. (1887). Stability of fluid motion: rectilinear motion of viscous fluid between two parallel plates. *Phil. Mag*, 24(5), 188-196.

Kirchhoff, G. (1869). Zur Theorie freier Flüssigkeitsstrahlen. *Journal für die reine und angewandte Mathematik*, 70, 289-298

Kim, H., Leong, Z. Q., Ranmuthugala, D., & Forrest, A. (2015). Simulation and validation of an AUV in variable accelerations. *International Journal of Offshore and Polar Engineering*, 25(01), 35-44.

Kopp, C. (2012). Defining future submarine capabilities. *Defence Today*, 10(1), 10-13.

Lamb, H. (1913). On some cases of wave-motion on deep water. *Annali di Matematica Pura ed Applicata* (1898-1922), 21(1), 237-250.

Lamb, H. (1926). On Wave Resistance. *Proceedings of the Royal Society of London. Series A, Containing Papers of a Mathematical and Physical Character*, 111(757), 14-25. doi: 10.2307/94660

Lamb, H. (1916). *Hydrodynamics*. Cambridge University Press

Lamb, H. (1932). *Hydrodynamics*. Cambridge University Press

Laplace P-S Marquis de. (1776). Suite des recherches sur plusieurs points du systeme du monde (XXV–XVII). Mem. Presentes Divers Savans Acad. R. Sci. Inst. France, pp. 525–52.

Larsson, L., & Kim, K. J. (1992). Hydrodynamic optimisation using Shipflow. In *5th Intl Symp on the Practical Design of Ships and Mobile Units*, 1, 1-16. Newcastle upon Tyne, U.K.

Lazauskas, L. V. (2005). *Hydrodynamics of Advanced High Speed Sealift Vessels*. (Master of Science, University of Adelaide, Adelaide).

Liu, H. L., & Huang, T. T. (1998). *Summary of DARPA SUBOFF experimental program data*, (DTIC Report CRDKNSWC/HD-1298-11). Bethesda, Maryland: Naval Surface Warfare Center, Carderock Division

Leong, Z., Ranmuthugala, D., Penesis, I., & Nguyen, H. (2012). Numerical simulation of spheres in relative motion using dynamic meshing techniques. *Proceedings of the 18th Australasian Fluid Mechanics Conference*, 1, 1-4.

Leong, Z. Q., Saad, K. A. M., Ranmuthugala, D., & Duffy, J. (2013). Investigation into the hydrodynamic interaction effects on an AUV operating close to a submarine. In *Pacific 2013 International Maritime Conference*, 1, 251. Sydney, Australia.

Leong, Z. Q. (2014). *Effects of hydrodynamic interaction on an AUV operating close to a moving submarine* (Doctoral dissertation, University of Tasmania, Launceston, Australia).

Leong, Z., Ranmuthugala, D., Penesis, I., & Nguyen, H. (2015). RANS-based CFD prediction of the hydrodynamic coefficients of DARP SUBOFF geometry in straight-line and rotating arm manoeuvres. *International Journal of Maritime Engineering*, 157(A1), A41-A52.

Liu, T.-L., & Guo, Z.-M. (2013). Analysis of wave spectrum for submerged bodies moving near the free surface. *Ocean Engineering*, 58, 239-251. doi: 10.1016/j.oceaneng.2012.10.003

MacCamy, R. (1964). The motion of cylinders of shallow draft. *Journal of Ship Research*, 7, 1-11.

Menter, F. R. (1994). Two-equation eddy-viscosity turbulence models for engineering applications. *AIAA journal*, 32(8), 1598-1605.

Menter, F. R. (2011). *Turbulence modeling for engineering flows*. (Technical Paper, ANSYS Inc), 1-25.

Menter, F. R., Langtry, R., Likki, S., Suzen, Y., Huang, P., & Völker, S. (2006). A correlation-based transition model using local variables—Part I: model formulation. *Journal of Turbomachinery*, 128(3), 413-422.

Michell, J. H. (1893). XLIV. The highest waves in water. *The London, Edinburgh, and Dublin Philosophical Magazine and Journal of Science*, 36(222), 430-437.

Michell, J. H. (1898). XI. The wave-resistance of a ship. *The London, Edinburgh, and Dublin Philosophical Magazine and Journal of Science*, 45(272), 106-123.

Nahon, M. (1996). A simplified dynamics model for autonomous underwater vehicles. In *Autonomous Underwater Vehicle Technology*, 1, 373-379.

Neulist, D. (2011). *Experimental investigation into the hydrodynamic characteristics of a submarine operating near the free surface*. (Undergraduate Thesis, Australian Maritime College, Launceston, Australia.)

Newman, J. (1964). A slender-body theory for ship oscillations in waves. *Journal of Fluid Mechanics*, 18(04), 602-618.

Newman, J., & Tuck, E. (1964). Current progress in the slender body theory for ship motions. In *5th Symposium on Naval Hydrodynamics*, 1, 129-165. Bergen, Norway.

Newton, I. (1687). *Philosophiae naturalis principia mathematica*, 3.

Perrault, D., Bose, N., O'Young, S., & Williams, C. D. (2003). Sensitivity of AUV added mass coefficients to variations in hull and control plane geometry. *Ocean Engineering*, 30(5), 645-671.

Poisson, S.-D. (1818). Mémoire sur la théorie des ondes. *Mém. Acad. R. Sci. Inst. France*, 2, 70-186.

Polis, C., Ranmuthugala, D., & Duffy, J, Renilson, M. (2013). Enabling the prediction of manoeuvring characteristics of a submarine operating near the free surface. In *Pacific 2013 International Maritime Conference*, 1, 281-291. Sydney, Australia

Pope, S.B., (1975). A more general effective-viscosity hypothesis. *J. Fluid Mech*., 72, 331–340.

Prestero, T. (2001). *Verification of a six-degree of freedom simulation model for the REMUS autonomous underwater vehicle*. (Doctoral Thesis, Massachusetts Institute of Technology)

Shenoi, R. R., Krishnankutty, P., Selvam, R. P., & Kulsreshtha, A. (2012). Prediction of maneuvering coefficients of a container ship by numerically simulating HPMM using RANSE based solver. In *Third International Conference on Ship Manoeuvring in Shallow and Confined Water*, 1, 3-5.

Renilson, M. (2015). *Submarine Hydrodynamics*. Springer.

Renilson, M. R., Polis, C., Ranmuthugala, D., & Duffy, J. (2014). Prediction of the hydroplane angles required due to high speed submarine operations near the surface. In *Warship 2014: Naval Submarines & UUVs*, 1, 147-155.

Reynolds, O. (1894). On the dynamical theory of incompressible viscous fluids and the determination of the criterion. *Proceedings of the Royal Society of London*, 56(336-339), 40-45.

Rider, B. & Mattsson, A. (2013) *CFD Before CFD*, retrieved from http://dept.ku.edu/~cfdku/JRV/Rider.pdf

Roddy, R. F. (1990). *Investigation of the stability and control characteristics of several configurations of the DARPA SUBOFF model from captive-model experiments*. (DTIC Document DTRC/SHD-1298-08). Bethesda, Maryland: David Taylor Research Center.

Sen, D. (2000). A study on sensitivity of maneuverability performance on the hydrodynamic coefficients for submerged bodies. *Journal of Ship Research*, 44(3), 186-196.

SNAME (1952), *Nomenclature for Treating the Motion of a Submerged Body through a Fluid*. (SNAME Technical and Research Bulletin, I-5.)

Stokes, G. G. (1847). On the theory of oscillatory waves. *Trans Cambridge Philos Soc*, 8, 441-473.

Thomson, W. & Tait, P.G. (1867). *Treatise on natural philosophy (Vol. 1)*. Claredon Press..

Toxopeus, S. (2008). Viscous-flow calculations for bare hull DARPA SUBOFF submarine at incidence. *International Shipbuilding Progress*, 55(3), 227-251.

Toxopeus, S., Atsavapranee, P., Wolf, E., Daum, S., Pattenden, R., Widjaja, R., Gerber, A. (2012). Collaborative CFD exercise for a submarine in a steady turn. In *ASME 2012 31st International Conference on Ocean, Offshore and Arctic Engineering.*

Toxopeus, S., & Vaz, G. (2009). Calculation of current or manoeuvring forces using a viscous-flow solver. In *ASME 28th International Conference on Ocean, Offshore and Arctic Engineering*, 5, 717-728. Honolulu, Hawaii. doi:10.1115/OMAE2009-79782.

Tuck, E. (1971). Irrotational flow past bodies close to a plane surface. *Journal of Fluid Mechanics*, 50(03), 481-491.

Tuck, E. (1987). *Wave resistance of thin ships and catamarans*. (Report T8701, Applied Mathematics Department, The University of Adelaide)

Tuck, E. O. (1989). A submerged body with zero wave resistance. *Journal of Ship Research*, 33(2), 81-83.

Tuck, E. O. (1989). The wave resistance formula of Michell, J.H. (1898) and its significance to recent research in ship hydrodynamics. *Journal of the Australian Mathematical Society Series B-Applied Mathematics*, 30, 365-377.

Vassilopoulos, L., & Mandel, P. (1964). A new appraisal of strip theory. In *Fifth Symposium of Naval Hydrodynamics*, Office of Naval Research, Department of the Navy.

VonNeumann, J., & Richtmyer, R. D. (1950). A method for the numerical calculation of hydrodynamic shocks. *Journal of Applied Physics*, 21(3), 232-237.

Wallin, S., & Johansson, A. V. (2000). An explicit algebraic Reynolds stress model for incompressible and compressible turbulent flows. *Journal of Fluid Mechanics*, 403, 89-132.

Weinblum, G., Amtsberg, H., & Bock, W. (1936). Bodies of revolution with minimum wave resistance, *Ingenieur Archiv,* VII, 104.

Wilcox, D. (1988). Reassessment of the scale-determining equation for advanced turbulence models. *AIAA Journal*, 26(11), 1299-1310.

Wilson-Haffenden, S., Renilson, M., Ranmuthugala, D., & Dawson, E. (2010). An Investigation into the Wave Making Resistance of a Submarine Travelling Below the Free Surface. In *International Maritime Conference 2010, 1, 495-504*. Sydney, Australia.

Enabling the Prediction of Manoeuvring Characteristics of a Submarine Operating Near the Free Surface

Presented at PACIFIC 2013 by Christopher Polis

C Polis[1], D Ranmuthugala[1], J Duffy[1], M Renilson[1,2]

1. Australian Maritime College, 2. Higher Colleges of Technology, UA

Appendix A has been removed for copyright or proprietary reasons.

Prediction of The Hydroplane Angles Required Due To High Speed Submarine Operations Near The Surface

Presented at WARSHIP 2014 by Martin Renilson

M R Renilson, Higher Colleges of Technology, UAE, and Australian Maritime College, University of Tasmania, Australia

C Polis, Australian Maritime College, University of Tasmania, Australia

D Ranmuthugala, Australian Maritime College, University of Tasmania, Australia

J Duffy, Australian Maritime College, University of Tasmania, Australia

Appendix B has been removed for copyright or proprietary reasons.

APPENDIX C – FELDMAN (1979) EQUATIONS OF MOTION

For reference.

AXIAL FORCE EQUATION

$$m\left[\dot{u} - vr + wq - x_G(q^2 + r^2) + y_G(pq - \dot{r}) + z_G(pr + \dot{q})\right] =$$

$$+ \frac{\rho}{2} \ell^4 \left[X_{qq'} q^2 + X_{rr'} r^2 + X_{rp'} rp\right]$$

$$+ \frac{\rho}{2} \ell^3 \left[X_{\dot{u}'} \dot{u} + X_{vr'} vr + X_{wq'} wq\right]$$

$$+ \frac{\rho}{2} \ell^2 \left[X_{vv'} v^2 + X_{ww'} w^2\right]$$

$$+ \frac{\rho}{2} \ell^2 \left[X_{\delta r \delta r'} u^2 \delta_r^2 + X_{\delta s \delta s'} u^2 \delta_s^2 + X_{\delta b \delta b'} u^2 \delta_b^2\right]$$

$$-(W-B) \sin\theta + F_{xp}$$

NORMAL FORCE EQUATION

$$m\left[\dot{w} - uq + vp - z_G(p^2 + q^2) + x_G(rp - \dot{q}) + y_G(rq + \dot{p})\right] =$$

$$+ \frac{\rho}{2} \ell^4 Z_{\dot{q}}' \dot{q}$$

$$+ \frac{\rho}{2} \ell^3 \left[Z_{\dot{w}}' \dot{w} + Z_q' uq + Z_{vp}' vp\right]$$

$$+ \frac{\rho}{2} \ell^2 \left[Z_u' u^2 + Z_w' uw\right]$$

$$+ \frac{\rho}{2} \ell^2 \left[Z_{|w|}' u|w| + Z_{ww}' |w(v^2 + w^2)^{1/2}|\right]$$

$$+ \frac{\rho}{2} \ell^2 \left[Z_{\delta s}' u^2\delta_s + Z_{\delta b}' u^2\delta_b + Z_{\delta s\eta}' u^2\delta_s \left(\eta - \frac{1}{C}\right) C\right]$$

$$- \frac{\rho}{2} C_d \int_{\ell} b(x)\, w(x) \left\{[w(x)]^2 + [v(x)]^2\right\}^{1/2} dx$$

$$+ \frac{\rho}{2} \ell \bar{C}_L \int_{x_2}^{x_1} v(x)\, \bar{v}_{FW}(t - \tau[x])\, dx$$

$$+ (W - B) \cos\Theta \cos\phi$$

PITCHING MOMENT EQUATION

$$I_y \dot{q} + (I_x - I_z)rp - (\dot{p} + qr)I_{xy} + (p^2 - r^2)I_{zx} + (qp - \dot{r})I_{yz}$$

$$+ m\left[z_G(\dot{u} - vr + wq) - x_G(\dot{w} - uq + vp)\right] =$$

$$+ \frac{\rho}{2} \ell^5 \left[M_{\dot{q}}' \dot{q} + M_{rp}' rp\right]$$

$$+ \frac{\rho}{2} \ell^4 \left[M_{\dot{w}}' \dot{w} + M_q' uq\right]$$

$$+ \frac{\rho}{2} \ell^3 \left[M_u' u^2 + M_w' uw + M_{w|w|R}' w\left|(v^2 + w^2)^{1/2}\right|\right]$$

$$+ \frac{\rho}{2} \ell^3 \left[M_{|w|}' u|w| + M_{ww}' |w (v^2 + w^2)^{1/2}|\right]$$

$$+ \frac{\rho}{2} \ell^3 \left[M_{\delta s}' u^2\delta_s + M_{\delta b}' u^2\delta_b + M_{\delta s\eta}' u^2\delta_s\left(\eta - \frac{1}{C}\right) C\right]$$

$$+ \frac{\rho}{2} C_d \int_{\ell} x\, b(x)\, w(x) \left\{[w(x)]^2 + [v(x)]^2\right\}^{1/2} dx$$

$$- \frac{\rho}{2} \ell \bar{C}_L \int_{x_2}^{x_1} x\, v(x)\, \bar{v}_{FW}(t - \tau[x])\, dx$$

$$- (x_G W - x_B B)\cos\theta\cos\phi - (z_G W - z_B B)\sin\theta$$